Continuum damage mechanics with an application to fatigue

CONTINUUM DAMAGE MECHANICS WITH AN APPLICATION TO FATIGUE

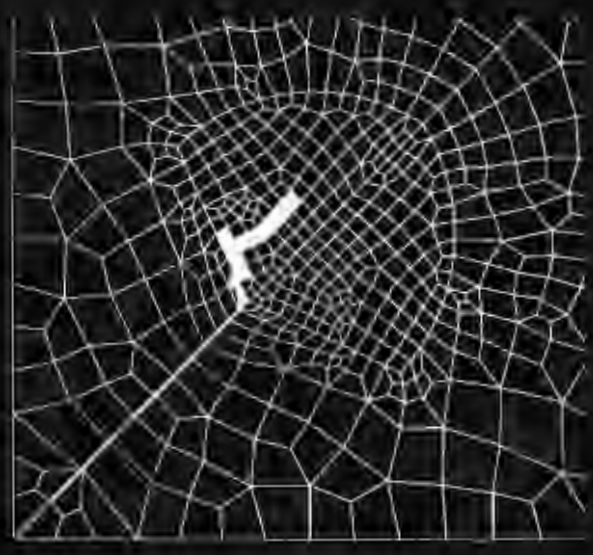

Michel Paas

CONTINUUM DAMAGE MECHANICS

WITH AN APPLICATION TO FATIGUE

CIP–DATA KONINKLIJKE BIBLIOTHEEK, DEN HAAG

Paas, Michel Hendrik Julius Wilhelm

Continuum damage mechanics with an application to fatigue /
Michel Hendrik Julius Wilhelm Paas. – [S.l. : s.n.]. – Ill.
Thesis Eindhoven. – With ref. – With a summary in Dutch.
ISBN 90–9003688–1
SISO 533 UDC 531(043.3)
Subject heading: continuum damage mechanics.

Druk: Febodruk, Enschede

CONTINUUM DAMAGE MECHANICS

WITH AN APPLICATION TO FATIGUE

PROEFSCHRIFT

ter verkrijging van de graad van doctor
aan de Technische Universiteit Eindhoven,
op gezag van de Rector Magnificus, prof.ir. M. Tels,
voor een commissie aangewezen door het College van Dekanen
in het openbaar te verdedigen
op vrijdag 19 oktober 1990 om 16.00 uur

door

MICHEL HENDRIK JULIUS WILHELM PAAS

geboren te Heerlen

Dit proefschrift is goedgekeurd door de promotoren

prof.dr.ir. J.D. Janssen

en

prof.dr.ir. A.M.A. v.d. Heijden

co–promotor

dr.ir. P.J.G. Schreurs

Contents

Abstract

In the modeling of failure mechanisms the application of advanced theoretical and numerical methods is indispensable. In the present study continuum damage mechanics (CDM) is adopted to describe these mechanisms. CDM is a branch in continuum mechanics, which is characterized by the introduction of a continuous damage variable that represents the local distribution of microdefects. The introduction of the damage variable requires the establishment of an additional equation, the so–called (damage) evolution equation, that expresses how the damage changes. In CDM a continuous coupling between damage and deformations is obtained. General expressions for the constitutive equations, i.e. the stress–strain relation and the evolution equation, can be derived from two potentials: the Helmholtz free energy and the dissipation potential.

The present research focuses on brittle failure mechanisms, implying that damage evolution is the predominant dissipative mechanism. Additionally, the current state does not depend on the rate at which this state has been realized. A distinction, which is based on the criterion for damage growth, is made between brittle and fatigue damage. Models are developed for both mechanisms. The model for brittle damage is capable of describing the behaviour of concrete and polystyrene in simple loading situations. The model for fatigue can be reduced to some widely accepted cumulative damage models. Anisotropic damage is considered by taking the directional nature of damage into account with dyadic vector products.

For a complete description of failure mechanisms, the evolution equation and the initial damage must be supplied. To characterize the parameters in the evolution law, it is hypothesized that microcrack growth and macrocrack growth are given by identical relationships. Then, the evolution equation can be derived using concepts from fracture mechanics. Based on the fact that failure processes actually are stochastic processes, it can be argued that the initial damage is a random quantity. By associating the initial damage with a characteristic size, the so–called elementary cell, its statistical properties can be established. The validity of the developed statistical model is demonstrated for fatigue in rubbers and polystyrene.

For practical applications the equilibrium equation and the constitutive equations are solved numerically. Based on the principle of weighted residuals, an iterative procedure is derived for the solution of the nonlinear equations. A substantial reduction in computing time is obtained by the application of an adaptive stepsize algorithm for the numerical integration of the evolution equation

and by uncoupling the constitutive equations.

Simulation techniques are applied to analyze stochastic failure processes. The simulations consist of finite element calculations for different realizations of the initial state. The statistics of the failure processes follow from the total of responses. The simulations learn that the solutions obtained with the coupled and uncoupled constitutive equations display only small deviations. Moreover, the influence of the mesh on the solutions is reduced by the elementary cell.

In CDM crack growth is equivalent to the development of a zone of completely damaged elements. Both initiation and propagation of cracks are predicted.

Notation

Quantities

A	scalar
$\vec{A}$	vector
$\mathbf{A}$, ${}^4\mathbf{A}$	second, fourth order tensor
$\underset{\sim}{A}$	column
$\underline{\underline{A}}$	matrix
$\underline{A}$	stochastic quantity
$\mathbf{I}$, ${}^4\mathbf{I}$	second, fourth order unit tensor

Operations and functions

$\mathbf{A}^c$, ${}^4\mathbf{A}^c$	conjugation
$\vec{A}\,\vec{B}$, $\mathbf{A}\,\vec{B}$, $\vec{A}\,\mathbf{B}$, $\mathbf{A}\,\mathbf{B}$	dyadic product
$\vec{A}\cdot\vec{B}$, $\mathbf{A}\cdot\vec{B}$, $\vec{A}\cdot\mathbf{B}$, $\mathbf{A}\cdot\mathbf{B}$	inner product
$\mathbf{A}:\vec{B}$, ${}^4\mathbf{A}:\mathbf{B}$	double inner product
$\mathbf{A}^{-1}$, $\underline{\underline{A}}^{-1}$	inversion
$\underset{\sim}{A}^{-T}$, $\underline{\underline{A}}^{-T}$	transposition
$\underset{\sim}{A}^T\underset{\sim}{B}$, $\underline{\underline{A}}\,\underset{\sim}{B}$, $\underset{\sim}{A}^T\underline{\underline{B}}$, $\underline{\underline{A}}\,\underline{\underline{B}}$	matrix product
$\lvert\vec{A}\rvert$	magnitude
$\det(\mathbf{A})$	determinant
$\dot{A}$	material time derivative
$\vec{\nabla}$	gradient operator
$E(A)$	expected value
$p_{\underline{A}}(A)$	probability distribution function
$P_{\underline{A}}(A)$	cumulative distribution function

1 Introduction

1.1 Scope of the work

Structural design is concerned with developing structures of improved performance. At any stage of the development trade–offs must be made between performance and reliability on the one hand and performance and cost on the other. How such trade–offs are made and the criteria on which they are based, strongly depends on the operating conditions, which can be divided into mechanical loadings and environmental effects. Sometimes an improved performance is obtained by trial and error. Quite frequently this is unfeasible from a practical and economical point of view. Then, an improved performance should be attained through extensive analysis in the conceptual design phase. A promising approach is to apply optimization techniques, where some objective function, for instance the weight of a structure, is optimized. The objective function depends on several design variables. In many problems the values of the design variables are subject to some constraints, for instance the weight must have a non–negative value. In many cases the objective function can not be derived straightforwardly. Experimental design methods are helpful to determine which parameter studies should be carried out in order to establish the relationships between objective functions and design variables. The parameter studies are usually based on finite element calculations (Schoofs 1987). Minimization of the objective function with respect to the chosen design variables yields an optimal design.

As failure criteria in structural design are usually simple static criteria, the reliability of a design requires thorough investigation. In situations, where failure occurs after a long period of time, such as fatigue, an ubiquitous problem is having a limited time to complete testing. Various procedures are used to accelerate lifetests. Roughly, accelerated lifetests can be divided into two categories: compressed–time tests and advanced stress tests. In compressed–time tests the amplitudes of the loadings are maintained at the level expected in normal use, but the loading frequencies are much higher. In advanced stress tests increased loads and harsher environments are applied. Accelerated testing is useful, but it must be carried out with care to ensure that the results are not erroneous, since the failure mechanisms that are dominant at high loading levels or frequencies may no longer be important at nominal conditions.

An example of the design phases mentioned above can be found in the heart valve research project at the Eindhoven University of Technology. This project aims at the development of a heart valve prosthesis with synthetic (fibre reinforced) leaflets. It was founded upon the opinion that specifications for an improved design must be obtained by a detailed analysis of the behaviour of a natural aortic valve. Early studies (Van Steenhoven 1979, Sauren 1981) revealed stress reducing mechanisms in natural valves, such as gradual valve closure, leaflet reinforcement and flexible leaflet suspension. In a follow–up study by Rousseau (1985) a valve prosthesis was analyzed, which exhibited the main characteristics of the natural aortic valve. In order to specify an optimal design, the effects of geometry and material properties on the stress distribution in the leaflets were evaluated for static loading in the closed phase. It is questionable, whether this approach really leads to a valve prosthesis that performs well, since another unfavourable situation occurs, when the valve is opening or closing. During these phases the leaflets are bended and wrinkled, which may cause microcracks in combination with leaflet calcification. In fact, an optimal design must account for both phases. Naturally, this leads to conflicting demands, which are to design a valve prosthesis that behaves like the natural valve on the one hand and that shows a high reliability on the other. For this purpose a better insight into the failure mechanisms involved is essential. This can be obtained with the aid of experimental methods (compressed–time tests) in combination with advanced theoretical and numerical methods to predict the observed physical phenomena.

A suitable theory should incorporate the fact that within a solid all sorts of microdefects are present, whose dimensions depend on the material, the production process and the environment. From experience it is known that increased loadings and larger defects will accelerate failure processes. Hence, it is stated that defect growth depends on the stress state and the defect dimensions. Since the exact positions and dimensions of the microdefects are unknown, local stress states are unknown as well. Consequently failure processes are stochastic processes.

In this thesis failure mechanisms are modeled by representing the local distribution of microdefects as internal state or rather damage variables. The introduction of the damage variables requires the establishment of an additional equation, the so–called (damage) evolution equation, that describes how the damage state changes. This phenomenological approach is called continuum damage mechanics (CDM). In CDM a continuous coupling between local damage processes and local deformations is obtained. The application of CDM has various attractive

features:

- CDM has a sound thermodynamical basis,
- internal variables can be used to characterize various dissipative mechanisms,
- complex material behaviour, involving geometrical and physical nonlinearities and anisotropic damage, can be taken into account,
- experimental characterization of the parameters in the damage evolution equation is feasible,
- both initiation and propagation of macrocracks can be predicted,
- CDM is based on continuum mechanics, such that implementation in existing finite element codes is relatively straightforward; advantage can be taken of similarities with other dissipative mechanisms such as plasticity.

1.2 Further considerations

In the foregoing CDM was selected as a tool for the analysis of failure mechanisms. Particular interest is directed towards fatigue. In fatigue, damage evolution is the predominant dissipative mechanism and the current state does not depend upon the rate at which this state has been realized. The evolution equation and a criterion which indicates, whether the current state changes, must be specified. Most of the existing models for fatigue were developed for metals (Lemaitre 1986a, Chaboche and Lesne 1988). The application of these models to polymer materials may produce incorrect results, since different microstructural mechanisms may be prevalent. For example, the model derived by Lemaitre (1986a) is based on the presence of micro plasticity. This mechanism, however, is unlikely to occur in polymer materials. Since no suitable models were found in literature, part of this work focuses on the development of brittle damage models.

With regard to the experimental characterization the number of model parameters should be kept as low as possible. Lemaitre and Dufailly (1987) stated that due to the localization of damage, conventional methods are not suitable for damage characterization, since these methods are based on measuring variations in global material properties, such as the Young's modulus, density and electrical resistance. The lack of experimental methods for damage measurements in case of fatigue and the resulting scarcity of experimental data encourages for contributions in this field.

Due to the presence of microdefects with unknown dimensions and positions, failure processes are stochastic processes. As yet the random nature of damage has

not been under much investigation. In fact, in CDM this randomness is neglected by assuming that initially a material is in a perfect state, resulting in a deterministic analysis. In this work the randomness in the initial state is taken into account and it is endeavoured to develop a theory for determining its statistical distribution. The probability distribution function (PDF) of the initial damage together with an evolution equation enable us to predict lifetime distributions. Another interesting application can be found in the experimental field. Suppose that an experimental lifetime distribution and an evolution equation are available. Then, it is possible to determine the initial damage distribution. With respect to the establishment of the evolution equation it is assumed that microcrack growth and macrocrack growth are expressed by identical relationships. A sound basis for this assumption is given in this thesis. Provided that a relationship between the local defect state and the damage variable is available, an evolution equation can be derived. This assumption has the additional advantage that data from fracture mechanics can be used.

Besides reflections on the theoretical and experimental facets of failure mechanisms, an important issue is the numerical solution of the resulting equations. Currently much effort is spent on the modeling of macrocrack initiation and propagation using so–called local approaches. In a local approach to fracture the crack tip is a process zone in a finite element mesh in which the damage state increases, resulting in a decrease of the rigidity. Crack growth is identified with the evolution of a completely damaged zone with recalculation of the stress–strain state. Although CDM provides a viable tool to model fracture, a more general use of the local approaches is delayed by the cost of the calculations and the dependence on the finite element modeling (Chaboche 1988). On the subject of fatigue Lemaitre (1986b) states in a review paper that "only few papers deal with fatigue, which means that we have to work hard in this field! But the difficulty is that fatigue is much more localized than other kinds of damage". This remark gives rise to further research on the numerical aspects of damage models concerning computing times, the influence of the mesh on the results (mesh sensitivity) and damage localization.

The key to developments on the mesh sensitivity and damage localization in failure processes is hidden in the stochastic nature of damage. By associating the PDF of the initial damage to a characteristic size, which is independent of the element dimensions, the mesh sensitivity is reduced. Additionally, the evolution equation, which displays a sudden explosive increase in the damage, causes a natural localization of the failure process. Because of the randomness in the initial damage, a localization can be found even in nearly homogeneous stress fields.

A substantial reduction in computing time can be obtained by the application of an adaptive stepsize algorithm. In situations where an explosive increase in the damage state is observed, it is convenient to uncouple the constitutive equations. The solutions obtained with this approach show small deviations from the solutions obtained with the coupled equations, however with much less computational effort. Finally, it is noted that polymer materials may exhibit large deformations. Hence, a viable numerical tool must provide for geometrical nonlinearities.

1.3 Contents of the thesis

In this thesis the following subjects will be discussed.

In chapter 2 the basic equations in continuum mechanics are presented and internal variables are introduced to represent dissipative mechanisms. Some concepts in formulating damage variables are discussed in chapter 3. A model is developed for the analysis of brittle failure mechanisms. A distinction, which is based on the formulation of the damage criterion, is made between brittle and fatigue damage. Besides isotropic damage, anisotropic damage is considered as well using dyadic vector products. In all cases a criterion for damage evolution and an evolution equation, indicative of the mechanisms involved, must be supplied.

The stochastic nature of damage is discussed in chapter 4. A theory is developed for characterizing the statistical distribution of the initial damage, which is an essential quantity in the prediction of fatigue mechanisms. The validity of the model is examined for fatigue in rubbers and glassy polymers.

The numerical elaboration of the theory is exposed in chapter 5. Based on the principal of weighted residuals a plane stress element is derived. Methods for the reduction of computing times are presented involving the application of an adaptive stepsize control algorithm and the uncoupling of the constitutive equations. To demonstrate the capabilities of the numerical tool, simulations concerning the stochastic aspects of damage and the initiation and propagation of macrocracks are carried out in chapter 6. In chapter 7 the conclusions of the present research are given and some recommendations for future research are put forward.

2 Thermodynamical framework

2.1 Introduction

In this chapter a general framework of the theory used in this thesis is presented. In section 2.2 some important kinematical quantities are defined. In section 2.3 the so–called balance laws are introduced. In order to determine all variables in the balance laws, constitutive equations, which characterize the material behaviour, are required. In section 2.4 some widely accepted constitutive principles are discussed, which restrict the possible forms of the functional dependence on the assumed independent variables in the constitutive equations. In section 2.5 some assumptions concerning the constitutive equations are made. It is assumed that the state of a continuum can be described completely by the instantaneous values of the independent variables together with a set of internal independent variables. The consequences of the introduction of the internal variables with respect to the Clausius–Duhem inequality will be considered. This leads to the introduction of a dissipation potential by which the generalized fluxes can be determined as functions of the conjugate generalized forces.

2.2 Kinematical quantities

In this section some important kinematical quantities used in continuum mechanics are defined. Each material point of a body can be identified by a column ξ of three material coordinates. The set of columns ξ for all material points of the body is denoted by B. Let $\vec{x} = \vec{x}(\xi, t)$ be the current position vector of $\xi \in B$. It is assumed that $\vec{x}$ is differentiable with respect to both ξ and t. The position vector of $\xi \in B$ in the reference configuration is written as $\vec{x}_0 = \vec{x}(\xi, t_0)$. Defining the rate $\dot{\alpha}$ of a quantity $\alpha = \alpha(\xi, t)$ as the time derivative of α for fixed values of ξ, the velocity vector $\vec{v}$ of a material point is denoted as

$$\vec{v}(\xi, t) = \dot{\vec{x}}(\xi, t) = \frac{\partial \vec{x}}{\partial t} \tag{2.2.1}$$

The deformation of the body is characterized by the deformation tensor $\mathbf{F}$

$$\mathbf{F} = \mathbf{F}(\vec{x}_0, t) = (\vec{\nabla}_0 \vec{x})^c \tag{2.2.2}$$

where $\vec{\nabla}_0$ is the gradient operator with respect to the reference configuration. The deformation tensor is regular and its determinant J is positive and describes the change in volume of an infinitesimal material element

$$J = \det(\mathbf{F}) = \frac{\mathrm{d}V}{\mathrm{d}V_0} > 0 \tag{2.2.3}$$

The deformation tensor can be decomposed uniquely into the product of a rotation tensor $\mathbf{R}$ and a symmetric positive definite tensor $\mathbf{U}$, the so–called stretch tensor

$$\mathbf{F} = \mathbf{R}\cdot\mathbf{U} \quad ; \quad \mathbf{U}^2 = \mathbf{F}^c\cdot\mathbf{F} \tag{2.2.4}$$

A useful measure for the deformations in a body is the Green–Lagrange strain tensor, which is defined as

$$\mathbf{E} = \tfrac{1}{2}\,(\,\mathbf{F}^c\cdot\mathbf{F} - \mathbf{I}) \tag{2.2.5}$$

The rate of deformation tensor $\dot{\mathbf{F}}.\mathbf{F}^{-1}$, which is independent of the reference configuration, can be written as the sum of the symmetric deformation rate tensor $\mathbf{D}$ and the skew–symmetric spin tensor $\mathbf{\Omega}$

$$\dot{\mathbf{F}}\cdot\mathbf{F}^{-1} = \mathbf{D} + \mathbf{\Omega} = (\vec{\nabla}\,\vec{\mathrm{v}})^c \tag{2.2.6}$$

2.3 Balance laws

At every instant during the deformation of a continuum, the balance laws must be satisfied. If polar media are left out of consideration, the laws of conservation of mass, momentum, moment of momentum and energy (first law of thermodynamics) can be written in the following local forms

$$\dot{\rho} + \rho\,\vec{\nabla}\cdot\vec{\mathrm{v}} = 0 \quad \Leftrightarrow \quad J = \frac{\rho_0}{\rho} \tag{2.3.1}$$

$$\vec{\nabla}\cdot\sigma + \rho\vec{\mathrm{b}} = \rho\dot{\vec{\mathrm{v}}} \tag{2.3.2}$$

$$\sigma = \sigma^c \tag{2.3.3}$$

$$\rho\dot{e} = \sigma : D + \rho r - \vec{\nabla}\cdot\vec{h} \tag{2.3.4}$$

Here ρ, σ, $\vec{b}$, e, r and $\vec{h}$ denote, respectively, the density, the Cauchy stress tensor, the specific (i.e. per unit mass) load vector, the specific internal energy, the specific heat production and the heat flow vector.

The second law of thermodynamics states, that every thermomechanical process has a direction, such that not every conceivable state can be reached from the current state. In a more formal way, it is stated that the local rate of entropy production of any volume element in a continuum is positive regardless of the nature of the process, leading to (Malvern 1969)

$$\dot{\gamma} \equiv \dot{\eta} - \frac{r}{\theta} + \frac{1}{\rho}\vec{\nabla}\cdot\left[\frac{\vec{h}}{\theta}\right] \geq 0 \tag{2.3.5}$$

where $\dot{\gamma}$ is the specific internal entropy production rate, θ is the absolute temperature and η is the specific entropy. The inequality implies internal entropy production in an irreversible process, the equality holds for a reversible process.
The Helmholtz free energy ψ is introduced as

$$\psi = e - \theta\eta \tag{2.3.6}$$

Using the first law of thermodynamics (2.3.4) and (2.3.6), the second law of thermodynamics is expressed as

$$\rho\dot{\gamma}\theta \equiv -\rho(\dot{\psi} + \dot{\theta}\eta) + \sigma : D - \frac{1}{\theta}\vec{h}\cdot\vec{\nabla}\theta \geq 0 \tag{2.3.7}$$

The state of a body is known when for any material particle the density ρ, the position vector $\vec{x}$ and the absolute temperature θ are known for the whole time interval under consideration (Müller 1984). According to eq. (2.3.1), the density can be expressed in terms of the position vector $\vec{x}$. Although the number of the remaining equations of balance is seven, the position vector field and the temperature field can not be determined, since new variables η, ψ, σ and $\vec{h}$ have appeared (it is tacitly assumed that r and $\vec{b}$ are known). Thus the system (2.3.2)–(2.3.4) is underdetermined. However, the so–called constitutive variables η, ψ, σ and $\vec{h}$ are related to the independent variables through constitutive equations. Thus, in order to close the system of equations (2.3.2)–(2.3.4) it is necessary to

determine the constitutive equations for η, ψ, σ and $\vec{h}$. The constitutive variables have to satisfy a number of principles, which will be discussed in the next section.

2.4 Constitutive principles

It is recalled that a constitutive variable C at a material particle ξ can only depend on the histories of the position vector field $\vec{x}$ and temperature field θ

$$C(\xi, t) = C(\vec{x}(\zeta, \tau), \theta(\zeta, \tau)\,;\ \tau \leq t,\ \zeta \in B) \tag{2.4.1}$$

In this section some widely accepted constitutive principles will be discussed, which restrict the possible forms of the functional dependence on the independent variables in (2.4.1). Details of these principles can be found in Malvern (1969) and Müller (1984). The principle of local action states that the current values of the constitutive variables in a material point are determined completely by the history of the independent variables in the neighbourhood of that point. Materials satisfying this principle are called simple materials. As a result of this principle the constitutive variables at ξ are determined by the histories of $\vec{x}$, $\mathbf{F}$, θ and $\vec{\nabla}\theta$ at ξ. The principle of equipresence states that each of the constitutive variables is a function of all independent variables until proven otherwise, hence

$$C(\xi,t) = C(\vec{x}(\xi,\tau), \mathbf{F}(\xi,\tau), \theta(\xi,\tau), \vec{\nabla}\theta(\xi,\tau);\ \tau \leq t) \tag{2.4.2}$$

For brevity the dependence on the material coordinates will not be written explicitly below. The principle of objectivity states that constitutive equations must be invariant under changes of the frame of reference. From this principle it immediately follows that the spatial position $\vec{x}$ of a material point cannot be an independent variable (Müller 1984). Then, the constitutive equations are given by

$$\sigma(t) = \frac{1}{J}\,\mathbf{F}(t)\cdot\mathbf{P}[\mathbf{E}(\tau), \theta(\tau), \vec{g}_o(\tau);\ \tau \leq t]\cdot\mathbf{F}^c(t) \tag{2.4.3}$$

$$\vec{h}(t) = \frac{1}{J}\,\mathbf{F}(t)\cdot\vec{h}_o[\mathbf{E}(\tau), \theta(\tau), \vec{g}_o(\tau);\ \tau \leq t] \tag{2.4.4}$$

$$\psi(t) = \psi[\mathbf{E}(\tau), \theta(\tau), \vec{g}_o(\tau);\ \tau \leq t] \tag{2.4.5}$$

$$\eta(t) = \eta[\mathbf{E}(\tau), \theta(\tau), \vec{g}_o(\tau);\ \tau \leq t] \tag{2.4.6}$$

where $\vec{g}_o = \vec{\nabla}_o\theta = \mathbf{F}^c \cdot \vec{\nabla}\theta$ and P is called the second Piola–Kirchhoff stress tensor. The constitutive variables $\mathbf{P}$, $\vec{h}_o$, ψ and η are invariant quantities (Van Wijngaarden 1988). A convenient property of invariant quantities is, that their material time derivatives are also invariant.

From the constitutive equations (2.4.3)–(2.4.6) it follows, that the state of a body can not be determined, unless the histories of the independent variables are known up to the current time t. In order to avoid the inconveniences of such a formulation in terms of functionals, an alternative point of view will be adopted in the next section by the introduction of internal variables.

2.5 Internal variables

From a purely mathematical point of view, the introduction of a finite number of internal variables of scalar, vectorial or tensorial nature can be regarded as a strategy adopted for the purpose of parametrizing the histories of the independent variables in the constitutive equations (Coleman and Gurtin 1967, Rice 1970, Kestin and Bataille 1977, Germain et al. 1983). The resulting gain in simplicity is purely formal unless it is possible to identify the parametrization with a clear physical meaning. Internal variables have the common property that they describe micro–structural changes or rather dissipative mechanisms. Experimental investigations have led to the identification of a wide variety of internal variables, e.g. reflecting the extent of a chemical reaction, the growth of dislocations or microcrack growth.

Next two assumptions are made concerning the constitutive equations. The first assumption is about the class of materials to be considered. It is proposed, that the state of a body can be described completely by the instantaneous values of E, $\dot{\mathbf{E}}$, θ, $\vec{g}_o$ and a set of internal variables for the modeling of history dependent material behaviour (Van Wijngaarden 1988). The strain rate dependence will be useful at a later stage in the modeling of brittle failure mechanisms. For convenience all internal variables are stored into a column $\underset{\sim}{z}$

$$\underset{\sim}{z} = \{ \underset{\sim}{s} , \vec{\underset{\sim}{s}} , \underset{\sim}{S} \}^T \tag{2.5.1}$$

that contains scalar, vectorial and tensorial variables. Then the constitutive variables $\mathbf{P}$, $\vec{h}_o$, ψ and η are denoted as

$$C = C(\underset{\sim}{\omega}) \; ; \; \underset{\sim}{\omega} = \{\mathbf{E}(t), \dot{\mathbf{E}}(t), \theta(t), \vec{g}_o(t), \underset{\sim}{z}(t)\}^T \tag{2.5.2}$$

For notational simplicity the dependence on the current time will not be written explicitly in the sequel. The fact that the internal variables must account for the influence of the past on the current values of the constitutive variables, leads to the second assumption: the rate of the internal variables and the constitutive variables $\mathbf{P}$, $\vec{h}_o$, ψ and η depend on the same variables (Coleman and Gurtin 1967), hence

$$\dot{\underset{\sim}{z}} = \dot{\underset{\sim}{z}}\,(\underset{\sim}{\omega}) \tag{2.5.3}$$

The Clausius–Duhem inequality (2.3.7) places further restrictions on the possible forms of the constitutive equations (Malvern 1969). For the particular set of independent variables in (2.5.2) the consequences of the restrictions with respect to the Clausius–Duhem inequality will be investigated. If $\boldsymbol{\sigma}$, $\mathbf{D}$, $\vec{h}$ and $\vec{\nabla}\theta$ are replaced by the invariant quantities $\mathbf{P}$, $\dot{\mathbf{E}}$, $\vec{h}_o$ and $\vec{g}_o$, the Clausius–Duhem inequality becomes

$$\rho_o(-\dot{\psi} - \dot{\theta}\eta) + \mathbf{P} : \dot{\mathbf{E}} - \frac{1}{\theta}\vec{h}_o \cdot \vec{g}_o \geq 0 \tag{2.5.4}$$

The rate of the free energy is given by

$$\dot{\psi} = \frac{\partial\psi}{\partial\mathbf{E}} : \dot{\mathbf{E}} + \frac{\partial\psi}{\partial\dot{\mathbf{E}}} : \ddot{\mathbf{E}} + \frac{\partial\psi}{\partial\theta}\,\dot{\theta} + \frac{\partial\psi}{\partial\vec{g}_o} \cdot \dot{\vec{g}}_o + \frac{\partial\psi}{\partial\underset{\sim}{z}}^{T} \otimes \dot{\underset{\sim}{z}} \tag{2.5.5}$$

where the symbol $\otimes$ denotes a product operator according to

$$\frac{\partial\psi}{\partial\underset{\sim}{z}}^{T} \otimes \dot{\underset{\sim}{z}} = \frac{\partial\psi}{\partial\underset{\sim}{s}}^{T} \dot{\underset{\sim}{s}} + \frac{\partial\psi}{\partial\vec{\underset{\sim}{s}}}^{T} \cdot \dot{\vec{\underset{\sim}{s}}} + \frac{\partial\psi}{\partial\underset{\sim}{S}}^{T} : \dot{\underset{\sim}{S}} \tag{2.5.6}$$

Substitution of (2.5.5) into the Clausius–Duhem inequality yields

$$\left[\mathbf{P} - \rho_o\frac{\partial\psi}{\partial\mathbf{E}}\right] : \dot{\mathbf{E}} - \rho_o\frac{\partial\psi}{\partial\dot{\mathbf{E}}} : \ddot{\mathbf{E}} + \rho_o\left[-\eta - \frac{\partial\psi}{\partial\theta}\right]\dot{\theta} +$$

$$-\rho_o\frac{\partial\psi}{\partial\vec{g}_o} \cdot \dot{\vec{g}}_o - \rho_o\frac{\partial\psi}{\partial\underset{\sim}{z}}^{T} \otimes \dot{\underset{\sim}{z}} - \frac{1}{\theta}\vec{h}_o \cdot \vec{g}_o \geq 0 \tag{2.5.7}$$

The quantities $\dot{\mathbf{E}}$, $\ddot{\mathbf{E}}$, $\dot{\theta}$ and $\dot{\vec{g}}_0$ form a set of independent variables, whereas $\dot{\underset{\sim}{z}}$ depends among others on $\dot{\mathbf{E}}$ and $\vec{g}_0$. Requiring that the Clausius–Duhem inequality must hold for all possible choices of the aforementioned quantities we must have

$$\frac{\partial \psi}{\partial \dot{\mathbf{E}}} = \mathbf{0} \quad ; \quad \eta = -\frac{\partial \psi}{\partial \theta} \quad ; \quad \frac{\partial \psi}{\partial \vec{g}_0} = \vec{0} \tag{2.5.8}$$

$$\left[\mathbf{P} - \rho_0 \frac{\partial \psi}{\partial \mathbf{E}} \right] : \dot{\mathbf{E}} - \rho_0 \frac{\partial \psi^{\mathrm{T}}}{\partial \underset{\sim}{z}} \otimes \dot{\underset{\sim}{z}} - \frac{1}{\theta} \vec{h}_0 \cdot \vec{g}_0 \geq 0 \tag{2.5.9}$$

Inequality (2.5.9) is satisfied for

$$\mathbf{P} = \rho_0 \frac{\partial \psi}{\partial \mathbf{E}} \tag{2.5.10}$$

$$-\rho_0 \frac{\partial \psi^{\mathrm{T}}}{\partial \underset{\sim}{z}} \otimes \dot{\underset{\sim}{z}} - \frac{1}{\theta} \vec{h}_0 \cdot \vec{g}_0 \geq 0 \tag{2.5.11}$$

Inequality (2.5.11) contains two terms, respectively, a term due to irreversible heat conduction in the presence of a thermal gradient and a term due to the internal work of the internal variables. The quantities entering the Clausius–Duhem inequality are often called generalized irreversible forces $\underset{\sim}{X}$ and generalized fluxes $\underset{\sim}{J}$. The generalized forces and fluxes in the formulation of (2.5.11) are given by

$$\underset{\sim}{X}^{\mathrm{T}} = \left[-\frac{\partial \psi^{\mathrm{T}}}{\partial \underset{\sim}{z}} , -\frac{1}{\rho_0 \theta} \vec{g}_0 \right] \quad ; \quad \underset{\sim}{J}^{\mathrm{T}} = \left[\dot{\underset{\sim}{z}}^{\mathrm{T}}, \vec{h}_0 \right] \tag{2.5.12}$$

Then (2.5.11) is expressed as

$$\underset{\sim}{X}^{\mathrm{T}} \otimes \underset{\sim}{J} \geq 0 \tag{2.5.13}$$

According to $(2.5.12)_2$ the generalized fluxes depend on all independent variables. The generalized fluxes can be expressed in a manner, such that the preceding inequality is always obeyed. The basic step in the derivation of a general solution for (2.5.13) is the assumption that the generalized fluxes and forces are

related to each other by functions, which contain as parameters the independent variables (Germain et al. 1983). This leads to

$$\underset{\sim}{X}^T \otimes \underset{\sim}{J}(\underset{\sim}{X}, \underset{\sim}{\omega}) \geq 0 \quad ; \quad \underset{\sim}{J}(\underset{\sim}{0}, \underset{\sim}{\omega}) = \underset{\sim}{0} \tag{2.5.14}$$

where the restriction $(2.5.14)_2$ has a physical background, since without a driving force, the fluxes are zero, e.g. no heat conduction occurs without a thermal gradient. The solution of inequality $(2.5.14)_1$ consists of two parts, respectively, a non–dissipative part, which does not influence the production of entropy and a dissipative part, which contributes a term in the entropy production and which is derivable from a so–called dissipation potential ϕ. Mathematically this implies that every solution $\underset{\sim}{J}$ of (2.5.14) of class C^1 in $\underset{\sim}{X}$ and of class C^o in $\underset{\sim}{\omega}$ must be of the form

$$\underset{\sim}{J}(\underset{\sim}{X}, \underset{\sim}{\omega}) = \underset{\sim}{\nabla}_{\underset{\sim}{X}}\phi(\underset{\sim}{X}, \underset{\sim}{\omega}) + \underset{\sim}{U}(\underset{\sim}{X}, \underset{\sim}{\omega}) \tag{2.5.15}$$

where $\underset{\sim}{U}(\underset{\sim}{X}, \underset{\sim}{\omega})$ is a vector function, which satisfies the conditions

$$\underset{\sim}{X}^T \otimes \underset{\sim}{U}(\underset{\sim}{X}, \underset{\sim}{\omega}) = 0 \quad ; \quad \underset{\sim}{U}(\underset{\sim}{0}, \underset{\sim}{\omega}) = \underset{\sim}{0} \tag{2.5.16}$$

Hence the entropy inequality $(2.5.14)_1$ becomes

$$\underset{\sim}{X}^T \otimes \underset{\sim}{\nabla}_{\underset{\sim}{X}}\phi(\underset{\sim}{X}, \underset{\sim}{\omega}) \geq 0 \tag{2.5.17}$$

From (2.5.17) it follows that the dissipation potential ϕ must possess a non–negative radial derivative and an absolute minimum at $\underset{\sim}{X} = \underset{\sim}{0}$. In literature the non– dissipative part $\underset{\sim}{U}$ in (2.5.15) is disregarded (Krajcinovic 1983, Lemaitre 1986a, Chaboche 1988), yielding

$$\underset{\sim}{J}(\underset{\sim}{X}, \underset{\sim}{\omega}) = \underset{\sim}{\nabla}_{\underset{\sim}{X}}\phi(\underset{\sim}{X}, \underset{\sim}{\omega}) \tag{2.5.18}$$

This form is accepted throughout this thesis for the modeling of damage phenomena.

To conclude this chapter, it is stated that general expressions for the constitutive equations were obtained from a thermodynamical framework by the introduction of the free energy potential and the dissipation potential.

3 Damage modeling

3.1 Introduction

The mechanical properties of materials depend on the damage state, which can be defined by the existing density, distribution and type of microdefects. Depending on their sizes and orientations some of the microdefects will start growing under certain loading conditions. In this chapter these phenomena are treated from a phenomenological perspective. An attractive theory is offered by continuum damage mechanics. CDM is a branch of continuum mechanics, which is characterized by the introduction of internal field or rather damage variables that represent the local distribution of microdefects in an averaged sense (Krajcinovic 1984). In section 3.2 some concepts in formulating damage variables are discussed. In section 3.3 brittle failure mechanisms are modeled, implying that damage evolution is the predominant dissipative mechanism and that the current state does not depend on the rate at which this state has been realized. A restriction is made to isotropic damage states. A distinction, which is based on the formulation of the criterion for damage evolution, is made between brittle and fatigue damage. In section 3.4 anisotropic damage is considered. In this case the directional nature of damage is taken into account using dyadic products of vector variables.

3.2 Damage variables

The practical utility of the selected damage variable, depends on its description of the macroscopic effects. If the damage is distributed isotropically in a representative volume element, a scalar variable will produce satisfactory results (Davison et al. 1977, Chaboche 1988, Billardon and Moret–Bailly 1987, Paas et al. 1990a,b,c). For highly directional fields a better description may be obtained by the introduction of a vector variable (Davison and Stevens 1973, Krajcinovic and Fonseka 1981, Talreja 1985) or a tensorial variable (Simo and Ju 1987, Murakami 1988, Weitsman 1988). In literature three methods can be distinguished in the modeling of damage.

1 Taylor series expansions of constitutive equations
Using the theory of invariants (Spencer 1971) the restrictions, placed on the constitutive equations by the assumption of some material symmetry, are taken into account. Once a suitable damage variable is chosen, a basis of scalar invariants of

the independent variables, reflecting the symmetries characteristic of the material, can be determined. The constitutive equations are obtained by Taylor series expansions in the scalar invariants. This approach has a great generality, since it is not confined to small deformations. However, without further simplifications of the constitutive equations the experimental characterization is unfeasible due to the large number of model parameters. For this reason in literature an evolution equation is either disregarded (Talreja 1985, Murakami 1988), given only in a symbolic form (Davison and Stevens 1973, Allen et al. 1987, Weitsman 1988a,b) or elaborated for simple loading situations (Krajcinovic and Fonseka 1981, Simo and Ju 1987). In section 3.4 a procedure for the modeling of anisotropic damage states using dyadic vector products is discussed.

2 Micromechanical approach

For infinitesimally small deformations, it is convenient to adopt a micro–mechanical approach, in which the underlying physics of the failure mechanisms is reflected (Krajcinovic and Sumarac 1989, Singh and Digby 1989). The damage state is characterized with effective field theories (Budianski and O'Connel 1976, Laws and Brockenbrough 1987), which determine the effects of microcrack systems on the material behaviour. The criteria for damage evolution and the evolution equations are derived using linear elastic fracture mechanics on the microscale. Since many materials in structural design, like composites, ceramics and concrete, show linear elastic behaviour further study in this direction seems worthwhile. Extensions to nonlinear models can be made in combination with Taylor series expansions of the constitutive equations.

3 Effective stress concept

Consider the representative volume element (RVE) in Fig. 3.1. A surface of intersection δS is defined by the normal $\vec{n}$. Due to the formation of microdefects in the RVE the effective load–carrying area, associated with the direction of the normal $\vec{n}$, is reduced from δS to δS_e. The damage variable associated with the direction of $\vec{n}$ can be defined as (see section 3.4)

$$D_n = 1 - \frac{\delta S_e}{\delta S} \tag{3.2.1}$$

If the damage state is isotropic, D_n does not depend on the direction of the normal $\vec{n}$ and the damage can be characterized by a scalar quantity $D = D(\vec{x},t)$, for

which $D = D(\vec{x},t_o) = D_o \geq 0$ corresponds to the initial state and $D = D(\vec{x}, t_c) = D_c < 1$ corresponds to complete local rupture. The effective stress tensor can be related to the Cauchy stress tensor by (see e.g. Chaboche 1988 and Murakami 1988)

$$\hat{\sigma} = \frac{\sigma}{1-D} \tag{3.2.2}$$

The preceding equation is referred to as the effective stress concept. Considerable effort has been put in the extension of the effective stress concept to anisotropic damage (Kachanov 1986, Murakami 1988).

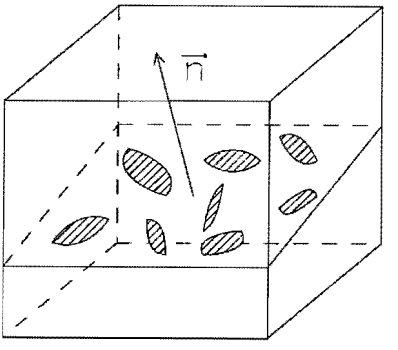

Figure 3.1 Damaged volume element

The effective stress concept is commonly applied in combination with the hypothesis of strain equivalence (Lemaitre 1986a, Chaboche 1988). The hypothesis of strain equivalence states that the effective stress tensor for a damaged material can be derived from the same Helmholtz free energy as for a virgin material, i.e. $\psi^o(\mathbf{E}) = \psi(\mathbf{E}, D = 0)$. Using (2.5.10) and (3.2.2) the second Piola–Kirchhoff stress tensor is written as

$$\mathbf{P} = (1 - D)\hat{\mathbf{P}} \quad ; \quad \hat{\mathbf{P}} = \rho_o \frac{\partial \psi^o}{\partial \mathbf{E}} \tag{3.2.3}$$

For isotropic damage the effective stress concept and the hypothesis of strain equivalence render an easy to use stress–strain relation, that is generally accepted in the field of CDM. In the next section we will adopt these concepts for the modeling of brittle failure mechanisms.

3.3 Brittle failure mechanisms

3.3.1 General theory

In the following we are concerned with the modeling of brittle failure mechanisms. These mechanisms are characterized by the fact that damage evolution is the predominant dissipative mechanism. Additionally, the current damage depends on the deformation path, but not on the rate at which this path has been followed. Then, in the integration of the evolution equations time acts as a pseudo variable (time–independent behaviour).

In the ensuing subsections we distinguish between brittle and fatigue damage. Brittle damage develops if relatively large loadings are applied resulting in a small number of loading reversals until failure occurs. Models for brittle damage have been developed for rock and concrete (Krajcinovic and Fonseka 1981, Mazars 1982, Simo and Ju 1987, Singh and Digby 1989) and for spalling in case of impact loading (Davison and Stevens 1973). For loadings well below the material strength, leading to a large number of loading reversals until failure, different processes are prevalent. Throughout, these processes are designated as fatigue damage. Next, the compulsory specifications for a complete description of brittle mechanisms are given.

Independent variables

A restriction is made to isotropic damage. Neglecting thermal effects, the independent variables are given by the Green–Lagrange strain tensor $\mathbf{E}$, its material time derivative $\dot{\mathbf{E}}$ and a scalar internal field variable D, that represents the damaged state. According to the principle of equipresence, the dependent variables $\mathbf{P}$, ψ and $\dot{\mathrm{D}}$ depend on all independent variables

$$\mathbf{P} = \mathbf{P}(\underset{\sim}{\omega}) \; ; \; \psi = \psi(\underset{\sim}{\omega}) \; ; \; \dot{\mathrm{D}} = \dot{\mathrm{D}}(\underset{\sim}{\omega}) \; ; \; \underset{\sim}{\omega}^{\mathrm{T}} = \{\mathbf{E}, \dot{\mathbf{E}}, \mathrm{D}\} \tag{3.3.1}$$

Following the theory in section 2.5 (see (2.5.8)–(2.5.11)) we obtain

$$\mathbf{P} = \rho_0 \frac{\partial \psi}{\partial \mathbf{E}} \; ; \; \frac{\partial \psi}{\partial \dot{\mathbf{E}}} = \mathbf{0} \; ; \; -\frac{\partial \psi}{\partial \mathrm{D}} \dot{\mathrm{D}} = \mathrm{X}\,\dot{\mathrm{D}} \geq 0 \tag{3.3.2}$$

Stress–strain relation

The stress–strain relation $(3.3.2)_1$ can be refined by accepting the effective stress

concept and the hypothesis of strain equivalence, yielding

$$\mathbf{P} = \rho_0 \, (1 - \mathrm{D}) \, \frac{\partial \psi^o}{\partial \mathbf{E}} \tag{3.3.3}$$

Then the generalized irreversible force X is given by

$$\mathrm{X} = -\frac{\partial \psi}{\partial \mathrm{D}} = \psi^o(\mathbf{E}) \tag{3.3.4}$$

Damage growth criterion

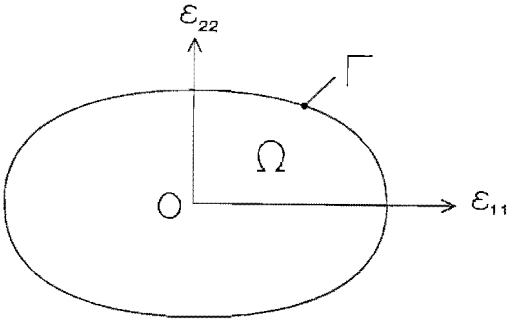

Figure 3.2 Damage criterion in strain space

The formulation of a damage model requires the establishment of a criterion for damage growth. Here the existence of a reversible domain Ω in strain space is proposed, which contains the origin and which is bounded by the surface Γ. The damage does not change if $\mathbf{E} \in \Omega$, but may evolve if $\mathbf{E}$ lies on the boundary Γ or outside the domain Ω. Formally the domain Ω and its boundary Γ can be expressed as (Fig. 3.2)

$$\Omega = \{ \, \mathbf{E} | \; g(\mathbf{E}, \kappa) < 0 \, \} \; ; \; \Gamma = \{ \, \mathbf{E} | \; g(\mathbf{E}, \kappa) = 0 \, \} \tag{3.3.5}$$

where κ is a parameter that serves as a threshold. In general its value depends on the deformation history and the material. The following set g is chosen

$$g(\mathbf{E}, \kappa) = \bar{\epsilon}(\mathbf{E}) - \kappa \leq 0 \tag{3.3.6}$$

where $\bar{\epsilon}$ is an equivalent strain. In section 3.3.3 $\bar{\epsilon}$ will be specified.

Damage evolution equation

According to the theory in section 2.5, $(3.3.2)_3$ is satisfied under the assumption that the evolution equation can be derived from a dissipation potential

$$\dot{D} = \nabla_X \phi(X, \underset{\sim}{\omega}) \tag{3.3.7}$$

which must be a monotonic increasing function of X. In brittle mechanisms the current state does not depend upon the rate at which this state has been realized. Then, the evolution function (3.3.7) must be positively homogeneous of degree 1 with respect to $\dot{E}$

$$\nabla_X \phi(X, \lambda \dot{E}, E, D) = \lambda \, \nabla_X \phi(X, \dot{E}, E, D) \quad \forall \, \lambda \geq 0 \tag{3.3.8}$$

Additionally, it is required that the current state can only change if the equivalent strain rate is positive. Then, the following evolution equation is proposed, which satisfies the aforementioned requirements

$$\dot{D} = \dot{\mu} \, \nabla_X \tilde{\phi}(X, E, D) \tag{3.3.9}$$

$$\dot{\mu} = \begin{cases} 0 & \text{if} \quad g < 0 \vee (g > 0 \wedge \dot{g} < 0) \\ A(E) : \dot{E} & \text{if} \quad g = 0 \vee (g > 0 \wedge \dot{g} > 0) \end{cases}$$

In the next subsections a detailed discussion concerning the specific choices of the dissipation potential and damage criterion is presented for brittle and fatigue damage.

3.3.2 Brittle damage

For brittle damage it is assumed that the boundary Γ can not be crossed, thus $E(t) \in \{ \Omega \cup \Gamma \}$. The current state can only change if $E(t) \in \Gamma$. Then, using (3.3.6), the following consistency condition must be satisfied on Γ

$$g = \dot{g} = 0 \implies \dot{\kappa} = \dot{\bar{\epsilon}} \tag{3.3.10}$$

This condition describes how the boundary Γ changes. In fact it states that the damage may grow, when the equivalent strain $\bar{\epsilon}$ reaches the current threshold κ. If the material property κ_0 denotes the initial threshold before any loading is applied, we must have that $\kappa \geq \kappa_0$. Combining (3.3.9) and (3.3.10) the evolution law is expressed as

$$\dot{D} = \dot{\mu}\, \nabla_X \hat{\phi}(X, E, D) \quad ; \quad \dot{\mu} \geq 0 \quad ; \quad \dot{\mu}\, g = 0 \tag{3.3.11}$$

If $g < 0$ the damage criterion is not satisfied. Accordingly $\dot{\mu} = 0$ must hold and the damage does not alter. If on the other hand $g = 0$ further damage may develop ($\dot{\mu} \geq 0$). Without a supplementary specification of the scalar function $\dot{\mu}$ the damaged state can not be determined. For this reason we propose

$$A = \frac{\partial \bar{\epsilon}}{\partial E} \quad \Longrightarrow \quad \dot{\mu} = \dot{\bar{\epsilon}} \quad \text{if } g = \dot{g} = 0 \tag{3.3.12}$$

Using (3.3.6), (3.3.11) and (3.3.12) the damage evolution equation becomes

$$\dot{D} = \begin{cases} 0 & \text{if } \bar{\epsilon} < \kappa \\ \nabla_X \hat{\phi}(X, E, D)\, \dot{\bar{\epsilon}} & \text{if } \bar{\epsilon} = \kappa \end{cases} \tag{3.3.13}$$

where the current boundary Γ must be determined by integration of the consistency condition (3.3.10).

Frequently, there is no need for distinction between tensile and compressive loadings and it suffices to formulate a damage criterion in the generalized force space, hence $g = g(X, \check{X})$ with $\check{X}$ the current threshold. Then, the evolution equation can be rewritten as

$$\dot{D} = \begin{cases} 0 & \text{if } X < \check{X} \\ \nabla_X \hat{\phi}(X, E, D)\, \dot{X} & \text{if } X = \check{X} \end{cases} \tag{3.3.14}$$

The damage variable is obtained by integration of (3.3.14), which requires the precise nature of the damage criterion and the potential $\hat{\phi}$ to be specified. Taking into account that this potential must be a monotonic increasing function of X, we choose

$$\hat{\phi} = \frac{c}{d+1} X^{d+1}(D_c - D)^{-e} \tag{3.3.15}$$

where $d \neq -1$ and $c, e \geq 0$ and D_c is a critical damage. Using (3.3.15) and (3.3.12) the evolution law is written as

$$\frac{dD}{dX} = \begin{cases} 0 & \text{if } X < \check{X} \\ c\, X^d (D_c - D)^{-e} & \text{if } X = \check{X} \end{cases} \tag{3.3.16}$$

Integration of the evolution law between the initial threshold X_o and the maximum generalized force $\check{X}$ yields.

$$D = D_c - \left[(D_c - D_o)^{\alpha} - \beta(\check{X}^{\gamma} - X_o^{\gamma})\right]^{\frac{1}{\alpha}} \tag{3.3.17}$$

where $\alpha = 1+e$, $\gamma = d+1$ and $\beta = c\alpha\gamma^{-1}$. Using $D_c = D(\check{X} = X_c)$, with X_c the generalized force at complete rupture, we obtain

$$D = D_c - (D_c - D_o)\left[\frac{X_c^{\gamma} - \check{X}^{\gamma}}{X_c^{\gamma} - X_o^{\gamma}}\right]^{\frac{1}{\alpha}} \tag{3.3.18}$$

Damage in uni–axial tests

The developed damage model will be illustrated with two examples concerning the mechanical behaviour of concrete and polystyrene (PS). These materials show linear elastic behaviour. In one–dimensional situations, the generalized force X and the stress–strain relation are written as

$$\begin{aligned} X &= \psi^o(\epsilon) = \tfrac{1}{2}E_o\epsilon^2 \\ \sigma &= (1-D)\frac{\partial\psi^o}{\partial\epsilon} = (1-D)E_o\epsilon \implies \frac{\sigma}{E_o\kappa_c} = (1-D)\frac{\epsilon}{\kappa_c} \end{aligned} \tag{3.3.19}$$

where E_o is the Young's modulus of the virgin material and κ_c is the rupture strain. Substitution of $(3.3.19)_1$ into (3.3.18) yields

$$D = 1 - \left[\frac{\kappa_c^{2\gamma} - \breve{\epsilon}^{2\gamma}}{\kappa_c^{2\gamma} - \kappa_0^{2\gamma}} \right]^{\frac{1}{\bar{\alpha}}} \tag{3.3.20}$$

where κ_0 is the threshold strain below which no damage growth occurs and $\breve{\epsilon}$ is the maximum strain that has been reached during the loading process. In accordance with most of the literature on CDM we take $D_0 = 0$ in the initial state and $D_c = 1$ in the final ruptured state.

Concrete is known to behave as a brittle material that contains numerous microcracks and microvoids. From experimental observations, failure in concrete is a continuous process, that initiates at low loading levels, with an increasing amount of damage for increasing loading levels. The model parameters are listed in table 3.1 for two different types of concrete (type I and II). The parameters E_0, κ_0 and κ_c for tension and compression were obtained from Mazars (1982), and Krajcinovic and Fonseka (1981) respectively. A typical stress–strain curve for tension loading is depicted in Fig. 3.3. (Mazars 1982) together with the model curve resulting from (3.3.19) and (3.3.20). In Fig. 3.4 the normalized stress–strain curve for compressive loadings, as determined with the present model, is shown. The experimental results from Krajcinovic and Fonseka (1981) are marked also, showing good agreement with the model curve.

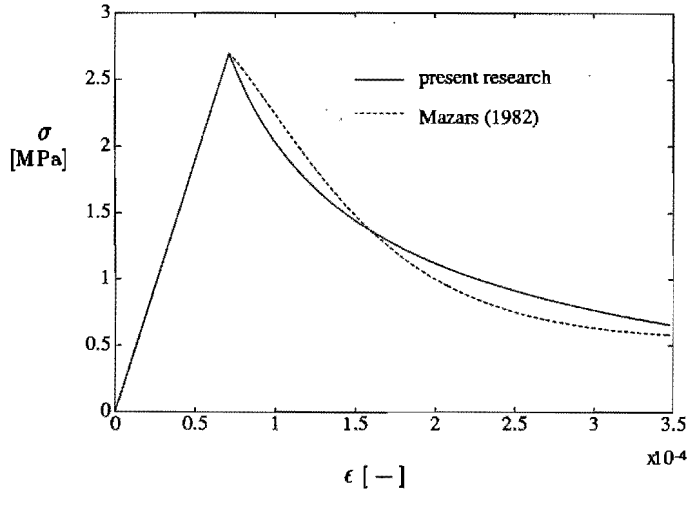

Figure 3.3 Concrete under tensile loading

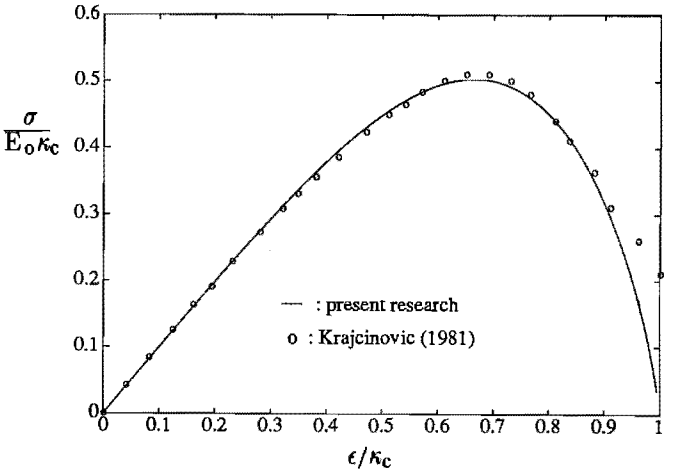

Figure 3.4 Concrete under compressive loading

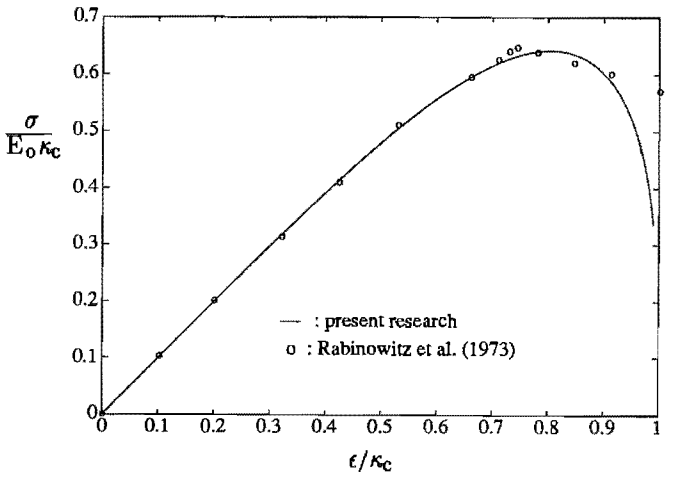

Figure 3.5 PS under tensile loading

Polystyrene (PS) is an amorphous glassy polymer. The tensile behaviour of PS has been the subject of extensive investigations and in particular the role of crazing in fracture has been studied in detail (Rabinowitz et al. 1973, Chen et al. 1981). The breakdown of the craze structure to form a macrocrack is modeled by (3.3.20). The data for PS under tension loading are given in table 3.1, where E_0, κ_0 and κ_c were obtained from Rabinowitz (1973). In Fig. 3.5 the stress–strain curve according to the present model is shown together with an experimental curve (Rabinowitz 1973).

Table 3.1

	Concrete I tension	Concrete II compression	PS tension
E_0	38 GPa	27.5 GPa	3.3 GPa
κ_0	$.71 \cdot 10^{-4}$	0	0
κ_c	$1 \cdot 10^{-3}$	$-6 \cdot 10^{-3}$	$2.04 \cdot 10^{-2}$
α	1	1.25	3.25
γ	-1	1.5	1.5

From these results it may be stated that a reasonably accurate description of brittle damage under uni–axial loadings is provided by (3.3.19) and (3.3.20).

3.3.2 Fatigue damage

Damage evolution equation

Under alternating loads materials will fail at stress levels much lower than they can withstand under monotonic loading conditions. This phenomenon is called fatigue. Since the number of loading reversals until failure occurs, usually is very large, it is also referred to as high cycle fatigue. Fatigue failure involves initiation and growth of a damaged zone, generally developing from a stress concentration site at the surface. This is followed by the initiation of a macrocrack with subsequent crack propagation untill some critical crack size is reached at which catastrophic fracture occurs (Sauer and Richardson 1980, Lemaitre 1986a).

A general theory for the modeling of brittle mechanisms was presented in section 3.3.1. In the following the damage growth criterion and the evolution equation are specified. In fatigue it is assumed that the boundary Γ of the domain Ω is not influenced by the deformation history and that the damage state changes if $\mathbf{E} \notin \Omega$. The damage criterion (3.3.6) now becomes

$$g = \bar{\epsilon}(\mathbf{E}) - \kappa_0 \tag{3.3.21}$$

where κ_0 is a fixed threshold, which is a true material property. We further assume

that (3.3.12) holds, whence the evolution law (3.3.9) takes the form

$$\dot{D} = \begin{cases} 0 & \text{if } \bar{\epsilon} < \kappa_0 \\ \nabla_X \tilde{\phi}(X, E, D) \langle \dot{\bar{\epsilon}} \rangle & \text{if } \bar{\epsilon} \geq \kappa_0 \end{cases} \tag{3.3.22}$$

In this equation the so–called McAuley brackets have been introduced, which are defined as

$$\langle x \rangle = \begin{cases} x & \text{if } x \geq 0 \\ 0 & \text{if } x < 0 \end{cases} \tag{3.3.23}$$

The McAuley brackets express that the current state can only change if the equivalent strain is increasing. A close similarity between the models for brittle and fatigue damage can be observed. In fact the only distinction is caused by the damage surface Γ, which in case of fatigue is fixed, whereas for brittle damage Γ is determined by the consistency condition (3.3.10). For notational simplicity, (3.3.22) is rewritten as

$$\dot{D} = H(\bar{\epsilon} - \kappa_0)\, \nabla_X \tilde{\phi}(X, E, D) \langle \dot{\bar{\epsilon}} \rangle \tag{3.3.24}$$

where $H(\cdot)$ is the Heaviside step function, which is defined as

$$H(x) = \begin{cases} 0 & \text{if } x < 0 \\ 1 & \text{if } x \geq 0 \end{cases} \tag{3.3.25}$$

A proper evolution law for fatigue damage should display the following features:
- in connection with experimental characterization the number of model parameters should be kept as low as possible,
- the contribution of tensile and compressive loadings is different.

Based on these characteristics $\tilde{\phi}$ is chosen as

$$\tilde{\phi} = \alpha\, D^{\beta}\, \bar{\epsilon}^{\gamma}\, X \tag{3.3.26}$$

where α, β, $\gamma \geq 0$ are material parameters. Using (3.3.24) and (3.3.26) the evolution equation is written as

$$\dot{D} = H(\bar{\epsilon} - \kappa_0)\ \alpha\, D^{\beta}\, \bar{\epsilon}^{\gamma}\, \langle\, \dot{\bar{\epsilon}}\, \rangle \tag{3.3.27}$$

Chaboche and Lesne (1988), who studied fatigue mechanisms in metals using an evolution law in which the term D^{β} also occurred, found that the material parameter β may depend on the loading.

With regard to the choice of the equivalent strain it is noted that for brittle materials this quantity should express the important part played by tension strains. Therefore, the equivalent strain is defined as

$$\bar{\epsilon} = \sqrt{\sum_{i=1}^{3} [\langle \epsilon_i \rangle^2 + h \langle -\epsilon_i \rangle^2]} \quad ; \quad h \in [0,1] \tag{3.3.28}$$

where ϵ_i are principal strains and h is a parameter, which expresses the fact that compressive strains are less harmful to damage growth than tensile strains. In Fig. 3.6 the influence of h on the damage surface as defined by (3.3.21), is demonstrated for $\kappa_0 = 1.7 \cdot 10^{-2}$ and $\epsilon_3 = 0$.

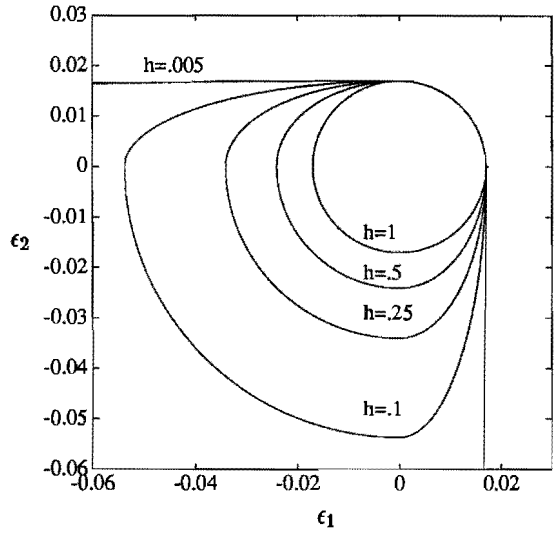

Figure 3.6 Influence of h on the damage surface

Damage growth per cycle

In case of fatigue one is interested in the damage growth per loading cycle. Integration over one period $[t_{i-1}, t_i]$ with $D(t_i) = D_i$ yields

$$\int_{D_{i-1}}^{D_i} D^{-\beta} dD = \int_{t_{i-1}}^{t_i} \alpha\, H(\bar{\epsilon} - \kappa_0)\, \bar{\epsilon}^{\gamma} \langle \dot{\bar{\epsilon}} \rangle \, d\tau \equiv \delta \tag{3.3.29}$$

The preceding equation is rewritten as

$$\frac{1}{1-\beta}\left[\left[1 + \frac{\Delta D_i}{D_{i-1}}\right]^{1-\beta} - 1\right] = \delta\, D_{i-1}^{\beta-1} \quad ; \quad \beta \neq 1 \tag{3.3.30}$$

Bearing in mind that $\beta \frac{\Delta D_i}{D_{i-1}} \ll 1$ with $\Delta D_i = D_i - D_{i-1}$, the left–hand side of (3.3.30) is linearized, yielding

$$\Delta D_i = \delta\, D_{i-1}^{\beta} \tag{3.3.31}$$

The damage after N cycles must be computed by summation over all previous cycles. This can be circumvented by rewriting the incremental damage growth per cycle ($\Delta N = 1$) as

$$\Delta D_i = \frac{\Delta D_i}{\Delta N} \Delta N = \frac{1}{f} \frac{\Delta D_i}{\Delta t} \equiv \frac{dD}{dN} \tag{3.3.32}$$

where f is the frequency of the periodical loading. Then the recurrence equation (3.3.31) is replaced by a differential equation for D(N), where N acts as a dimensionless time.

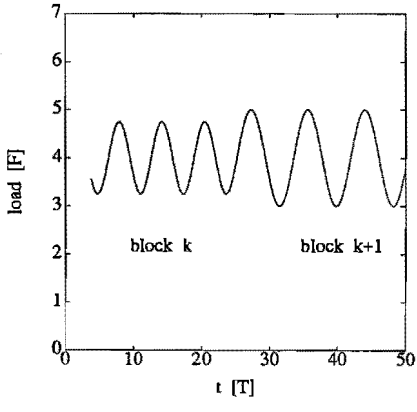

Figure 3.7 Block loading

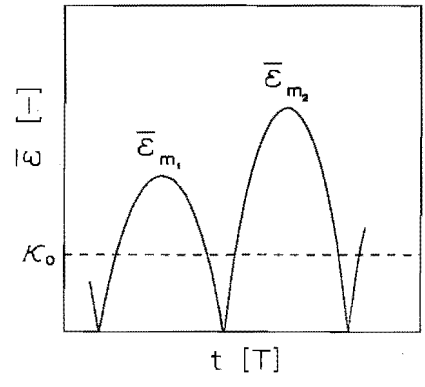

Figure 3.8 $\bar{\epsilon}$ as a function of time

Consider a body that is loaded in blocks. A block is defined as a series of loading reversals between two fixed amplitudes. The kth loading block takes place for $N_{k-1} \leq N < N_k$ cycles with $k = 1,...,n$ (Fig. 3.7). The damage evolution in block k is expressed as an initial value problem

$$\frac{dD}{dN} = \delta_k D^{\beta_k} \quad ; \quad \delta_k = \int_{t_{i-1}}^{t_i} \alpha H(\bar{\epsilon} - \kappa_0)\, \bar{\epsilon}^{\gamma} \langle \dot{\bar{\epsilon}} \rangle \, d\tau$$

$$D(N = N_{k-1}) = D_{k-1} \tag{3.3.33}$$

where D_{k-1} is the initial value at the start of block k. The integral δ_k must be calculated for specific loading situations. Consider, for example, the effective strain as sketched in Fig. 3.8. We then have

$$\delta_k = \int_{\kappa_0}^{{}_{(k)}\bar{\epsilon}_{m1}} \alpha\, \bar{\epsilon}^{\gamma}\, d\bar{\epsilon} + \int_{\kappa_0}^{{}_{(k)}\bar{\epsilon}_{m2}} \alpha\, \bar{\epsilon}^{\gamma}\, d\bar{\epsilon} =$$

$$\frac{\alpha}{\gamma+1} \left({}_{(k)}\bar{\epsilon}_{m1}^{\gamma+1} + {}_{(k)}\bar{\epsilon}_{m2}^{\gamma+1} - 2\, \kappa_0^{\gamma+1} \right) \tag{3.3.34}$$

In order to solve the evolution equation, the initial damage $D(N=0) = D_0$ is required. This quantity depends on the local microstructure. If the damage is homogeneously distributed in a testing specimen, its effects are apparent on a global scale. Thus damage growth can be detected by measuring variations in material properties, such as the Young's modulus and the density. Due to the localization of damage in fatigue, the characterization of the initial damage D_0 becomes a difficult task. This problem is tackled in chapter 4 by regarding D_0 as a random variable, whose probability distribution function is established with statistics of extremes.

Uncoupled constitutive equations

Under the assumption that the stress tensor is not influenced by the damage, until a critical damage D_c has been reached at which local rupture occurs, we write

$$\mathbf{P} = [1 - D_c\, H(D - D_c)]\, \hat{\mathbf{P}} \tag{3.3.35}$$

As a result of (3.3.35) the stress–strain relation and the evolution equation have become uncoupled. Since the stress–strain relation is not influenced by the damage growth, the deformation state is left unaltered during the failure process, implying that (3.3.33) can be solved analytically. Then, the damage after $N_k = N_{k-1} + \Delta N_k$ cycles is obtained as

$$\int_{D_{k-1}}^{D_k} D^{-\beta_k}\, dD = \delta_k \int_{N_{k-1}}^{N_k} dN \Rightarrow$$

$$D_k = \left[\Delta N_k/\tilde{N}_{c_k} + D_{k-1}^{1-\beta_k} \right]^{\frac{1}{1-\beta_k}} \; ; \quad \tilde{N}_{c_k} = \frac{1}{(1-\beta_k)\delta_k} \tag{3.3.36}$$

The number of cycles to failure for loading in one block is obtained by substitution of $\Delta N_k = N_{c_k}$, $D_{k-1} = D_o$ and $D_k = D_c$ into (3.3.36)

$$N_{c_k} = [D_c^{1-\beta_k} - D_o^{1-\beta_k}]\, \tilde{N}_{c_k} \; ; \tag{3.3.37}$$

Consider a loading in two blocks (k = 1, 2). The damage after $N = \Delta N_1 + \Delta N_2$ cycles is obtained as

$$D(N) = \left[\Delta N_2/\tilde{N}_{c_2} + \left[\Delta N_1/\tilde{N}_{c_1} + D_o^{1-\beta_1} \right]^{\frac{1-\beta_2}{1-\beta_1}} \right]^{\frac{1}{1-\beta_2}} \tag{3.3.38}$$

Application of the loading in reversed order, first block 2 and then block 1, yields

$$D(N) = \left[\Delta N_1/\tilde{N}_{c_1} + \left[\Delta N_2/\tilde{N}_{c_2} + D_o^{1-\beta_2} \right]^{\frac{1-\beta_1}{1-\beta_2}} \right]^{\frac{1}{1-\beta_1}} \tag{3.3.39}$$

If $\Delta N_1 = \Delta N_2$ the damage at $N = \Delta N_1 + \Delta N_2$ cycles will have different values for both loading regimes. Thus, the order in which the loading is applied influences the current state. If the parameter β does not depend on the loading ($\beta_1 = \beta_2$) the damage is given by

$$D(N) = \left[\Delta N_1/\tilde{N}_{c_1} + \Delta N_2/\tilde{N}_{c_2} + D_o^{1-\beta} \right]^{\frac{1}{1-\beta}} \tag{3.3.40}$$

If $\Delta N_1 = \Delta N_2$ identical final damage states are reached for both regimes. For loading in n blocks and constant β, it can readily be shown that (3.3.36) takes the form

$$D(N) = \left[\sum_{k=1}^{n} \Delta N_k/\tilde{N}_{c_k} + D_o^{1-\beta}\right]^{\frac{1}{1-\beta}} \tag{3.3.41}$$

Let the initial damage be given by $D_o = 0$ and the critical damage by $D_c = 1$. Then (3.3.41) reduces to

$$D(N) = \left[\sum_{k=1}^{n} \Delta N_k/N_{c_k}\right]^{\frac{1}{1-\beta}} \quad ; \quad \beta \in [0,1\rangle \tag{3.3.42}$$

It is noted that if $D_o = 0$, we must have $\beta \in [0,1\rangle$, since the left–hand side integral in (3.3.36) is divergent for $\beta \geq 1$. In literature the preceding equation is referred to as the modified Palmgren–Miner rule (Hwang 1986). If $\beta = 0$ (3.3.42) reduces to Palmgren–Miner's linear damage rule

$$D(N) = \sum_{k=1}^{n} \Delta N_k/N_{c_k} \quad ; \quad N_{c_k}^{-1} = \delta_k \tag{3.3.43}$$

Because this rule does not require extensive information about the particular material being considered, it has found a widespread application in modern engineering science.

3.4 Anisotropic damage

Introduction

In the previous section isotropic damage states were modeled using scalar quantities. In case of highly directional damage fields more accurate descriptions of the material behaviour are obtained by the introduction of vectorial or tensorial damage variables. The resulting anisotropic damage models can be used to study the constitutive behaviour of composite materials (Talreja 1985, Allen et al. 1987, Weitsman 1988b, Allix et al. 1987), concrete (Krajcinovic and Fonseka 1981, Simo and Ju 1987, Singh and Digby 1988) and metals (Murakami and Ohno 1981). At the present state of the development there is no concensus about the choice of a proper damage variable. On the one hand a damage variable should be capable of

describing the most salient features of damage, on the other hand experimental validation of the resulting models should be possible. Furthermore the numerical implementation should also be taken into account. Even though an anisotropic damage model is to be preferred to an isotropic model on physical grounds, the latter may have definite advantages with regard to the numerical solution process. Below, the damage formulation and the basic steps in the derivation of a theory for anisotropic damage are discussed.

Damage formulation

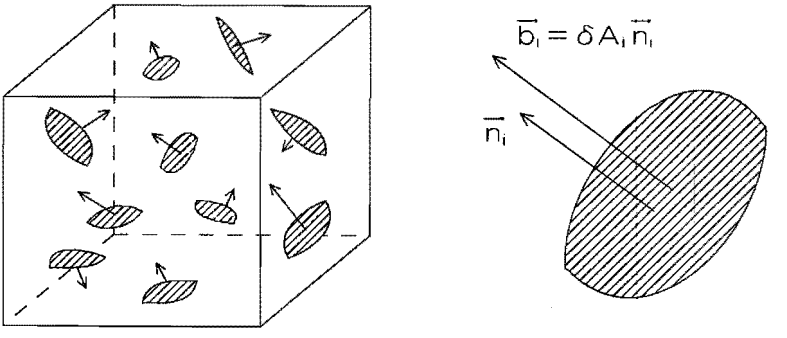

Figure 3.9 Vector representation of damage

Consider a representative volume element dV, situated around a point with momentary position vector $\vec{x}$ (Fig. 3.9). Let this volume contain m planar cracks. Each microdefect is characterized by a vector $\vec{b}_i(\vec{x}, t)$, $i = 1,...,m$, whose direction is perpendicular to the plane of the microdefect and whose magnitude is a function of the defect geometry. It is assumed that the effect of the defect geometry can be stored into a single parameter, the effective defect area δA_i:

$$\vec{b}_i(\vec{x}, t) = b_i \vec{n}_i \ ; \ b_i = b(\delta A_i) \tag{3.4.1}$$

where $\vec{n}_i$ is a unit vector normal to the ith defect. If n defect plane orientations in dV, each containing k_s cracks, can be distinguished, then for each orientation a vector $\vec{d}_s$ with $s = 1,...,n$ is defined such that

$$\vec{d}_s(\vec{x},t) = \sum_{i=1}^{k_s} \vec{b}_i = \vec{n}_s \sum_{i=1}^{k_s} b_i = d_s \vec{n}_s \tag{3.4.2}$$

Due to the paucity of detailed information regarding the exact size and location of the microdefects, it is proposed that $b_i = \delta A_i$. Consequently, the joint effect of the defects is accounted for by means of the sum of all effective defect areas contained in the defect plane, thus $d_s = \Sigma\ \delta A_i = \delta A_s$. From (3.4.2) it follows that $\vec{d}_s$ is not dimensionless. For infinitesimally small deformations, this measure can be nondimensionalized through division by a characteristic area δS, e.g. any one of the walls of the volume element (Weitsman 1988a,b), leading to

$$\vec{d}_s = \frac{\delta A_s}{\delta S}\,\vec{n}_s = \frac{\delta S - \delta A_e}{\delta S}\,\vec{n}_s = d_s\,\vec{n}_s \tag{3.4.3}$$

where δA_e is the effective load–carrying area associated with the direction of the normal $\vec{n}$. If δS is the surface of intersection in the RVE (Fig. 3.1), this expression is equivalent to the definition given in (3.2.1).

The vector $\vec{d}_s$ describing the defects in the deformed configuration is transformed to the vector $\vec{D}_s$, belonging to the reference configuration. Consider a defect plane, in which the effective defect area δA_s is spanned by two vectors $d\vec{x}$ and $d\vec{y}$. The following transformations must hold

$$\vec{d}_s = \delta S\,\vec{d}_s = \delta A_s\,\vec{n}_s = d\vec{x} * d\vec{y} = (\mathbf{F}\cdot d\vec{x}_o)*(\mathbf{F}\cdot d\vec{y}_o) = J\,\mathbf{F}^{-c}\cdot(d\vec{x}_o * d\vec{y}_o) \Rightarrow$$

$$\vec{d}_s = J\,\mathbf{F}^{-c}\cdot\frac{\delta A_{os}}{\delta S}\,\vec{N}_s = J\,\mathbf{F}^{-c}\cdot\vec{D}_s \tag{3.4.4}$$

In the sequel the joint effect of the microdefects in all planes in the volume element is accounted for by representing the damage as a summation of dyadic products

$$\mathbf{A} = \sum_{s=1}^{n} \mathbf{A}_s = \sum_{s=1}^{n} \vec{d}_s\vec{n}_s = J\,\mathbf{F}^{-c}\cdot\sum_{s=1}^{n} \vec{D}_s\vec{N}_s\cdot\mathbf{F}^{-1} \tag{3.4.5}$$

From (3.4.5) the following symmetric damage tensor can be derived

$$\mathbf{D} = J^{-1}\,\mathbf{F}^{c}\cdot\mathbf{A}\cdot\mathbf{F} = \sum_{s=1}^{n} \vec{D}_s\vec{N}_s \tag{3.4.6}$$

D is an invariant quantity, since it is not influenced by rigid body rotations.

In case of isotropically distributed damage consisting of microdefects of equal areas, (3.4.5) can be rewritten as

$$\mathbf{A} = \lim_{n\to\infty} \frac{1}{n} \sum_{s=1}^{n} \mathbf{A}_s = \lim_{n\to\infty} \frac{1}{n} \sum_{s=1}^{n} d\, \vec{n}_s \vec{n}_s = \frac{d}{3} \mathbf{I} \tag{3.4.7}$$

Hence, the damage tensor is no longer dependent on the direction of the normal $\vec{n}$ and the macrosymmetry of a material is not affected by homogeneously distributed microdefects. Since a vector representation does not satisfy this expectation, the dyadic representation is to be preferred.

Constitutive theory

For brittle damage and isothermal conditions, the independent variables are represented by the Green–Lagrange strain tensor $\mathbf{E}$, its material time derivative $\dot{\mathbf{E}}$ and the tensor $\mathbf{D}$. Using the principle of equipresence the dependent variables P, ψ and $\dot{\mathbf{D}}$ are functions of all independent variables

$$\mathbf{P} = \mathbf{P}(\underset{\sim}{\omega}) \;;\; \psi = \psi(\underset{\sim}{\omega}) \;;\; \dot{\mathbf{D}} = \dot{\mathbf{D}}(\underset{\sim}{\omega}) \;;\; \underset{\sim}{\omega}^{T} = \{\mathbf{E}, \dot{\mathbf{E}}, \mathbf{D}\} \tag{3.4.8}$$

Following the theory described in section 2.5 (see (2.5.8)–(2.5.11)), we obtain

$$\mathbf{P} = \rho_0 \frac{\partial \psi}{\partial \mathbf{E}} \;;\; \frac{\partial \psi}{\partial \dot{\mathbf{E}}} = \mathbf{0} \;;\; -\frac{\partial \psi}{\partial \mathbf{D}} : \dot{\mathbf{D}} = \mathbf{X} : \dot{\mathbf{D}} \geq 0 \tag{3.4.9}$$

where $\mathbf{X}$ is the irreversible generalized force associated with the flux $\dot{\mathbf{D}}$.

Inequality $(3.4.9)_3$ is satisfied if a potential ϕ exists, such that the damage evolution is given by

$$\dot{\mathbf{D}} = \nabla_{\mathbf{X}} \phi(\mathbf{X}, \underset{\sim}{\omega}) \tag{3.4.10}$$

where ϕ must possess a non–negative radial derivative and an absolute minimum at $\mathbf{X} = \mathbf{0}$. The damage criterion and the evolution equation can be established analogously to the procedure followed in sections 3.3.1 and 3.3.2. The existence of a reversible domain Ω in strain space is proposed, which can not be crossed. The damage state can only change for $\mathbf{E} \in \Gamma$ (Fig. 3.2). The domain and its boundary

can be defined by (3.3.5) and (3.3.6). Since the boundary Γ can not be crossed, the following damage consistency condition holds

$$g = \dot{g} = 0 \quad \Longrightarrow \quad \dot{\bar{\epsilon}} = \dot{\kappa} \tag{3.4.11}$$

In correspondence with (3.3.11) the evolution law is written as

$$\dot{\mathbf{D}} = \dot{\mu}\, \nabla_{\mathbf{X}} \tilde{\phi}(\mathbf{X}, \mathbf{E}, \mathbf{D}) \quad ; \quad \dot{\mu} \geq 0 \quad ; \quad \dot{\mu}\, g = 0 \tag{3.4.12}$$

where $\dot{\mu}$ is a scalar function that defines damage growth. If $g < 0$ the criterion (3.3.6) is not satisfied and hence $\dot{\mu} = 0$. If $g = 0$ damage growth may take place and using (3.3.12) the scalar function $\dot{\mu}$ is defined by

$$\dot{\mu} = \dot{\bar{\epsilon}} \tag{3.4.13}$$

Thus the evolution equation reads

$$\dot{\mathbf{D}} = \begin{cases} 0 & \text{if } \bar{\epsilon} < \kappa \\ \nabla_{\mathbf{X}} \tilde{\phi}\, (\mathbf{X}, \mathbf{E}, \mathbf{D})\, \dot{\bar{\epsilon}} & \text{if } \bar{\epsilon} = \kappa \end{cases} \tag{3.4.14}$$

The current damage surface follows from integration of (3.4.11).

The constitutive theory is completely defined by the stress–strain relation $(3.4.9)_1$, the consistency condition (3.4.11) and the evolution equation (3.4.14). In Appendix A the stress–strain relation is elaborated for isotropic material behaviour by expanding the dependent variables into Taylor series of scalar invariants of the independent variables. It is demonstrated, that even for a linear stress–strain relation extremely complex models are obtained, which require drastic simplifications to accomplish the model characterization.

4 A stochastic approach to damage modeling

4.1 Introduction

Due to the presence of flaws with unknown dimensions and positions, the strength and the lifetimes of solids act as statistical variables. In structural design the modeling of the scatter in strength and in fatigue data is carried out with so–called statistical strength theories (Weibull 1953, Cassenti 1984, Sheikh and Ahmad 1987). In these theories failure is commonly based on a weakest link assumption, which expresses that a structure will fail, if in some component a strength criterion is exceeded. Statistical strength theories have been implemented in finite element method codes for analyzing brittle failure mechanisms (Georgiadis 1984, Kam 1987, Van der Ven 1988).

In CDM the randomness in the damage state is neglected by assuming that initially a material is in a perfect state, which results in a deterministic analysis. In this chapter the probabilistic aspects of failure processes are taken into account by considering damage as a stochastic quantity. The theory will be applied to fatigue. The characterization of the model parameters in the evolution law is discussed in section 4.2. For this purpose it is hypothesized that microcrack growth and macrocrack growth can be described by identical relationships. Hence, the concepts of classical fracture mechanics can be applied on a microstructural level. The effects of the cracks on the stress–strain relation are expressed by a scalar damage variable. Combining this relationship with concepts from fracture mechanics, a damage evolution law is obtained, which is a particularization of the form that was derived in section 3.3.3. The parameters in this law are explicit functions of constants that emanate from fracture mechanics.

In section 4.3 a model is developed for characterizing the statistical distribution of the initial damage. For this purpose a solid is divided into cells, that contain random intrinsic damage. If the loading of the solid is globally homogeneous, its durability is limited by the largest initial damage of all cells. This maximum damage also is a random variable, whose distribution can be determined from the statistics of the damage in a single cell. Using experimental data, the best–fit values for the cell dimensions, the so–called elementary cell (EC), and the parameters in the damage distribution are obtained. The EC can be related to the scale at which micrographic damage measurements should be done. Additionally, in chapter 6 it will be demonstrated that in the numerical field, where CDM is used to

analyze the initiation and growth of macrocracks, the dependence of the mesh on the results is reduced by the introduction of the EC.

Once the probability distribution of the initial damage and the evolution equation have been established, the damage state can be computed. The integration of the evolution equation can be performed either numerically with simulation techniques or analytically in case of uncoupled constitutive equations. The fatigue lifetime distribution of an elastomeric biomaterial (Biomer) is derived in section 4.4. The resulting distributions are compared with test data reported in literature. In section 4.5 fatigue in polystyrene (PS) is discussed. In contrast with Biomer, the observable phenomena in PS under static and dynamic loadings are different. This necessitates different approaches for characterizing damage. Finally, the damage growth according to the developed model is compared with optical measurements.

4.2 Application of fracture mechanics in CDM

Brittle fracture

With regard to the establishment of the damage evolution equation, some concepts of classical fracture mechanics will be discussed in this section. Classical fracture mechanics is concerned with the growth of cracks from pre–existing flaws in brittle solids. These flaws could be either scratches or cracks which both have the effect of causing a stress concentration. This means that the local stress in the vicinity of the crack tip is higher than that applied to the body as a whole.

The starting point in classical fracture mechanics is the energy balance criterion of Griffith (1920). According to this hypothesis a crack in a stressed elastic and infinitely extended body will increase if the loss of elastically stored energy occasioned by such growth exceeds the surface energy of the freshly created crack surface. The hypothesis can be stated quantitatively in the following terms

$$-\frac{\partial U}{\partial A} \geq S \tag{4.2.1}$$

where U is the total elastically stored energy in the specimen, A is the interfacial crack area and S is the surface energy. For a linear elastic material it is possible to evaluate the left–hand side of (4.2.1) by integration of the strain energy over the whole specimen containing the crack. In case of an elliptical crack of length 2Q in an infinitely extended plate, loaded at infinity by a stress σ_0 in the direction perpendicular to the direction of the crack, the Griffith criterion predicts that no

growth of the crack can occur under conditions where

$$\pi \sigma_0^2 Q/E < 2S \tag{4.2.2}$$

It is noted that once the crack begins to grow, the stress necessary to maintain growth is continually reduced. Under constant stress, therefore, catastrophic propagation should ensue.

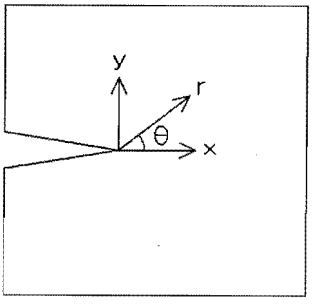

Figure 4.1 Crack tip

The theory of brittle fracture provides a good qualitative description of the fracture behaviour of brittle polymers such as PS and PMMA. However, the measured values of S are much larger than the theoretical surface energies. This discrepancy arises because the Griffith approach assumes that the material does not undergo plastic deformation. It is known that even if a material appears to behave in a brittle manner there is invariably a small amount of plastic deformation at the tip of the crack. The energy absorbed during plastic deformation is much higher than the theoretical surface energy. Therefore, the term 2S in (4.2.2) is replaced with G_c, which represents the total work of fracture. Thus, a crack will start to grow in an unstable manner when

$$\sigma_0^2 \pi Q = E G_c \tag{4.2.3}$$

Linear elastic fracture mechanics

LEFM considers the fracture condition in relation to the geometry of a crack. In LEFM three different modes of near crack tip deformation can be distinguished, mode I: opening, mode II: in–plane sliding (shear), mode III: antiplane sliding

(tearing). In the sequel we are concerned only with mode I loading, which is by far the most important case in practice. The stress distribution at the tip of the crack, i.e. for $r \to 0$ in an infinite plate, is given by

$$\sigma_{ij} = \sigma_o \sqrt{Q/2r}\, p_{ij}(\theta) = \frac{K_I}{\sqrt{2\pi r}}\, p_{ij}(\theta) \tag{4.2.4}$$

where K_I is known as the mode I stress intensity factor (SIF), which is a parameter that determines the height of the stress distribution ahead of the crack tip. For brevity the subscript in the SIF will be omitted. The function p_{ij} is independent of the geometry of the cracked body. Hence, the crack tip stresses and the deformation fields are fully determined by the SIF. For bi–axial stress conditions (4.2.4) takes the form (Broek 1986)

$$\begin{Bmatrix} \sigma_{11} \\ \sigma_{21} \\ \sigma_{22} \end{Bmatrix} = \frac{K}{\sqrt{2\pi r}} \cos(\theta/2) \begin{Bmatrix} 1-\sin(\theta/2)\sin(3\theta/2) \\ \sin(\theta/2)\cos(3\theta/2) \\ 1+\sin(\theta/2)\sin(3\theta/2) \end{Bmatrix} \tag{4.2.5}$$

In LEFM two cracks are supposed to behave identically if they have the same SIF. It is convenient to express the fracture conditions in terms of a critical value of the SIF. Thus, sudden crack growth occurs when $K = K_c$, where the critical value K_c is considered as a material constant. The constraints imposed by the edges in a finite specimen will actually make the value of the SIF larger than is predicted from the infinite plate assumption. Then K is a function of the ratio Q/W, where W is the width of the plate. It is customary to write the definition of K in the form

$$K = Y\sigma_o\sqrt{Q} \tag{4.2.6}$$

where $Y = f(Q/W)$, so that $Y = \sqrt{\pi}$ for $Q/W \to 0$. The values of the shape factor Y can be obtained either experimentally or by means of stress analysis. The LEFM solutions predict infinite stresses at the crack tip. Since real materials yield at finite stresses, the LEFM solutions loose their validity in the immediate vicinity of the crack tip. However, the basic assumptions of fracture mechanics remain valid, if yielding is confined to a very small plastic zone at the crack tip surrounded by an elastic region in which the stress field is governed by eq. (4.2.4).

In fracture mechanics fatigue crack growth is described by the empirical Paris law (Williams 1984)

$$\frac{dQ}{dN} = a(\Delta K)^b \tag{4.2.7}$$

where $\Delta K = K_{max} - K_{min}$ is the SIF range and a and b are material constants.

Damage evolution equation

The evolution equation (3.3.33) contains three parameters. With respect to the characterization of these parameters it is hypothesized that microdefect growth and macrocrack growth can be represented by identical relationships. Consequently, the theory of fracture mechanics can be applied to describe microdefect growth and possibly damage growth, if a relation between the damage variable and the microcrack configuration is available. Several reasons in support of this assumption can be given.

- Due to the localization of damage the conventional experimental methods, which measure variations in global material properties, are not suited.
- Measurements are disturbed by the uncertainty in the initial damage state.
- The resulting model forms a particularization of eq. (3.3.33). The model parameters are explicit functions of the constants in the Paris law, such that the model characterization becomes a straightforward task.
- Andrews (1969) succesfully applied this assumption to microcrack growth in polymers.
- In sections 4.4. and 4.5 its validity is demonstrated for real materials.
- From optical measurements an identical damage evolution is observed (see section 4.5).

Next, the relation between the damage variable and the microdefect configuration is discussed. For specimens containing microcracks, the stress–strain relation is influenced, resulting in a stiffness reduction in comparison with a virgin specimen. Effective field theories have been developed to determine the dependence of the crack density and the crack geometry on the mechanical behaviour (Budianski 1976, Horii 1983, Laws 1987). For a small density of isotropically distributed microcracks, the SIF and displacement jumps of each crack are given accurately by those of one crack in an infinite medium. In case of an array of m randomly oriented cracks of constant length 2Q in the surface element δS, and considering plane loading conditions, the material deterioration is expressed as (Budianski 1976)

$$D = \frac{m\pi Q^2}{\delta S} \tag{4.2.8}$$

For the procedure to be employed, the damage variable is written as

$$D = 1 - \delta S_e/\delta S = c^2/\delta S \leq D_c \tag{4.2.9}$$

where an equivalent crack length c is introduced, which must be thought of as the crack that has the same effect as the ensemble of smaller cracks within the surface element δS. Using (4.2.8) and (4.2.9) the effective defect size for cracks of constant length 2Q must necessarily be given by

$$c = \sqrt{\pi m}\, Q \tag{4.2.10}$$

Using (4.2.7) to predict the microdefect growth in a surface element δS together with (4.2.9), the damage evolution becomes

$$\frac{dD}{dN} = 2\sqrt{\frac{D}{\delta S}}\, a(\Delta K)^b \tag{4.2.11}$$

In sections 4.4. and 4.5 it is demonstrated that elaboration of this equation leads to particularizations of the damage growth equation (3.3.33). The evolution equation actually is an initial value problem requiring an initial value. Next, attention is given to the characterization of the initial damage.

4.3 The stochastic nature of damage

A characteristic of fatigue failure processes is that a scattering in lifetimes will be observed for identically shaped materials under identical loading conditions. This phenomenon is caused by different initial damage states, i.e. the exact positions and dimensions of microdefects in the material are unknown. The resulting stochastic failure processes can be modeled by considering the damage and consequently the effective defect size as stochastic variables. In the following a model is developed for determining the corresponding probability distribution functions. In order to distinguish between deterministic variables and stochastic variables, the latter are marked with an underscore. Consider a body that is divided into n cells with surface δS_i (i = 1,2,...,n). According to eq. (4.2.9) the relation between the damage and the effective defect size in cell i is written as

$$D_i = D(c_i) = c_i^2/\delta S_i \leq D_c \tag{4.3.1}$$

In a globally homogeneous stress field failure is initiated in the cell with the largest initial defect size. The magnitude of the largest defect size is a stochastic variable as well, which is denoted as $\underline{c}_m$. The cumulative distribution function (CDF) of the maximum defect size is expressed in terms of those of the $\underline{c}_i$ by realizing that

$$F_{\underline{c}_m}(c) \equiv P(\underline{c}_m \leq c) = P\{(\underline{c}_1 \leq c) \cap \ldots \cap (\underline{c}_n \leq c)\} \tag{4.3.2}$$

If the defect sizes are independent (4.3.2) can be written as

$$F_{\underline{c}_m}(c) = P(\underline{c}_1 \leq c)P(\underline{c}_2 \leq c)\ldots P(\underline{c}_n \leq c) = \prod_{i=1}^{n} F_{\underline{c}_i} \tag{4.3.3}$$

If all the $\underline{c}_i$ are identically distributed, the CDF of the defect size in a cell with area δS_i is given by

$$F_{\underline{c}_i}(c) = F_{\underline{c}}(c;\, \delta S_i) = \int_0^c f_{\underline{c}}(c;\, \delta S_i)\, dc \tag{4.3.4}$$

where $f_{\underline{c}}$ is the probability distribution function (PDF) of each of the c_i. The cell surface δS_i acts as a parameter in the PDF. If, in addition, the body consists of n equally sized cells, (4.3.3) reduces to

$$F_{\underline{c}_m}(c) = [F_{\underline{c}}(c)]^n \tag{4.3.5}$$

In this expression $F_{\underline{c}}$ is referred to as the parent distribution and $F_{\underline{c}_m}$ is the maximum extreme–value distribution of the effective defect sizes (Augusti 1984). The PDF of $\underline{c}_m$ is obtained by differentiating (4.3.5) with respect to c

$$f_{\underline{c}_m}(c) = n[F_{\underline{c}}(c)]^{n-1} f_{\underline{c}}(c) \tag{4.3.6}$$

The PDF of $\underline{D}$ is determined by the following transformation

$$f_{\underline{D}}(D) = f_{\underline{c}}(c) \left| \frac{dc}{dD} \right| \tag{4.3.7}$$

Combining (4.3.7) and (4.3.6) the PDF of the maximum damage in a body of n cells

is given by

$$f_{\underline{D}_m}(D) = n[F_{\underline{c}}(c)]^{n-1} f_{\underline{c}}(c) \left|\frac{dc}{dD}\right| \tag{4.3.8}$$

Let the PDF of the damage in a cell be distributed exponentially

$$f_{\underline{D}}(D;\ \lambda) = \lambda exp(-\lambda D) \tag{4.3.9}$$

This choice is a particularization of the parent distribution function for a so–called Gumbel or type I maximum extreme value distribution (Lewis 1987), which results from letting n in (4.3.6) become large. Using (4.3.9), (4.3.1) and (4.3.7), we obtain

$$f_{\underline{c}}(c;\ \lambda,\delta S) = (2c\lambda/\delta S)exp(-\lambda c^2/\delta S) \tag{4.3.10}$$

From (4.3.4) it follows that the CDF of the defect size is given by

$$F_{\underline{c}}(c;\ \lambda,\delta S) = 1 - exp(-\lambda c^2/\delta S) \tag{4.3.11}$$

After substitution of (4.3.10) and (4.3.11) into (4.3.6) the PDF for the maximum defect size distribution in a body containing n cells is given by

$$f_{\underline{c}_m}(c;\ \lambda,\ \delta S) = 2nc\lambda\delta S^{-1}exp(-\lambda c^2/\delta S) *$$

$$[1 - exp(-\lambda c^2/\delta S)]^{n-1}\ ;\ n = A/\delta S \tag{4.3.12}$$

where A is the specimen area. Using (4.3.8) and (4.3.9) the PDF of the maximum damage in a specimen is obtained as

$$f_{\underline{D}_m}(D;\ \lambda,n) = n\lambda exp(-\lambda D)[1 - exp(-\lambda D)]^{n-1} \tag{4.3.13}$$

The PDF (4.3.12) contains two unknown model parameters $\{\lambda,\ \delta S\}$, which need to be determined from experimental observations. Suppose an experimental distribution $\hat{f}$ is available, then the best–fit parameters $\lambda = \hat{\lambda}$ and $\delta S = A_{ec}$ are

obtained by minimizing the merit function

$$R = \sum_{i=1}^{s} \left| f_{c_m}(c_i;\ \delta S, \lambda) - \hat{f}(c_i) \right|^2 \tag{4.3.14}$$

that measures the agreement between the experimental frequency distribution $\hat{f}$ and the theoretical PDF. The best–fit parameter A_{ec} is referred to as the elementary cell (EC) size. The minimization is carried out with a Levenberg–Marquardt algorithm for nonlinear optimization problems (Press et al. 1986).

The derivation of the experimental frequency distribution for the maximum defect size is feasible only if the material shows localized failure under both static and dynamic loadings. For rubbery materials this condition holds. For glassy polymers, however, significant discrepancies between the failure processes under static and dynamic loadings may arise. For example, PS under static loadings exhibits a global decrease in rigidity (see Fig. 3.5), whereas in fatigue processes localized failure occurs. Under these circumstances the minimization procedure should be applied to lifetime distributions. Both procedures will be discussed in the next sections.

4.4 Fatigue in rubbers

Initial damage distribution

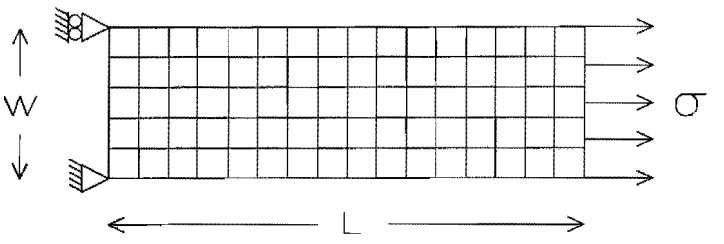

Figure 4.2 Testing specimen divided into n cells with area δS

In this section fatigue mechanisms in rubbers are discussed. Rubbers are highly flexible crosslinked networks. In common with other crosslinked polymers rubbers fracture in a brittle manner in the sense that any plastic flow is very local, but this is accompanied by large elastic deformations (Young 1983). Rubbers exhibit localized failure under both static and dynamic loadings. Then static tests can be

carried out to derive the experimental distribution of the maximum defect size in the specimen.

The experimental CDF of the maximum defect size follows from the fact that for any perfectly brittle material the breaking strength is controlled by the size of the defects present in the structure. The strength of a body can be increased by reducing the size of these defects. The reduction of the size of artificially induced cracks clearly also causes an increase in the strength of materials. When the crack size is reduced below a critical level, the breaking strength shows no further increase. The materials therefore behave as if they contain natural defects of these critical sizes. Two tests are required for the derivation of the experimental CDF.

1 A test, in which the distribution of the breaking strength g_σ in a population of virgin specimens is determined. To apply the theory of section 4.3 this test must be carried out under homogeneous loading conditions (Fig. 4.2).
2 A test, in which a relation between the breaking strength σ_b and the maximum effective defect size c_m is determined by varying the size of artificially induced cracks.

Combining the results of both tests, the experimental distribution of the maximum defect size in a specimen is expressed as

$$\hat{f}_{\underline{c}_m}(c_m) = g_{\underline{\sigma}}(\sigma_b) \left|\frac{d\sigma_b}{dc_m}\right| \tag{4.4.1}$$

An experimental maximum initial defect size distribution was obtained for the biomaterial biomer by Gadkaree and Kardos (1984). The specimen dimensions were L = 25.4 mm and W = 6.6 mm (Fig. 4.2). The specimen strength was described by a normal distribution with mean $\mu = 41.12$ Nmm^{-2} and standard deviation $s = 1.393$ Nmm^{-2}. The results of the second test are depicted in Fig. 4.3. The model distribution (4.3.12) was used to fit the experimental distribution. The best–fit model parameters were obtained as $\hat{\lambda} = 437.8$ and $A_{ec} = .385$ mm^2. The (parent) distribution of the initial defect size in an EC (4.3.10) and the maximum initial defect size distribution (4.3.12) are plotted in Fig. 4.4. The effect of the cell area on the damage state is demonstrated in Fig. 4.5, where the PDF of the maximum damage in a cell with dimensions kA_{ec} ($k = 1,2,...,\hat{n} = A/A_{ec} = 436$) is plotted for five distinct values of k. The values k = 1 and k = 436 correspond to the parent and the extreme value distribution in Fig. 4.4. It is noted that the dimensions of an EC are within the scale for a representative volume element (RVE), which for polymers ranges from 0.1 mm to 1 mm. Up to the present the scale of an RVE was

determined through micrographic measurements, which may lead to ambiguous results. The developed procedure can be used to compute the dimensions of an RVE, which might solve the question of scale as discussed by Lemaitre (1987).

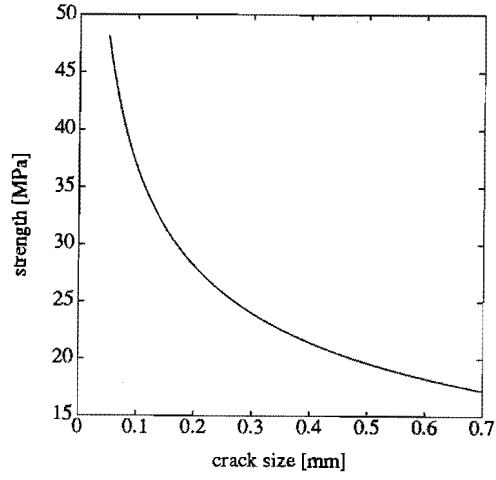

Figure 4.3 Breaking strength vs crack length from Gadkaree and Kardos (1984)

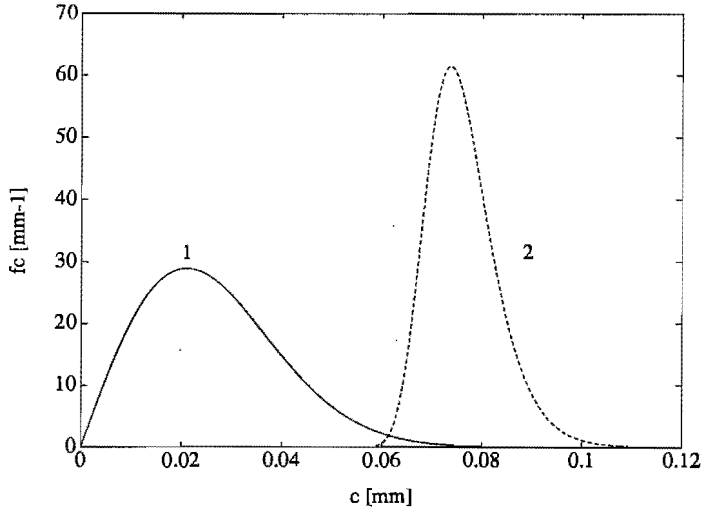

Figure 4.4 Parent PDF (curve 1) and extreme value PDF (curve 2) of initial defect sizes in Biomer

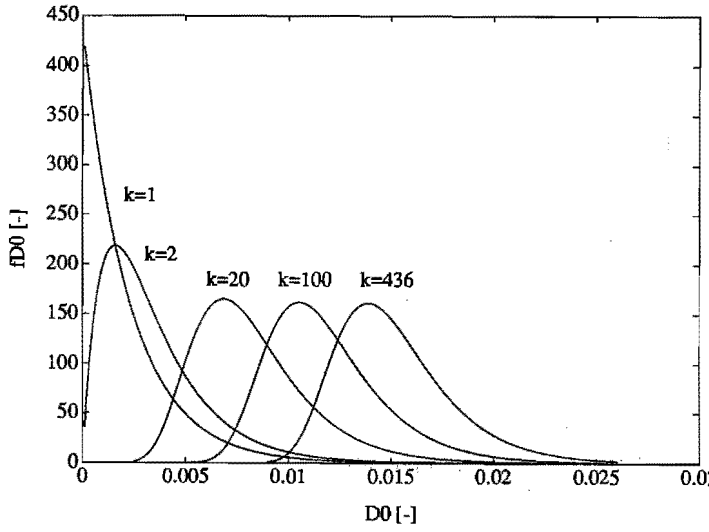

Figure 4.5 PDF of damage for different cell dimensions kA_{ec}

Failure of the specimen in Fig. 4.2 occurs, if the damage reaches a critical value D_c in one of the cells. Two failure definitions, which only differ in the choice of the cell size, are studied for both coupled and uncoupled constitutive equations.

(1) Failure occurs if the damage in an EC reaches a critical value, thus $\delta S = A_{ec}$.

(2) Failure occurs if the damage in a strip with dimensions $W*\sqrt{A_{ec}}$ (Fig. 4.2) has reached a critical value. This event corresponds to total rupture. Under these circumstances the Marquardt minimization is performed with a fixed cell size $\delta S = W\sqrt{A_{ec}}$, yielding $\hat{\lambda} = 2920$.

Damage evolution law

Because Griffith's criterion for crack propagation assumes linear elasticity, it can not be directly applied to materials which display large strains and nonlinear stress–strain behaviour. The so–called tearing energy approach, which has been worked out by Rivlin and Thomas (1953), gives a result more general than, but inclusive of, the Griffith criterion. It is still limited to elastic materials, but requires neither linearity nor small strains. For elastomeric materials the Paris law for fatigue crack growth is expressed as

$$\frac{dc}{dN} = a(\Delta T)^b \tag{4.4.2}$$

where a and b are crack growth constants and ΔT is the range of the tearing energy in a cycle. In what follows the minimum tearing energy is taken zero, i.e. loading between $\epsilon_l = 0$ and $\epsilon_m = \epsilon$. Following Gadkaree and Kardos (1984) the tearing energy for a crack in a specimen under uni–axial tension is taken as

$$T = 2B\, c\, \psi^o(\epsilon) \tag{4.4.3}$$

where ψ^o is the elastic potential of the undamaged material and B is a slowly varying function of strain, decreasing from its classical value of π at infinitesimal strains to a value around unity at very large extensions (Williams 1984). Using (4.2.9) and (4.4.3), the crack growth law (4.4.2) can be transformed to

$$\frac{dD}{dN} = p\, \psi^o(\epsilon)^b\, D^\beta \tag{4.4.4}$$

where $\beta = \frac{1}{2}(b+1)$ and $p = 2^{b+1} a\, B^b\, \delta S^{\beta-1}$.
The constitutive equation for the damaged material is expressed as (see (3.3.19))

$$\sigma = (1-D)\,\hat{\sigma} \quad ; \quad \hat{\sigma} = \frac{\partial \psi^o}{\partial \epsilon} = e\, \epsilon^m \tag{4.4.5}$$

where ϵ is the natural (logarithmic) strain and e and m are material constants.
Using (4.4.5) the evolution law is expressed as

$$\frac{dD}{dN} = \frac{\alpha}{\omega} D^\beta\, \epsilon^\omega = \frac{\eta D^\beta}{(1-D)^\omega} \tag{4.4.6}$$

$$\omega = \frac{b(m+1)}{m} \quad ; \quad \eta = p\left[\frac{e}{m+1}\right]^b \left[\frac{\sigma}{e}\right]^\omega$$

This evolution law is a particularization of eq. (3.3.33). The parameters β, η and ω are given explicitly in terms of the constants a, b in the Paris law and e, m in the free energy potential. The data for Biomer are given in table 4.1 (data in first column from Gadkaree and Kardos 1984).

Tests were performed at $\sigma = 10.89$ Nmm^{-2}, thus $\eta = 0.1$ for failure according to definition (1) and $\eta = 0.768$ for failure according to definition (2). It is remarked that with the evolution law and the initial damage distribution, all ingredients for the computation of lifetime distributions are available.

Table 4.1 Data for Biomer

$B = 1.6$	$\delta S = .385\ \mathrm{mm}^2$
$e = 11.1\ \mathrm{Nmm}^{-2}$	$\lambda = 437.8$
$m = 1.54$	$\beta = 1.75$
$b = 2.5$	$\omega = 4.123$
$a = 1.97 \cdot 10^{-4}\ \mathrm{N}^{-2.5}\mathrm{mm}^{-3.5}$	

Results

In what follows, the lifetime distribution of a population of Biomer specimens is determined. The CDF of the number of cycles to failure is defined as

$$F_{\underline{N}_c}(N_c) \equiv 1 - R(N_c) = \int_0^{N_c} f_{\underline{N}_c}(N)\, dN \tag{4.4.7}$$

where R is called the reliability. If the damage growth is described by the nonlinear differential equation (4.4.6), i.e. the constitutive equations are coupled, the lifetime distribution must be computed with simulation techniques. The solution process then consists of performing a series of numerical experiments. In each experiment a realization of the intrinsic damage is chosen as an input quantity. Then the damage is computed by a deterministic analysis. Finally, the lifetime distribution is obtained from the total of responses.

Using the data in table 4.1, eq. (4.4.6) is solved for three different maximum stresses with initial value $D_o = 1.46 \cdot 10^{-3}$ (see Fig. 4.6). The results confirm that it is extremely difficult to characterize the damage through variations in global material properties. Furthermore, the dominant role of the stresses in the failure process is demonstrated.

An analytical solution for the lifetime distribution can be derived, if the constitutive equations are uncoupled. In this case we have an explicit relation between the number of cycles to failure and the intrinsic damage $N_c = N_c(D_o)$. Hence, the PDF for the number of cycles to failure is given by

$$f_{\underline{N}_c}(N_c) = f_{\underline{D}_m}(D_o(N_c)) \left|\frac{dD_o}{dN_c}\right| \tag{4.4.8}$$

Using (4.3.13) and (4.4.8), (4.4.7) reads

$$F_{\underline{N}_c}(N_c) = \int_{D_0(N_c)}^{D_c} f_{\underline{D}_m}(D_0)\, dD_0$$

$$= [1 - exp(-\lambda D_c)]^n - [1 - exp(-\lambda D_0)]^n \tag{4.4.9}$$

Using (3.3.37) and $exp(-\lambda D_c) << 1$, (4.4.9) reduces to

$$F_{\underline{N}_c}(N_c) = 1 - \left[1 - exp\left[-\lambda[\, D_c^{1-\beta} - (1-\beta)\delta\, N_c]^{\frac{1}{1-\beta}}\right]\right]^n \tag{4.4.10}$$

The uncoupling is advantageous, since no computational effort has to be put in performing numerical experiments. However, the main benefit of this approach is that the derived lifetime distributions can be used in the characterization of the parameters in the damage distributions. The uncoupling is required if static loadings display nonlocal damaging. Therefore, it will be adopted in the next section, which deals with fatigue processes in polystyrene.

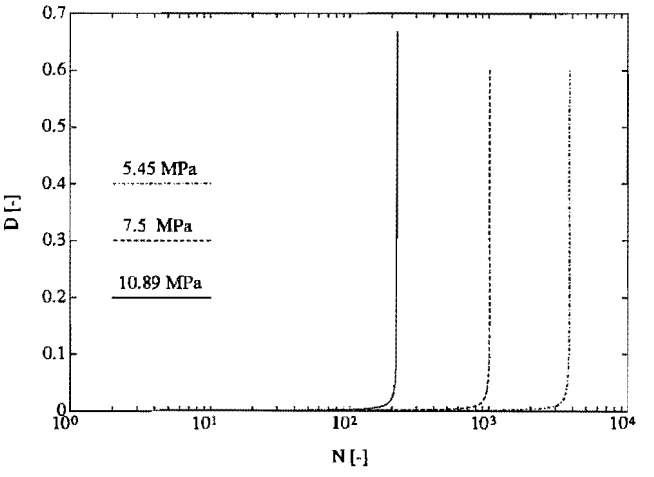

Figure 4.6 D as a function of N

Four situations were studied: failure according to definition (1) and (2) using either coupled or uncoupled equations. The CDF of the number of cycles to failure

for the coupled equations is calculated by performing 50 numerical experiments. The resulting lifetimes are fitted to a two–parameter Weibull distribution

$$F_{\underline{N}_c}(N_c) = 1 - exp\left[-\left[\frac{N_c}{N_o}\right]^v\right] \tag{4.4.11}$$

It is found that $v = 6.1$ and $N_o = 193$ for definition (1) and $v = 4.9$ and $N_o = 254$ for definition (2). The CDF for the uncoupled equations is given by eq. (4.4.10). The CDF's are depicted in Fig. 4.7. The results are compared with data from tensile fatigue experiments on Biomer specimens (Gadkaree and Kardos 1984). In these experiments 10 virgin specimens were loaded sinusoidally at a frequency of 0.1 Hz between 0 and 10.89 MPa, yielding curve 1 in Fig 4.7. It may be stated, that for failure according to definition (2) the CDF of the uncoupled constitutive equations shows only slight deviations from the CDF of the coupled constitutive equations, whereas for failure according to definition (1) larger deviations are observed. Besides, the conservative estimate of the lifetime distribution is improved by the uncoupling.

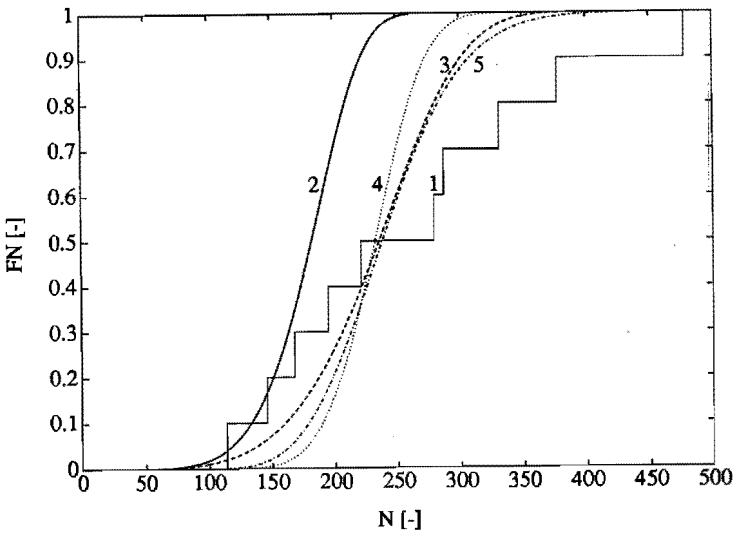

Figure 4.7 Lifetime distributions ; curve 1, experimental (Gadkaree and Kardos 1984) ; curve 2 coupled eq., def. (1) ; curve 3 coupled eq., def. (2); curve 4 uncoupled eq., def. (1) ; curve 5 uncoupled eq., def. (2)

A Kolmogorov–Smirnov test of goodness of fit (Augusti et al. 1984) is used to investigate whether the lifetime distributions (4.4.10) and (4.4.11) are capable of predicting the experimental distribution. To apply the test, the experimental CDF as well as the theoretical CDF must be evaluated for each distinct observation. The distribution Q of the maximum value of the absolute differences Δ between the two distributions is calculated giving the significance of any observed non–zero value of Δ. Considering the curves 1 and 3 we compute $\Delta = 0.2$ at $N_c = 279$. For $n = 10$ the significance level is $P(\underline{\Delta} < 0.2) = Q(\sqrt{10} \cdot 0.2) = 0.82$ (see Appendix B). Since the significance level is sufficiently large, there is no reason to reject the hypothesis that CDF (4.4.11) does describe the lifetime distribution. Similar tests can be performed on the curves 2, 4 and 5.

4.5 Fatigue in glassy polymers

Damage phenomena

In this section the fatigue behaviour of polystyrene (PS) will be investigated. The fatigue phenomena in PS are illustrated with experiments conducted by McMaster et al. (1974). The testing specimens were cylindrical and had a reduced diameter section. The tests were conducted in reversed tension–compression at 26 Hz. At this frequency the specimens could be tested without excessive heating. A typical fatigue fracture surface is sketched in Fig. 4.8. There are four distinct regions visible. Region R1, a region of slow stable crack growth, is a small, more or less semi–circular area surrounding the fracture source, generally a surface defect. Region R2, is a smooth region of increasing crack velocity. As the crack advances, the average stress rises and many crazes occur ahead of the crack tip, resulting in the much rougher zone R3. The line of demarcation between R3 and R4 represents the furthest penetration of the fatigue crack before catastrophic failure occurs.

In section 4.4 the experimental initial defect size distribution was derived from static experiments. This procedure worked because rubbers under static or dynamic loadings show localized damaging. For PS specimens in static tension tests, there is an extensive crazing over the entire specimen prior to fracture (Sauer and Richardson 1980). Phenomenologically the damaging of PS specimens under static tensile loads results in a global stiffness reduction (see Fig. 3.5), which is in contradiction with the local damage processes in fatigue. For this reason the PDF of the maximum initial damage can not be determined by performing static tests as was discussed in the previous section. In this section a different approach is applied.

In general, it is required to settle on an expression in which the parameters characteristic for the initial damage distribution occur. Such an expression is provided by eq. (4.4.10). It is noted that this CDF is valid for uncoupled constitutive equations. Using this expression in combination with data on lifetimes, a minimization procedure can be carried out to obtain the best–fit parameters. Choosing $D_c = 1$, the CDF contains four model parameters λ, n, β and δ. The parameters λ and n originate from the initial damage distribution and β and δ originate from the evolution law (3.3.33). Before computing the initial damage distribution, the parameters β and δ must be characterized.

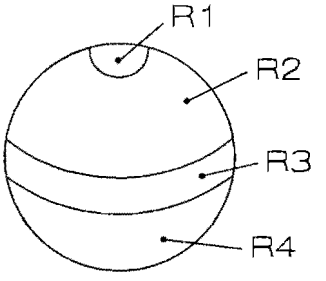

Figure 4.8 Fatigue fracture surface of PS specimen

Damage evolution law

The fatigue life of glassy polymers is controlled by the events leading to crack initiation and by the fatigue crack propagation in region R1. In fact the number of cycles spent in regions R2 to R4 amounts to a small fraction of the total life. The fracture source, which is situated at the specimen surface, can be modeled as an elliptical surface crack. In this case the mode I SIF is given by (Williams 1984)

$$K = \frac{\sigma\sqrt{\pi}}{E_2}\,(c^2\cos^2\varphi + q^2\sin^2\varphi)^{\frac{1}{4}}\sqrt{c/q} \tag{4.5.1}$$

$$E_2 = \int_0^{\frac{\pi}{2}} [1 - (1 - \frac{c^2}{q^2})\sin^2\phi]^{\frac{1}{2}}\, d\phi \tag{4.5.2}$$

where c and q are the minor and major axes of the ellipse and φ is a parametric angle, which is related to the real angle θ by $\tan\theta = (c/q)\tan\varphi$ (see Fig. 4.1). For

reasons of simplicity semi–circular cracks ($c/q = 1$) are considered, thus (4.5.1) takes the form

$$K = 2\sigma\sqrt{c/\pi} \tag{4.5.3}$$

Since the crack size c is many times smaller than the specimen diameter, the SIF will approach the value predicted by (4.5.3). Substitution of (4.5.3) into (4.2.11) yields the damage evolution for loading between $\sigma_l = 0$ and $\sigma_m = \sigma$

$$\frac{dD}{dN} = \tilde{\delta}\, D^{\beta}\, \sigma^{b} \;\; ; \;\; \beta = \tfrac{1}{4}b + \tfrac{1}{2} \;\; ; \;\; \tilde{\delta} = 2^{b+1}\, \pi^{-\frac{b}{2}}\, a\, \delta S^{\beta-1} \tag{4.5.4}$$

As this relation is a particularization of evolution equation (3.3.33), the parameters in the evolution law have become explicit functions of the constants in the Paris law, which for PS specimens, loaded at a frequency of 10 Hz, were determined by Skibo (1976) (see table 4.2).

Table 4.2 Data for Polystyrene

$A_{ec} = 30.21\ mm^2$	$b = 3.6$
$\lambda = 96311$	$h = 0.42$
$\mu_D = 2.65 \cdot 10^{-5}$	$\sigma_f = 0$
$a = 1.347 \cdot 10^{-8}\ N^{-3.6} mm^{-4.6}$	

Initial damage distribution

The maximum initial damage distribution is derived by dividing the testing specimen into cylindrical cells, which contain random surface defects. If the initial damage in one cell is distributed exponentially, the maximum initial defect size distribution is given by (4.3.12), whence the CDF for the lifetime is given by (4.4.10). The experimental lifetime distribution was obtained from Sauer et al. (1976). Now that we have disposal of an experimental lifetime distribution and a model distribution function, the minimization procedure can be carried out. For loadings ranging from $\sigma_m = 34.4$ MPa to $\sigma_l = 0$ the best–fit model parameters are

derived as $\hat{\lambda} = 96311$ and $\hat{n} = 6.708$. In Fig. 4.9 the parent distribution of the initial defect size (4.3.9) together with the maximum initial defect size distribution (4.3.12) are shown. The mean maximum defect size is $\mu_c = 2.83 \cdot 10^{-2}$ mm and the corresponding mean value of the maximum damage is given in table 4.2. This defect size agrees well with the maximum intrinsic defect size in a kindred glassy polymer PMMA, which was estimated to range between $3–3.5 \cdot 10^{-2}$ mm (Andrews 1969).

In order to investigate the magnitude of intrinsic defects in PS, artificial defects of various depth were made in the specimens by McMaster et al. (1974). The specimens were tested in reversed tension–compression at a stress ranging from –17.2 MPa to 17.2 MPa. Below a certain threshold defect size, i.e. the maximum initial defect size, no further increase in lifetime was possible. This threshold defect size corresponds to the mean defect size in unnotched specimens. McMaster et al. (1974) found $\mu_c = 0.021$ mm, which agrees well with the initial defect size that was derived from the minimization procedure.

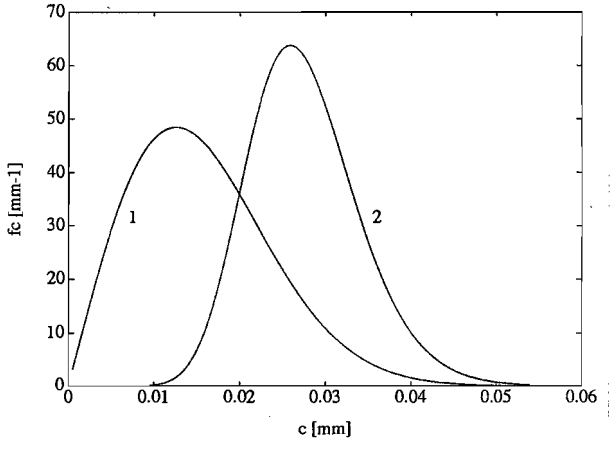

Figure 4.9 Parent PDF (curve 1) and extreme value PDF (curve 2) of initial defect sizes in PS

Effects of mean stress

The influence of the mean stress $\sigma_{mean} = {}^1/_2(\sigma_m + \sigma_l)$ on the fatigue lifetime was studied by Sauer et al. (1976). The alternating stress $\sigma_a = {}^1/_2(\sigma_m - \sigma_l)$ remained constant at 17.2 MPa during the experiments. The maximum stress acting on the specimen varied from 17.2 MPa to 34.4 MPa. In Fig. 4.10 the mean stress versus the number of cycles to failure is shown. In addition, calculations were carried out with

the data in table 4.2. Using (3.3.37) the fatigue lifetime for loading between two stress amplitudes is given by

$$N_c = \tilde{N}_c\,[1 - D_o^{1-\beta}] \quad ; \quad \tilde{N}_c^{-1} = (1-\beta)\,\delta \tag{4.5.5}$$

Extension of (4.5.4) to compressive loadings can be performed using (3.3.28) and (3.3.34). Then, we find

$$\delta = \tilde{\delta}\,[\,\sigma_m^b + \langle -\sqrt{h}\,\sigma_1\rangle^b\,] \quad ; \quad h \in [0,1] \tag{4.5.6}$$

The effects of the compressive stresses on damage evolution are accounted for by the factor h. The theoretical results are depicted in Fig. 4.10. As the mean stress increases, the number of cycles to failure decreases, which is predicted by the model. It is noted that for different mean stresses the deviations from the experimental results are small. This indicates that the parameters in the evolution equation are independent of the loading amplitudes. Hence, at every instant the current damage is represented by eq. (3.3.41).

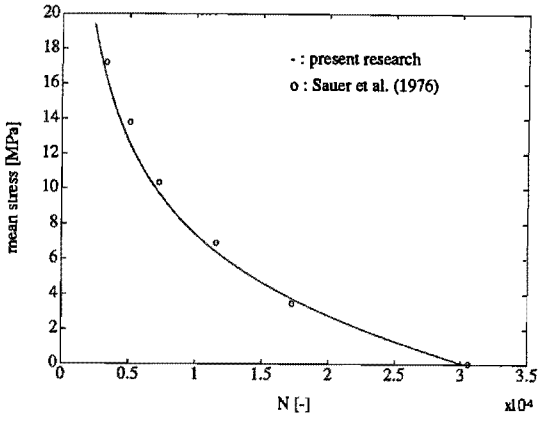

Figure 4.10 mean stress vs N

An optical method for damage measurements

In the foregoing it was assumed that microcrack growth and macrocrack growth are ruled by identical relations. Then damage evolution equations were derived from fracture mechanics. In the following the consequences of this assumption are set against optical measurements performed by Chen et al. (1981), who used a reflected

light method to determine the onset and growth of crazes during fatigue loading. Since PS is transparent and since crazes tend to form at right angles to the applied stress direction, the crazes act as a reflecting mirror and a beam of light will be transmitted if it does not meet any crack. Fig. 4.11 (a) shows the reflected light intensity for a PS specimen during fatigue loading as a function of the number of cycles. The test was conducted in completely reversed tension–compression at a stress level of 17.2 MPa and a frequency of 21 Hz. In this particular PS sample the first surface craze was detected at about 45% of the cycles required for fracture, which occurred at approximately 11800 cycles. Visual examination of the specimens during cycling and after fracture showed that crazing had developed in only one local area.

Using (3.3.41) the damage is computed as a function of the number of cycles. In this particular problem the initial damage value is chosen as $D_0 = 2.7 \cdot 10^{-4}$. The results are shown in Fig. 4.11 (b) for $D \leq 10^{-1}$. A close similarity between the reflected light intensity curve and the damage evolution curve can be observed. Indeed, it can be verified that the damage evolution is proportional to the increase in the reflected light intensity. This renders further evidence for the correctness of the developed theory. It is stated that reflected light measurements are appropriate for characterizing damage evolution. Optical measurements are non–destructive and easily carried out, while giving information about the local damage state. Their application, however is limited to translucent materials. In case of non–translucent materials ultrasonic waves measurements should be utilized.

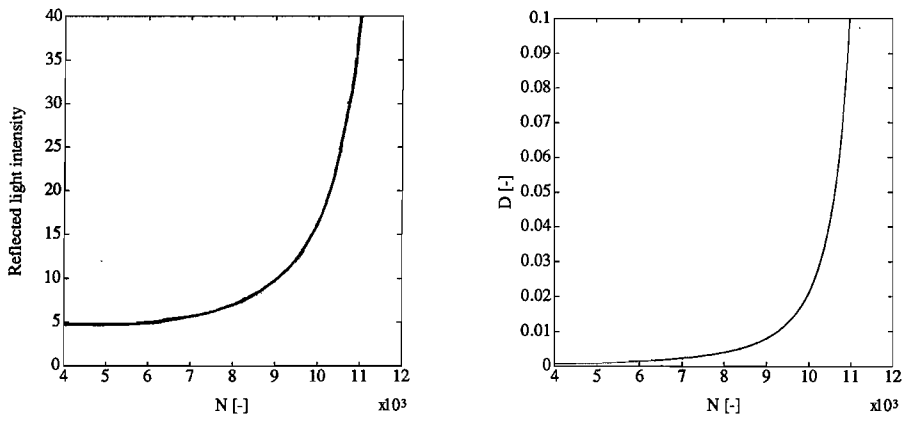

(a) (b)

Figure 4.11 (a) Reflected light intensity vs N, data from Chen et al. (1981)
Figure 4.11 (b) D vs N according to (3.3.41)

5 Numerical procedures

5.1 Introduction

For practical applications involving inhomogeneous deformations the equilibrium equation and the constitutive equations must be solved numerically. Since dissipative mechanisms take place, a particular analysis includes path dependent or time dependent phenomena. Dissipative mechanisms will be represented by a set of scalar internal variables. Throughout the complete history of load application, the equilibrium relation must be satisfied. The equilibrium state is susceptible for variations in the current values of the internal variables. The evolution equations for the internal variables in turn depend on the current state.

The response calculation is carried out by transforming the equilibrium relation into an integral form, using the principle of weighted residuals. Then, the time domain is discretized and an incremental solution process is applied. Here it is assumed that the solution for the discrete time t_n is known and that the solution for time t_{n+1} is required. After linearization of the integral equation an iterative procedure for the calculation of the position vector field at t_{n+1} is derived, which is exposed in section 5.2.

The current values of the internal variables are evaluated by integration of the rate equations, which is discussed in section 5.3. In the first iteration an estimate for the internal variables is computed with an explicit integration method. In the next iterations the successive corrections to this estimate are computed with an implicit method. In order to deal effectively with computing times, an automatic stepsize selection procedure is used.

In section 5.4 the iteration equation is discretized with the finite element method and an isoparametric plane stress element is derived. The solution process for the coupled equations consists of the following stages. In each iteration the evolution equations are integrated in order to evaluate the corrections to the internal variables. Then, the finite element equations are solved in order to evaluate corrections to the iterative changes of the nodal point positions. If some convergence criterion is satisfied the iterative procedure is terminated and the solution process is continued at the next time. Other solution strategies accept a weak coupling or use uncoupled equations. In section 5.5 the solution process is clarified for fatigue processes. In section 5.6 a test analysis is carried out to investigate some numerical aspects concerning accuracy and computing times.

5.2 Discretized equilibrium

Governing equations

Before describing the numerical solution process, the relevant equations are recalled. Omitting inertial effects and body forces the local balance equation of momentum (2.3.2) is given by

$$\vec{\nabla} \cdot \boldsymbol{\sigma} = \vec{0} \tag{5.2.1}$$

The constitutive equation for the stress tensor is given by

$$\boldsymbol{\sigma} = J^{-1}\mathbf{F}\cdot\mathbf{P}\cdot\mathbf{F}^{c} \quad ; \quad \mathbf{P} = \rho_0 \frac{\partial \psi}{\partial \mathbf{E}} \quad ; \quad \psi = \psi(\mathbf{E}, \underset{\sim}{z}) \tag{5.2.2}$$

The rate equation for the internal variables is expressed as an initial value problem

$$\dot{\underset{\sim}{z}} = \underset{\sim}{F}(\underset{\sim}{\omega}) \quad ; \quad \underset{\sim}{z}(t = 0) = \underset{\sim}{z}_0 \quad ; \quad \underset{\sim}{\omega}^{T} = \{ \mathbf{E}, \dot{\mathbf{E}}, \underset{\sim}{z} \} \tag{5.2.3}$$

Weigthed residuals

In order to establish a suitable form for the equilibrium equation the principle of weighted residuals is used, resulting in an integral equation, which forms the basis for the finite element approximations at discrete times in the loading history. According to the principle of weighted residuals the equilibrium equation is equivalent to the requirement that at every instant and for all admissible weighting functions $\vec{w}$, the following integral equation must be satisfied (Zienkiewicz 1977)

$$\int_V \vec{w} \cdot (\vec{\nabla} \cdot \boldsymbol{\sigma})\, dV = 0 \qquad \forall\, \vec{w} \tag{5.2.4}$$

where V is the current volume of the body. Using integration by parts and Gauss' theorem, the so–called weak form of the principle of weighted residuals is obtained

$$\int_V (\vec{\nabla}\vec{w})^{c} : \boldsymbol{\sigma}\, dV = \int_S \vec{w} \cdot \vec{p}\, dS \qquad \forall\, \vec{w} \tag{5.2.5}$$

where $\vec{p} = \boldsymbol{\sigma} \cdot \vec{n}$ is the external force on the deformed surface S and $\vec{n}$ is the outward

unit normal on S. Here the admissible weighting functions must be piecewise differentiable. Since the current configuration is unknown the integrals can not be evaluated. Therefore, all quantities will be formulated with respect to the initial configuration. Using (5.2.2) and the transformations

$$\vec{\nabla} = \mathbf{F}^{-c}\cdot\vec{\nabla}_o\,;\;\; dV = J\,dV_o\,;\;\; dS = \bar{J}\,dS_o\,;\; \vec{p}_o = \bar{J}\,\vec{p} \tag{5.2.6}$$

where the subscript $_o$ denotes that the quantities are defined with respect to the initial configuration, (5.2.5) takes the form

$$\int_{V_o} (\vec{\nabla}_o\vec{w})^c : \mathbf{P}\cdot\mathbf{F}^c dV_o = \int_{S_o} \vec{w}\cdot\vec{p}_o\, dS_o \qquad \forall\, \vec{w} \tag{5.2.7}$$

Time discretization and linearization

The requirement that the principle of weighted residuals must be satisfied at every instant will be relaxed and replaced by the requirement that this must be true for a discrete number of times $t = t_0, t_1, \ldots, t_n$. The time discretization results in an incremental solution process. It is assumed that the solutions up to time t_n are known and that the solution at $t_{n+1} = t_n + \Delta t_n$ is to be determined.

At time t_{n+1} the integral equation (5.2.7) is solved numerically. An iterative procedure, for determining the position vector field and its related quantities, is derived by writing all unknown quantities as the sum of an approximation of and a deviation from the exact solution. In the sequel we denote the real value of a quantity q at time t_{n+1} by $q(t_{n+1})$. An approximation for $q(t_{n+1})$ obtained in the ath iteration is denoted as q^a_{n+1} and the corresponding deviation is denoted as δq. The final computed value at t_n is denoted as q_n. Thus, we have

$$\vec{x}(t_{n+1}) = \vec{x}^a_{n+1} + \delta\vec{x}\,;\;\; \underset{\sim}{z}(t_{n+1}) = \underset{\sim}{z}^a_{n+1} + \delta\underset{\sim}{z}\,;\;\; \mathbf{P}(t_{n+1}) = \mathbf{P}^a_{n+1} + \delta\mathbf{P}$$
$$\vec{p}_o(t_{n+1}) = \vec{p}^a_{o_{n+1}} + \delta\vec{p}_o \tag{5.2.8}$$

Using (2.2.2) and (5.2.8) the deformation tensor is recast as

$$\mathbf{F}(t_{n+1}) = (\vec{\nabla}_o\vec{x}^a_{n+1})^c + (\vec{\nabla}_o\delta\vec{x})^c = \mathbf{F}^a_{n+1} + (\vec{\nabla}_o\delta\vec{x})^c \tag{5.2.9}$$

Using (2.2.5) the linearized iterative change of the Green–Lagrange strain tensor is expressed as

$$\delta\mathbf{E} = \tfrac{1}{2}\left[\mathbf{F}^{a\,c}_{n+1}\cdot(\vec{\nabla}_o\delta\vec{x})^c + (\vec{\nabla}_o\delta\vec{x})\cdot\mathbf{F}^a_{n+1}\right] \tag{5.2.10}$$

Then, the linearized iterative change in the second Piola–Kirchhoff stress tensor $\delta\mathbf{P}$ reads

$$\delta\mathbf{P} = \left.\frac{\partial\mathbf{P}}{\partial\mathbf{E}}\right|_{\mathbf{E}^a_{n+1},\underset{\sim}{z}^a_{n+1}} : \delta\mathbf{E} + \left.\frac{\partial\mathbf{P}^T}{\partial\underset{\sim}{z}}\right|_{\mathbf{E}^a_{n+1},\underset{\sim}{z}^a_{n+1}} \delta\underset{\sim}{z}(\mathbf{E}) \quad \Longrightarrow$$

$$\delta\mathbf{P} = \left[\frac{\partial\mathbf{P}}{\partial\mathbf{E}} + \frac{\partial\mathbf{P}^T}{\partial\underset{\sim}{z}}\frac{\delta\underset{\sim}{z}}{\delta\mathbf{E}}\right]_{\mathbf{E}^a_{n+1},\underset{\sim}{z}^a_{n+1}} : \delta\mathbf{E} = {}^4\mathbf{C}^a_{n+1} : \delta\mathbf{E} \tag{5.2.11}$$

Approximations for the current values of the internal variables are obtained by integration of the rate equations (5.2.3), which will be discussed in the next section. Since it is impossible to give a general procedure for representing the deviations of the boundary forces in terms of $\delta\vec{x}$, this term is omitted in the weighted residuals formulation. Using (5.2.8)–(5.2.11) the integral equation (5.2.7) is linearized to the following expression

$$\int_{V_o} (\vec{\nabla}_o\vec{w})^c : (\mathbf{P}^a_{n+1}\cdot{}^4\mathbf{I} + {}^4\mathbf{N}^a_{n+1}) : (\vec{\nabla}_o\delta\vec{x})\, dV_o =$$

$$-\int_{V_o} (\vec{\nabla}_o\vec{w})^c : \mathbf{P}^a_{n+1}\cdot\mathbf{F}^{a\,c}_{n+1}\, dV_o + \int_{S_o} \vec{w}\cdot\vec{p}^a_{o_{n+1}}\, dS_o \quad \forall\, \vec{w} \tag{5.2.12}$$

where ${}^4\mathbf{N}$ is defined by

$${}^4\mathbf{N} : \mathbf{A} = \tfrac{1}{2}\left[{}^4\mathbf{C} : \{\mathbf{F}^c\cdot\mathbf{A}^c + \mathbf{A}\cdot\mathbf{F}\}\right]\cdot\mathbf{F} \quad \forall\, \mathbf{A} \tag{5.2.13}$$

After having solved $\delta\vec{x}$ from the integral equation (5.2.12), a new approximation for the position vector field is derived. If the right–hand side of the integral equation is sufficiently small, the approximate solution is considered accurate enough. Then the iterative process is terminated and the solution process is continued at the next discrete time. If such is not the case the iterative process is continued, resulting in new approximations for the internal variables by integration of (5.2.3).

5.3 Integration of the evolution equations

In this section the numerical integration of the evolution equations is discussed. Eq. $(5.2.3)_1$ can readily be written in integral form as

$$\underset{\sim}{z}(t_{n+1}) = \underset{\sim}{z}(t_n) + \int_{t_n}^{t_{n+1}} \underset{\sim}{F}(\underset{\sim}{\omega}(\tau))d\tau \tag{5.3.1}$$

This integral equation can be evaluated with a large number of integration procedures. In practice care should be taken that an efficient method is employed. An implicit integration method is chosen in order to account for changes in the variables due to the coupling with the weigthed residuals formulation (5.2.12). A further advantage of implicit methods is their unconditional stability (Quinney 1985), implying that errors in intermediate results have little influence on the final result for any stepsize Δt. Therefore, the stepsize needs to be selected only on considerations of accuracy.

Consider a solution process that has been completed up till time t_n. If the function $\underset{\sim}{F}$ is approximated by a linear polynomial between the successive times t_n and t_{n+1}, the so–called trapezium rule is obtained

$$\underset{\sim}{z}_{n+1}^{a+1} = \underset{\sim}{z}_n + \tfrac{1}{2}\Delta t_n[\underset{\sim}{F}_n + \underset{\sim}{F}(\underset{\sim}{\omega}_{n+1}^{a})] \tag{5.3.2}$$

Since $\underset{\sim}{F}$ must be evaluated at the current time, the trapezium rule is an implicit method. The trapezium rule has second order accuracy, which means that the truncation error per step is $O(\Delta t^3)$. An initial estimate for the internal variables at t_{n+1} is obtained by substitution of the quantities at t_n in the trapezium rule

$$\underset{\sim}{z}_{n+1}^{1} = \underset{\sim}{z}_n + \Delta t_n \underset{\sim}{F}_n \tag{5.3.3}$$

If the integration procedure (5.3.3) is used exclusively to evaluate (5.3.1), it is commonly referred to as Euler's method. Euler's method is an explicit method with first order accuracy, i.e. the local truncation error is $O(\Delta t^2)$.

Stepsize selection

In order to deal efficiently with computing times, some mechanism for

automatically changing the stepsize as the integration proceeds, should be employed. Intuitively, if the solution is changing very slowly, then one can use a large stepsize, whereas in regions where the solution is changing rapidly a small stepsize must be used. The stepsize should be selected before the start of the next integration step. The usual approach is to estimate the truncation error for a step and, depending on its value, adjust the current stepsize either upward or downward. The local truncation errors for $\underset{\sim}{z}(t_{n+1})$ are defined by

$$\underset{\sim}{L}(t_{n+1}) = \underset{\sim}{z}(t_{n+1}) - \underset{\sim}{z}_{n+1} \tag{5.3.4}$$

The calculation of the truncation error $\underset{\sim}{L}(t_{n+1})$ is based on approximations of the internal variables for time t_{n+1}. Since at t_n no information is available concerning the quantities at t_{n+1}, explicit integration methods should be used to calculate approximations of the internal variables. A straightforward explicit method is to expand $\underset{\sim}{z}(t)$ into a Taylor series in the neighbourhood of $\underset{\sim}{z}_n$, thus

$$^{k}\underset{\sim}{z}_{n+1} = \sum_{p=0}^{k} \frac{1}{p!} \underset{\sim}{z}_n^{(p)} (\Delta t_n)^p \tag{5.3.5}$$

where $\underset{\sim}{z}_n^{(p)}$ is the pth derivative with respect to time. An approximation of the local truncation error $\underset{\sim}{L}_{n+1}$ of this k^{th} order integration method is found by comparing the integration method with a higher order method, e.g. one of order k+1

$$\underset{\sim}{L}_{n+1} = {}^{k+1}\underset{\sim}{z}_{n+1} - {}^{k}\underset{\sim}{z}_{n+1} = \frac{1}{(k+1)!} \underset{\sim}{F}_n^{(k)} (\Delta t_n)^{k+1} \tag{5.3.6}$$

Since the components of $\underset{\sim}{z}$ require different stepsizes, the stepsize must be determined to the needs of the worst–offender equation. The most critical component of $\underset{\sim}{z}$ is denoted as Z and the corresponding evolution function is denoted as T. Because Z may vary enormously in magnitude, a suitable criterion for the stepsize selection is obtained by requiring that the relative errors have a constant value e. Thus, we write

$$M_{n+1} = |{}^{k+1}Z_{n+1} - {}^{k}Z_{n+1}| = e\,|{}^{k+1}Z_n| \tag{5.3.7}$$

where M_{n+1} should be considered as the desired, i.e. highest admissible, truncation

error. Using (5.3.6) and (5.3.7) the stepsize is given by

$$\Delta t_n = \left[e\,(k+1)!\,|{}^{k+1}Z_n|\;|T_n^{(k)}|^{-1}\right]^{\frac{1}{k+1}} \tag{5.3.8}$$

The preceding equation can be cast into an equivalent form. Suppose we take the last step, i.e. $\Delta t = \Delta t_{n-1}$, and produce a local error M. Using (5.3.6) the step Δt_n, which would have given the desired truncation error M_{n+1}, is calculated as

$$\Delta t_n = \Delta t_{n-1} \left|\frac{M_{n+1}}{M}\right|^{\frac{1}{k+1}} \tag{5.3.9}$$

If M is larger than M_{n+1}, the preceding equation calculates how much to decrease the stepsize when the present step is retried, otherwise it calculates how much the stepsize can be increased safely for the next step.

5.4 Finite element equations

Using the principle of weighted residuals, an iterative procedure in integral form was derived in section 5.2. The integral form permits the solution of the unknown position vector field to be approximated with the finite element method. This method is based on separating a continuum into a finite number of elements. The elements are assumed to be interconnected at a discrete number of nodal points situated on their boundaries. A set of interpolation functions is chosen to define uniquely the position vector field and the weighting functions within each element in terms of their nodal values. The weighting functions are chosen according to the Galerkin method (Zienkiewicz 1977), which implies that the weighting functions and the position vectors are interpolated identically, thus giving

$$\vec{x} = \underset{\sim}{\phi}^T \underset{\sim}{\vec{x}}^e \quad ; \quad \vec{w} = \underset{\sim}{\phi}^T \underset{\sim}{\vec{w}}^e \tag{5.4.1}$$

where $\underset{\sim}{\vec{x}}^e$ and $\underset{\sim}{\vec{w}}^e$ are columns containing the nodal position vectors and weighting functions of element e, and $\underset{\sim}{\phi}$ is the corresponding column of interpolation functions.

As a result of this discretization eq. (5.2.12) can be written as a summation over all elements

$$\sum_e \vec{\underset{\sim}{w}}^{eT} \cdot \underline{\underline{K}}^e \cdot \delta\vec{\underset{\sim}{x}}^e = -\sum_e \vec{\underset{\sim}{w}}^{eT} \cdot \vec{\underset{\sim}{n}}^e + \sum_e \vec{\underset{\sim}{w}}^{eT} \cdot \vec{\underset{\sim}{h}}^e \tag{5.4.2}$$

$$\underline{\underline{K}}^e = \int_{V_0^e} (\vec{\nabla}_0 \underset{\sim}{\phi}) \cdot (\mathbf{P}^a_{n+1} \cdot {}^4\mathbf{I} + {}^4\mathbf{N}^a_{n+1}) \cdot (\vec{\nabla}_0 \underset{\sim}{\phi}^T) \, dV_0$$

$$\vec{\underset{\sim}{n}}^e = \int_{V_0^e} (\vec{\nabla}_0 \underset{\sim}{\phi}) \cdot \mathbf{P}^a_{n+1} \cdot \mathbf{F}^{a^c}_{n+1} \, dV_0$$

$$\vec{\underset{\sim}{h}}^e = \int_{S_0^e} \underset{\sim}{\phi} \, \vec{p}^a_{0_{n+1}} \, dS_0$$

where $\underline{\underline{K}}^e$ denotes the element stiffness matrix and the columns $\vec{\underset{\sim}{n}}^e$ and $\vec{\underset{\sim}{h}}^e$ respectively store the internal and external nodal forces of element e. Assemblage of all element stiffness matrices and internal and external element forces leads to

$$\vec{\underset{\sim}{w}}^T \cdot \underline{\underline{K}} \cdot \delta\vec{\underset{\sim}{x}} = \vec{\underset{\sim}{w}}^T \cdot (-\vec{\underset{\sim}{n}} + \vec{\underset{\sim}{h}}) = \vec{\underset{\sim}{w}}^T \cdot \vec{\underset{\sim}{r}} \quad \Rightarrow \quad \underline{\underline{K}} \cdot \delta\vec{\underset{\sim}{x}} = \vec{\underset{\sim}{r}} \tag{5.4.3}$$

In each iteration we calculate an out–of–balance load vector $\vec{\underset{\sim}{r}}$ and the stiffness matrix $\underline{\underline{K}}$, which yields an iterative change in the nodal point position vectors. Then, new approximations of the quantities that depend upon the nodal point position vectors are calculated. With these approximations, new approximations for the internal variables are determined by numerical integration of the evolution equations. The iterative process is continued until the out–of–balance load vector or the iterative changes in the position vectors are sufficiently small.

A four–node isoparametric element was chosen for the evaluation of the element stiffness matrix and the element nodal forces (Fig. 5.1). Plane stress conditions were assumed. The interpolation functions are bilinear functions, which depend on the isoparametric coordinates ξ_1 and ξ_2. In order to evaluate the integrals in (5.4.2) all quantities must be described as functions of the isoparametric coordinates, which involves some transformations (Bathe 1982) that will not be discussed in this thesis. The element was implemented in the HEEMP finite element package (Rooyackers 1988). Some numerical simulations will be presented in the next chapter.

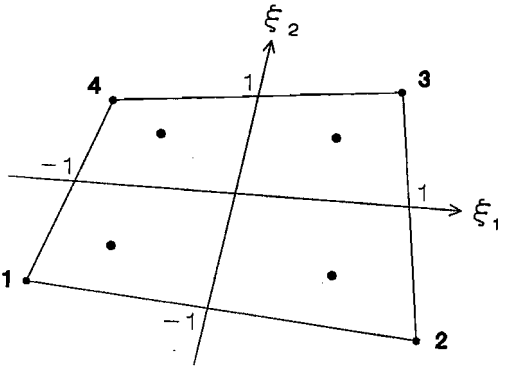

Figure 5.1 The plane stress element

5.5 Elaboration for fatigue

In the following it is assumed that the stress–strain relation is linear and that fatigue is the prevailing failure process. Then, damage is the only dissipative mechanism. Furthermore, the damage evolution law is positively homogeneous of degree one with respect to the strain rate, such that time can be considered as a pseudo variable. After integration of the evolution equation (3.3.24) over one loading cycle an incremental damage growth is obtained, which for computational convenience can be recast into a continuous form. The coupled constitutive equations (5.2.2) and (5.2.3) take the forms

$$\begin{aligned} \mathbf{P} &= (1-\mathrm{D})^4\mathbf{C}_0 : \mathbf{E} \\ \dot{\mathrm{D}} &\equiv f\,\frac{\mathrm{dD}}{\mathrm{dN}} = T(\bar{\epsilon}(\mathbf{E}), \mathrm{D}) \;\; ; \;\; \mathrm{D}(t=0) = \mathrm{D}_0 \end{aligned} \tag{5.5.1}$$

where ${}^4\mathbf{C}_0$ is a constant symmetric fourth order tensor. CDM is capable of modeling crack growth with a local approach to fracture (Lemaitre 1986b). Here a crack is represented as a zone in a finite element mesh, in which the damage has reached a critical level. Crack growth is identified with the growth of this zone. As will be demonstrated in the next section, it is convenient with respect to the reduction of computing time to uncouple the constitutive equations. Using (3.3.35) we obtain

$$\mathbf{P} = [1 - D_c H(D - D_c)]\ {}^4\mathbf{C}_0 : \mathbf{E}$$

$$\dot{D} = T(\bar{\epsilon} = \bar{\epsilon}(\tilde{t}), D) \quad ; \quad D(t = 0) = D_0 \tag{5.5.2}$$

In this case T is a function of the current damage state and the deformation state at $t = \tilde{t}$ with $\tilde{t}$ denoting the last discrete time, at which a critical damage level was reached in the solid.

The desired stepsize is computed according to (5.3.8). Choosing $k = 1$ the stepsize is based on the truncation error that is made when the initial approximation for the damage state is carried out with Euler's method (5.3.3), thus

$$\Delta t_n = \left[2\epsilon\ {}^2D_n \,|\, T_n^{(1)} \,|^{-1}\right]^{\frac{1}{2}} \tag{5.5.3}$$

The first order derivative, that is determined for the stepsize selection, can be used to calculate an improved initial estimate for the damage at t_{n+1}

$${}^2D_{n+1}^1 = D_n + \Delta t_n\ T_n + \tfrac{1}{2}(\Delta t_n)^2 T_n^{(1)}$$

$$T_n^{(1)} = \left.\frac{\partial T}{\partial D}\right|_{\bar{\epsilon}_n, D_n} T_n + \left.\frac{\partial T}{\partial \bar{\epsilon}}\right|_{\bar{\epsilon}_n, D_n} \dot{\bar{\epsilon}}_n \tag{5.5.4}$$

According to the trapezium rule (5.3.2) the $(a+1)^{th}$ correction to the damage variable at t_{n+1} is calculated as

$$D_{n+1}^{a+1} = D_n + \tfrac{1}{2}\Delta t_n[\ T_n + T(\bar{\epsilon}_{n+1}^a, D_{n+1}^a)\ ] \tag{5.5.5}$$

In Appendix C the solution process is summarized for both coupled and uncoupled constitutive equations for times $t_n > 0$.

5.6 Test analysis

The element, described in section 5.4, has been subjected to a number of tests, which can be divided into two categories. In the first category the correct implementation of the element is checked. Being relatively standard, these tests will

not be discussed in what follows. In the second category the performance of the algorithm for the numerical integration of the evolution equations is checked. In the following we will amplify on the integration of the evolution equation.

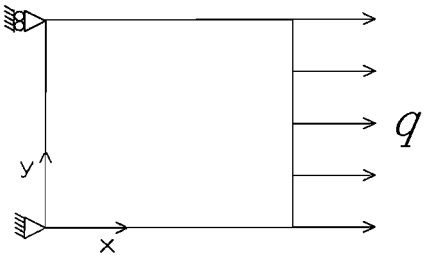

Figure 5.2 Plate subjected to uni–axial loading

Consider a plate of dimensions 25*25*0.5 [L^3]. The plate is loaded at the free end by a distributed periodical force q, which ranges from 0 to q_m (Fig. 5.2). The plate has an initial damage D_o. The external loading will cause the plate to deteriorate. Due to the imposed kinematic boundary conditions, the stress state in the plate is uni–axial. The deformation matrix is given by $F_{ij} = \lambda_j \delta_{ij}$, where λ_j is the elongation factor with respect to direction j. The deformed state is represented exactly by the plane stress element of section 5.4. For an isotropic linear elastic material the stress–strain relation is given by

$$\begin{bmatrix} \hat{P}_{11} \\ 0 \\ 0 \end{bmatrix} = \frac{E}{(1+\nu)(1-2\nu)} \begin{bmatrix} 1-\nu & \nu & \nu \\ \nu & 1-\nu & \nu \\ \nu & \nu & 1-\nu \end{bmatrix} \begin{bmatrix} E_{11} \\ E_{22} \\ E_{33} \end{bmatrix} \tag{5.6.1}$$

From (5.6.1) we obtain

$$E_{22} = E_{33} = -\nu E_{11} \quad ; \quad \hat{P}_{11} = \frac{P_{11}}{1-D} = E\, E_{11} \tag{5.6.2}$$

Using (5.2.2) the Cauchy stress σ_{11} is obtained as

$$\hat{\sigma}_{11} = \frac{\sigma_{11}}{1-D} = \lambda_1 \lambda_3^{-2} \hat{P}_{11} \tag{5.6.3}$$

Using $(5.6.2)_2$, (5.6.3) and $\sigma_{11} = q/b = q/(\lambda_3 b_o)$ with b the thickness of the plate, the elongation factor λ_1 is determined by

$$\chi^2\lambda_1^2(\lambda_1^2-1)^2 = \lambda_3^2 = 1 - \nu(\lambda_1^2-1) \quad ; \quad \lambda_1^2 \leq \frac{1+\nu}{\nu} \tag{5.6.4}$$

where $\chi = (E/2q)b_o(1-D) = \chi(D)$. Substitution of $u = \lambda_1^2-1$ yields a third order equation

$$\chi^2u^3 + \chi^2u^2 + \nu u - 1 = 0 \tag{5.6.5}$$

From the preceding equation the displacement field can be solved analytically.

The equivalent strain is chosen according to (3.3.28). Since the deformation in thickness direction will hardly influence the growth of surface defects, its contribution to the damage evolution is neglected. Then the equivalent strain is written as

$$\bar{\epsilon} = \sqrt{1+h\nu^2}\, E_{11} \tag{5.6.6}$$

Let the damage evolution law be given by (3.3.33). For fixed loading amplitudes 0 and q_m during the complete history, the equivalent strain varies between 0 and $\bar{\epsilon}_m$. Then, $(5.5.1)_2$ takes the form

$$\frac{dD}{dN} = \delta\, D^{\beta} \quad ; \quad \delta = \frac{\alpha}{\gamma+1}\left[\bar{\epsilon}_m^{\gamma+1} - \kappa_o^{\gamma+1}\right] \tag{5.6.7}$$

Through the parameter χ the displacement field is dependent upon the current damage state. Thus calculation of the damage involves a nonlinear initial value problem, for which in most cases no analytical solution can be derived. When the elastic and dissipative mechanisms are uncoupled according to $(5.5.2)_1$, an analytical solution is established as (see eq. (3.3.41))

$$D(N) = \left[\,(1-\beta)\,\delta\, N + D_o^{1-\beta}\,\right]^{\frac{1}{1-\beta}} \tag{5.6.8}$$

The material parameters used in the test example are summarized in table 5.1. It is noted that most values were taken from the data acquired for PS. The calculations were accomplished for loadings ranging from 0 to q_m = 17.2 Nmm^{-1}. Using (5.6.5) the elongation factor is determined as λ_1 = 1.011, which exactly matches the finite element calculation.

Table 5.1 Material data

$E = 3 \cdot 10^3$ [FL^{-2}]	$\alpha = 5.35 \cdot 10^5$
$\nu = 0.25$	$\beta = 1.4$
$h = 0.2$	$\gamma = 2.6$
$D_0 = 2 \cdot 4 \cdot 10^{-5}$	$\kappa_0 = 0$

In Fig. 5.3 the damage is depicted as a function of the number of cycles for different relative truncation errors e. For each e the numerical solutions for the coupled and uncoupled equations are shown together with the analytical solution for the uncoupled equations (5.6.8). It appears that the integration procedure works well, since the numerical and analytical solutions for the uncoupled equations almost coincide. The small deviations between the solutions for the coupled and uncoupled equations indicate that the application of the uncoupled equations should

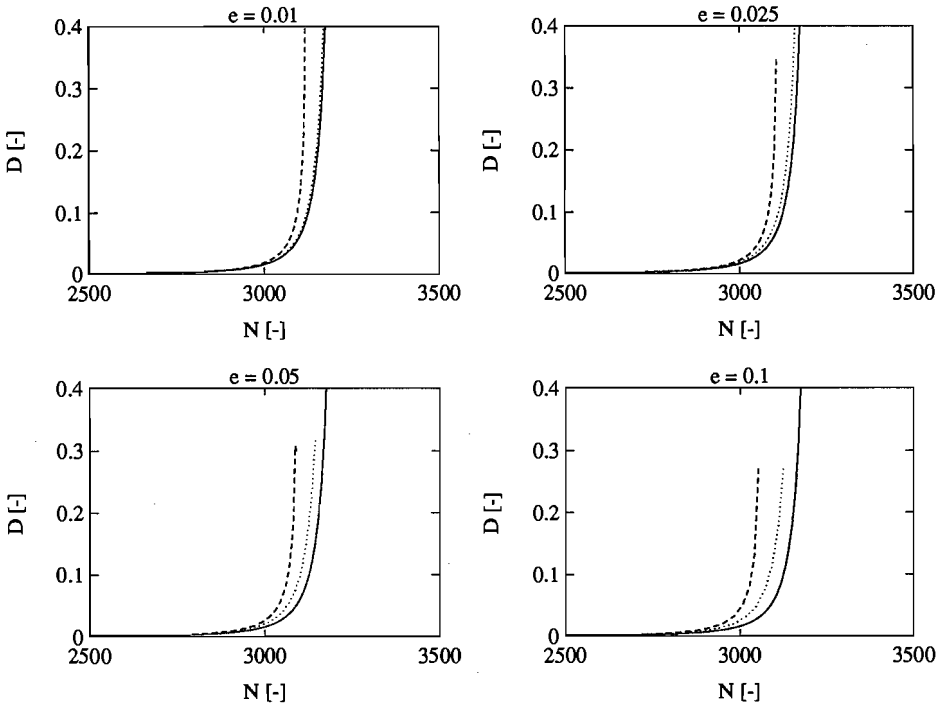

Figure 5.3 D vs N for different relative errors e
--- coupled eq., ···· uncoupled eq., — analytical solution

be favoured with regard to computing times. This is illustrated further in table 5.2, where the computing times for both solution methods are shown for different e. The computing times are scaled to the smallest value, which is obtained in the uncoupled situation with $e = 0.1$. For a relative error $e = 0.01$ the numerical integration shows greatest accuracy, but with associated larger computational cost.

Table 5.2 Relative CPU times

e	Coupled	Uncoupled
0.01	36.4	1.7
0.025	27.1	1.3
0.05	21.8	1.1
0.1	18	1

The stepsize selection procedure is illustrated for $e = 0.025$. In Fig. 5.4 the damage evolution is shown as a function of the number of cycles. The instants, at which the incremental analysis was carried out, are marked. In Fig. 5.5 the equivalent strain is depicted as a function of the number of cycles. For the uncoupled equations the equivalent strain has a constant value until a critical damage level has been reached. For the coupled equations the equivalent strain is a continuously increasing function that follows the damage evolution.

In Fig. 5.6 the stepsize (in cycles) is shown as a function of the number of steps. The stepsize selection procedure performs very well, computing relatively large steps when the damage is changing slowly and continuously decreasing steps as the damage increases. The deviations between the stepsize selections for the coupled and uncoupled equations result from a different first derivative in $(5.5.4)_2$, implying that a more conservative estimate for the stepsize must be made for the coupled equations due to the dependence on the deformed state. This effect is most pronounced for large variations in the deformation state.

The additional reduction in computational effort by the stepsize selection procedure can easily be imagined. Since without any stepsize selection procedure a correct description of the damage would require a stepsize, which is completely dictated by the explosive growth towards the end of the lifetime. Let us consider for example the stepsize selection of the uncoupled equations.

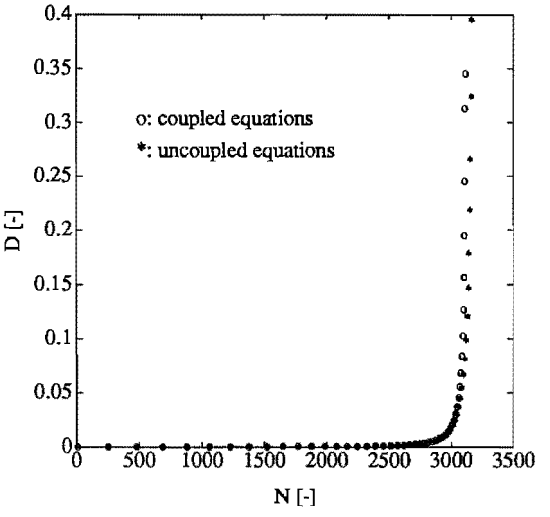

Figure 5.4 D as a function of N ($e = 0.025$)

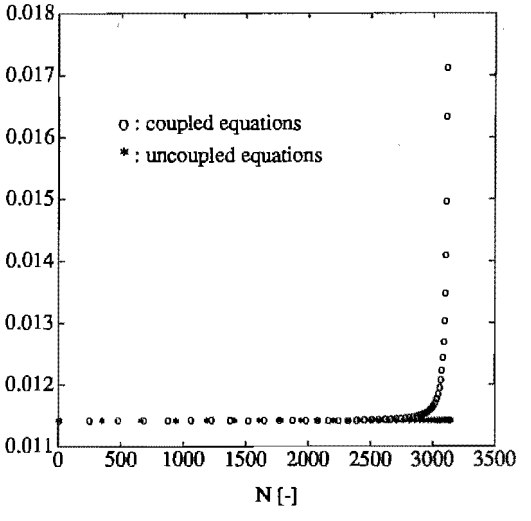

Figure 5.5 $\bar{\epsilon}$ as a function of N ($e = 0.025$)

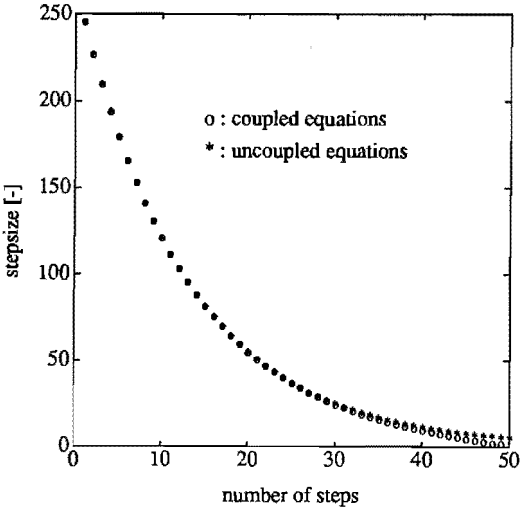

Figure 5.6 Stepsize vs number of steps ($e = 0.025$)

From Fig. 5.6 it follows that for a correct description of the constitutive behaviour, the stepsize should approximately be 5 cycles. Then without any stepsize control it is necessary to take 640 steps for failure at 3200 cycles. Compared to the 50 steps that were taken in the example at hand, an enormous reduction in CPU time is achieved solely on the basis of the stepsize selection procedure. For the coupled equations the reduction in c.p.u. time is even more pronounced, since towards the end of the lifetime the stepsize must be chosen more carefully (see Fig. 5.6).

In concluding this section it is worth remarking that the solution for the uncoupled equations leads to nearly as accurate solutions as for the coupled equations with much lesser computational effort. Thus for failure mechanisms, which show an explosive increase in the damage, the application of the uncoupled equations is highly recommended. Apart from these considerations, an enormous reduction in computing time is achieved with the adaptive stepsize control, which therefore is to be favoured under all circumstances.

6 Numerical simulations

6.1 Introduction

In the previous chapters a model for the description of fatigue processes was developed. Explicit forms for the stress–strain relation, the evolution equation and a criterion for damage growth, were derived in chapter 3. Since materials typically contain flaws of unknown dimensions and positions, the initial damage should be considered as a stochastic quantity. In chapter 4 it was argued that this assumption accounts for the scattering in the observed lifetimes in fatigue. The numerical solution process was discussed in chapter 5. Points of issue were the establishment of a linearized set of equations, the numerical integration of the evolution equation and the reduction of c.p.u. time.

In this chapter simulation techniques are adopted to analyze stochastic failure processes. The simulations consist of finite element calculations for different realizations of the initial (damage) state. The statistics of the failure processes (in terms of lifetimes) are derived from the computed responses. In section 6.2 this probabilistic analysis is applied to tensile loading and bending. The essential features of failure mechanisms in homogeneous and inhomogeneous deformations are highlighted. Case studies on the numerical solution process are performed concerning the application of coupled and uncoupled constitutive equations, the accuracy of numerical integration of the evolution equation and the influence of the element mesh on the results (mesh sensitivity). As regards the reduction of the mesh sensitivity the elementary cell (EC), introduced in chapter 4, is the key word.

In sections 6.3 and 6.4 CDM is used to predict crack growth in fatigue loading by representing a crack as a zone of completely damaged elements. The corresponding failure processes are dominated by the local deformation state. This implies that identical crack patterns are obtained regardless of the initial state. As our main concern is the prediction of crack patterns, just one calculation is carried out. The initial damage in the elements is given by the expected values of the associated probability distribution functions (PDF). In section 6.3 a plate with an elliptical hole is analyzed. Under the given type of loading the development of the completely damaged zone, corresponding to macrocrack growth, is evident. In section 6.4 crack growth in a plate with an induced crack is studied for three distinct loadings. In this problem the crack pattern is uncertain a priori.

6.2 Probabilistic damage analysis

6.2.1 Generation of the initial damage state

In this chapter numerical studies on fatigue in materials displaying linear elastic and isotropic material behaviour are carried out. It is recalled that the relevant equations are given by the equilibrium equation (5.2.1) and the constitutive equations for stress–strain and damage growth. In case of coupled constitutive equations (5.5.1) is used, whereas (5.5.2) is used for the uncoupled equations. For periodical loadings that vary between zero to a positive extreme, the evolution equation is given by the following initial value problem

$$\frac{dD}{dN} = \begin{cases} 0 & \text{if } \bar{\epsilon} < \kappa_0 \\ \frac{\alpha}{\gamma+1}\left[\bar{\epsilon}_m^{\gamma+1} - \kappa_0^{\gamma+1}\right] D^{\beta} & \text{if } \kappa_0 \leq \bar{\epsilon} < \kappa_c \\ \infty & \text{if } \bar{\epsilon} \geq \kappa_c \end{cases} \tag{6.2.1}$$

$$D(N = 0) = D_0$$

The equivalent strain $\bar{\epsilon}$ is defined according to (3.3.28). Compared with (5.6.7) a static criterion has been added to the evolution law, indicating that instantaneous rupture occurs if $\bar{\epsilon}$ exceeds the equivalent strain threshold κ_c.

Owing to the presence of randomly distributed flaws in materials, failure processes actually are stochastic processes, which will be analyzed using simulation techniques. The simulations consist of finite element calculations for different realizations of the initial damage state. The statistics of the failure processes can be derived from the computed responses.

In order to characterize the initial state each element in the finite element mesh is divided into four subareas S_i , $i \in \{1,2,3,4\}$ as is shown in Fig. 6.1. The subareas are the Gauss point influence zones. The Gauss points comprise the points where the constitutive equations are evaluated. A subarea consists of $k_i = S_i/A_{ec}$ elementary cells (EC). The stress gradients in S_i are small, resulting in approximately homogeneous stress fields. Subsequently failure is initiated in the EC with the largest initial damage (see section 4.3), which therefore is the limiting factor in the reliability of S_i. Hence, the PDF of the maximum initial damage in S_i must be established. If the initial damage has an exponential parent distribution, the maximum damage in S_i is distributed as (see (4.3.13))

$$f_{\underline{D}}(D) = k_i \, \lambda \, exp(-\lambda D) \, [1-exp(-\lambda D)]^{k_i-1} \;\; ; \; k_i = S_i / A_{ec} \tag{6.2.2}$$

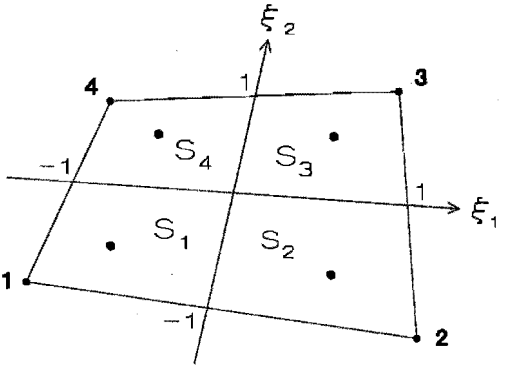

Figure 6.1 Plane stress element divided into four subareas

In each calculation a realization of the initial damage must be determined. For this purpose, the initial damage must be attributed to the Gauss points in the elements according to (6.2.2). The essential building block for generating probability distributions is a reliable random number generator (Press et al. 1986). The random number generator creates a uniform distribution, so that the probability of finding a number between x and $x+dx$ is given by

$$p_{\underline{x}}(x) \, dx = \begin{cases} dx & \text{if} \quad 0 < x < 1 \\ 0 & \text{if} \quad x \geq 1 \end{cases} \tag{6.2.3}$$

The PDF $p_{\underline{y}}$ of some function $y(x)$ is determined by the transformation law of probabilities

$$p_{\underline{y}}(y) = p_{\underline{x}}(x) \left| \frac{dx}{dy} \right| \tag{6.2.4}$$

If we want to generate the desired distribution function $p_{\underline{y}} = f_{\underline{D}}$, then using (6.2.3) and (6.2.4), we need to solve

$$\left| \frac{dx}{dD} \right| = f_{\underline{D}}(D) \quad \Rightarrow \quad x = F_{\underline{D}}(D) \tag{6.2.5}$$

where $F_{\underline{D}}$ is the indefinite integral of $f_{\underline{D}}$, i.e. the cumulative distribution function

(CDF). Inverting (6.2.5), the desired transformation, which takes a uniformly distributed random variable x into one distributed as $f_{\underline{D}}$, is given by

$$D = F_{\underline{D}}^{-1}(x) \tag{6.2.6}$$

Whether (6.2.6) can be used, depends on the existence of the inverse function.

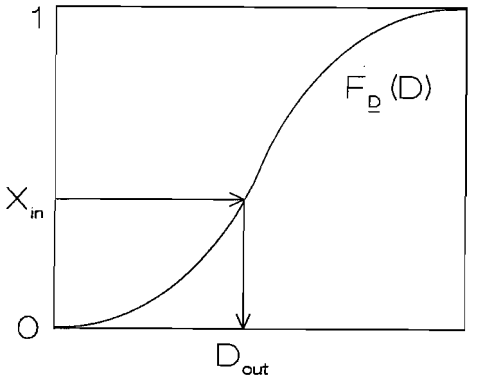

Figure 6.2 Transformation of random variables; the input values x_{in} are distributed uniformly, the output values D_{out} are distributed according to $f_{\underline{D}}$

A geometric interpretation of the transformation involved is given in Fig. 6.2. A uniformly distributed random number x_{in} is determined between 0 and 1. Then, the value $D = D_{out}$ is determined that has the fraction x_{in} of probability area to its left. If the desired PDF is given by (6.2.2), the transformation of x_{in} is given by

$$D_{out} = \frac{1}{\lambda} \ln(1 - x_{in}^{1/k_i}) \tag{6.2.7}$$

In the following subsections the generation of the initial damage is given by the preceding transformation.

6.2.2. Uni–axial tension

Consider the structure in Fig. 6.3 of dimensions 16*5*.1 [L^3]. The structure is loaded at x = 16 [L] by a distributed periodical force q_1 ranging from 0 to 2 [$F \cdot L^{-1}$]. The

stress state in the structure is approximately homogeneous. The PDF of the maximum initial damage in a subarea S_i is described by eq. (6.2.2.). The material dependent data used in this analysis are given in table 6.1. It is remarked that the parameters in the damage evolution equation, which are used throughout this chapter, are based on polystyrene (section 4.5). The remaining material data are chosen rather arbitrarily. Due to the paucity of experimental data on fatigue experiments no reference can be made to results from other studies. Nevertheless, the results of the computations are suited well for qualitative interpretations.

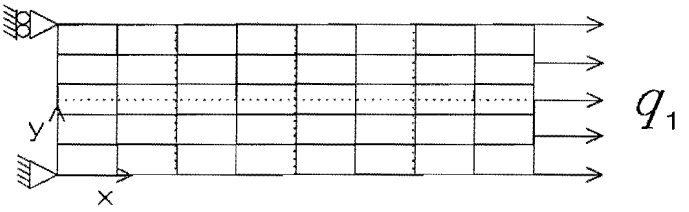

Figure 6.3 Uni–axially loaded structure, discretized using 8 or 40 elements

Table 6.1

$E = 10^3$ [F·L^{-2}]	$D_c = 0.98$
$\nu = 0.25$	$\kappa_0 = 0$
$\alpha = 3.69 \cdot 10^4$	$\kappa_c = 4 \cdot 10^{-2}$
$\beta = 1.4$	$\lambda = 5000$
$\gamma = 2.6$	$A_{ec} = 0.5$ [L^2]
$h = 0.2$	

In the following three case studies are carried out, involving the uncoupling of the constitutive equations, the integration accuracy and the mesh sensitivity. The integration accuracy is formulated in terms of the relative error e, which is defined by eq. (5.3.7). The mesh sensitivity is tested either using a mesh with 8 elements or a mesh with 40 elements. In each case two simulations are compared (see table 6.2). Each simulations consists of 15 finite element calculations with different initial states. In order to save computing time the calculations are, where possible, carried out for the uncoupled constitutive equations.

The first failure of any subarea is referred to as failure initiation or crack initiation. As the deterioration continues more and more subareas fail, until finally no convergence can be achieved anymore by the solution process. This stage corresponds to structural instability. In the sequel complete failure is identified either with first failure of a subarea, corresponding to a weakest link hypothesis, or with structural instability.

Table 6.2 Simulations for section 6.2.2

case	(Un)Coupled	e	n_e
1	U/C	0.025	40
2	U	0.025/0.05	40
3	U	0.025	8/40

1 *Coupled versus uncoupled constitutive equations*

In the structure in Fig. 6.3 a progressive deterioration and corresponding stiffness reduction take place. In order to study these phenomena a relative elongation u/u_o is introduced, where the subscript $_o$ refers to the maximum elongation in the first cycle. This definition is a good indicator of the damage, as can readily be seen in one–dimensional situations, where employing a linear strain definition we have

$$\frac{u}{u_o} = \frac{\epsilon}{\epsilon_o} = \frac{1-D_o}{1-D} \Rightarrow D = 1-(1-D_o)\frac{u_o}{u} \tag{6.2.8}$$

In Figs. 6.4 and 6.5 the relative elongations are shown as a function of the number of cycles for the coupled and uncoupled constitutive equations respectively. The stochastic nature of the failure process is obvious through the scattering in lifetimes for the respective realizations. As a result of the continuous coupling between the stress–strain relation and the damage evolution equation a smooth increase in the elongations is obtained (Fig. 6.4). In case of the uncoupled equations intermittent changes in the elongations occur, if somewhere in the structure a critical damage has been reached (Fig. 6.5). At all times the computed damage variables take on larger values for the coupled constitutive equations. This is a direct consequence of the effective stress concept, which induces the damage to grow more rapidly.

For every calculation the instant of failure initiation and structural instability

are recorded. Cumulative frequency distributions, giving the probability of failure as a function of the number of cycles, are obtained from the total of responses. These distributions are depicted in Fig. 6.6. Curves 1 and 2 show the distribution according to the weakest link hypothesis for the coupled and uncoupled equations respectively. The deviations between the curves are small. Curves 3 and 4 correspond to structural instability for the coupled and uncoupled equations respectively. The deviations between the coupled and uncoupled solutions remain small as the failure process continues.

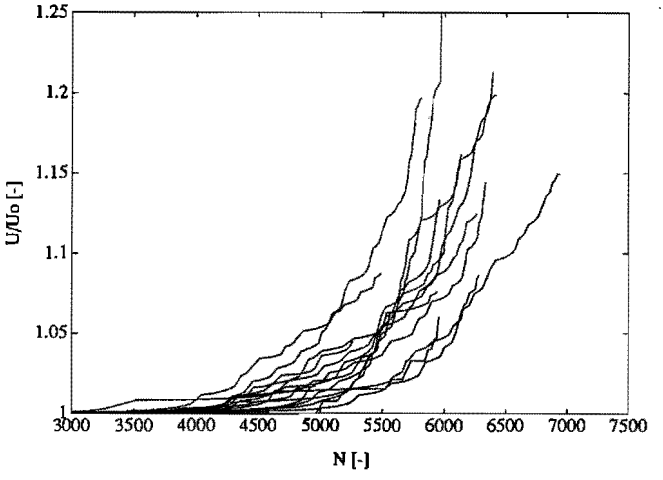

Figure 6.4 Relative elongation u/u_o vs N for the coupled equations

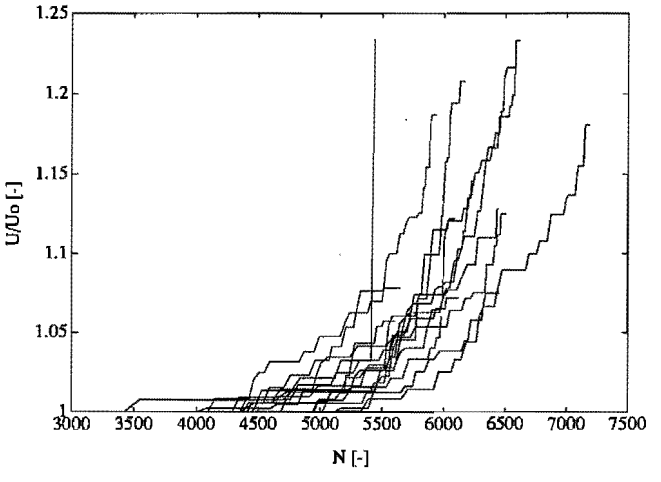

Figure 6.5 Relative elongation u/u_o vs N for the uncoupled equations

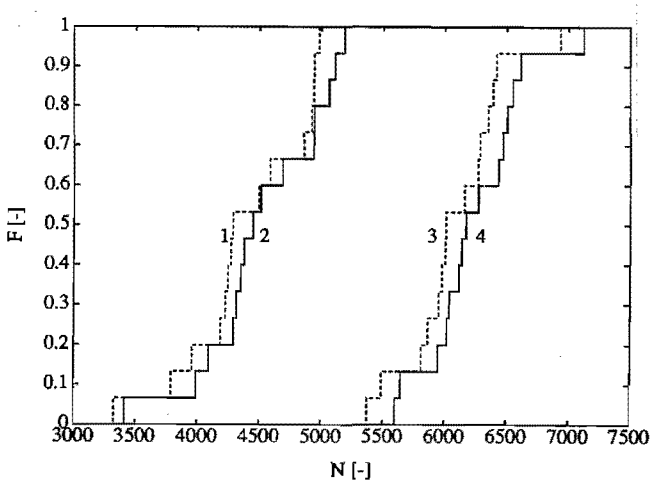

Figure 6.6 Lifetime distributions for uni–axial tension (case 1) ; ----- coupled eq., —— uncoupled eq. ; curves 1, 2 weakest link ; curves 3, 4 structural instability

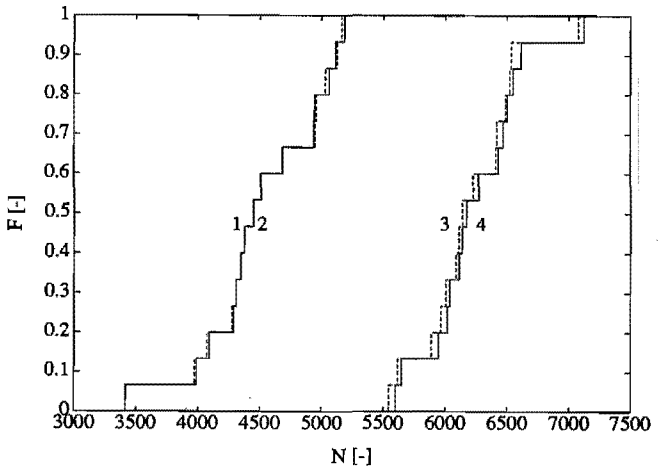

Figure 6.7 Lifetime distributions for uni–axial tension (case 2) ; ----- $e = 0.05$, —— e = 0.025 ; curves 1, 2 weakest link ; curves 3, 4 structural instability

2 *Integration accuracy*

The effects of the numerical integration on the solution accuracy are examined for two relative errors $e = 0.025$ and $e = 0.05$. The resulting lifetime distributions are plotted in Fig. 6.7. Curves 1 and 2 show the distribution according to the weakest link hypothesis; curves 3 and 4 correspond to structural instability. The computed

lifetime distributions show small deviations. Thus, in practical applications it suffices to use the larger relative error $e = 0.05$.

3 *Mesh sensitivity*

In finite element calculations the Gauss point influence zone (subarea S_i in Fig. 6.1) determines the dimensions of the completely damaged zone, representing the crack. However, there is no indication at all that these dimensions correspond to the characteristic dimensions of the failure mechanisms. The resulting mesh dependence (mesh sensitivity) is a major drawback in a more general use of CDM. Several solutions to this problem have been proposed (Billardon and Moret–Bailly 1987, Chaboche 1988, Bazant and Pijaudier–Cabot 1988). Billardon et al. (1987), proposed that local fracture occurs in a characteristic volume when the mechanical dissipation, associated with the damage process and integrated over the whole loading history, reaches a critical value. However, the size of the characteristic volume is unknown. Further, because of the volume integration, the spatial variation of damage should at least display C^0 continuity throughout the mesh. There are some points of similarity between Billardon's approach and the present approach, which involve the choice of a characteristic size. In the present study the elementary cell (EC) is identified with the characteristic size. It is demonstrated that the notion of the EC leads to a reduction of the mesh sensitivity without imposing requirements on the continuity of the damage.

In general, failure processes are influenced by the combined effects of damage and deformations. In order to completely focus on the mesh dependence associated with damage, it is most convenient to investigate problems involving homogeneous deformations. Then, the crack initiation is completely dictated by the maximum initial damage in the structure (see section 4.3). The PDF of the maximum damage is independent of the finite element mesh and is fully controlled by the number of EC's in the structure: $n = \sum_{n_e} \sum_{m} S_{e_m} / A_{ec} = S/A_{ec}$, with S_{e_m} the surface of subarea m in element e and S the total surface of the mesh. Hence, the PDF of the time to crack initiation is independent of the mesh.

Two parameter studies were carried out either using 8 or 40 elements (see table 6.2). The computed cumulative frequency distributions of the failure probability are shown in Fig. 6.8. Curves 1 and 2 represent the instants of failure initiation (weakest link hypothesis). The distributions show a reasonably good agreement. In case of uncoupled constitutive equations, an analytical solution is given by eq. (5.6.8). Then the CDF of the lifetimes according to the weakest link

hypothesis is given by eq. (4.4.10). This CDF is represented by curve 5. Curves 1 and 2 agree fairly well with the analytical solution, clearly demonstrating that the crack initiation is not influenced by the mesh. However, owing to the restricted number of calculations curves 1 and 2 do not perfectly match the analytical solution.

After failure initiation the deformation field is disturbed in the vicinity of the completely damaged zone and consequently the failure process is increasingly controlled by the local deformation state. Final failure is brought about by successive failure of subareas. Curves 3 and 4 show the cumulative frequency distributions for structural instability using 8– and 40–element meshes respectively. Regarding the number of cycles to failure the deviations amount to about 10 percent. These discrepancies arise from overrating the local stress state in the 8–element structure after failure initiation.

The simulations show that the mesh sensitivity with respect to the (crack) initiation, the (crack) propagation and ultimate failure, is reduced by the notion of the EC. It is noted that in processes, which produce smooth damage fields, such as plasticity coupled with damage, the energy criterion as proposed by Billardon and Moret–Bailly (1987) can be adopted by identifying the EC with the characteristic volume.

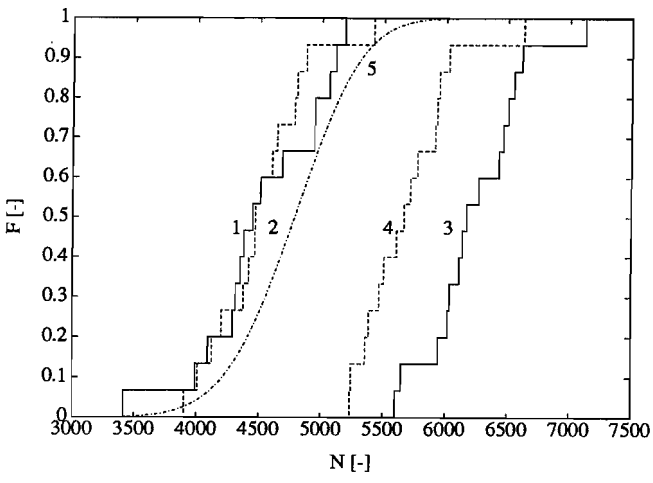

Figure 6.8 Lifetime distributions for uni–axial tension (case **3**) ;
----- 8 elements, —— 40 elements ; curves 1, 2 weakest link (numerical); curves 3, 4 structural instability (numerical) ; curve 5 weakest link (analytical)

6.2.3 Bending

In the following the effects of the local deformation state on the failure process are discussed. The structure in Fig. 6.9 is loaded at x = 16 [L] by a periodical force q_2, which ranges from 0 to 0.2 [$F \cdot L^{-1}$]. The effects of the local deformations, for both coupled and uncoupled constitutive equations, as well as the effects of the equivalent strain definition, through variation of the parameter h in (3.3.28), are examined (see table 6.3). All calculations are performed with a 40–element mesh and a relative error $e = 0.025$.

Table 6.3 Simulations for section 6.2.3

case	(Un)Coupled	h
1	C/U	0.2
2	U	0.2/1

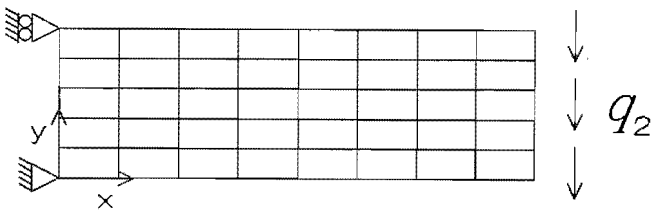

Figure 6.9 Structure loaded in bending

1 *Effects of the local deformation state*

In the previous subsection the location of failure initiation was a probabilistic quantity, which was determined by the maximum initial damage in the structure. If the sample size is large enough this location will show a uniform distribution. For the structure in Fig. 6.9 the deformation field is inhomogeneous. Fifteen finite element calculations were carried out. In Fig. 6.10 the number of observed failures is given versus the failure location. Undoubtedly, the local deformation state and not the initial damage is the dominating quantity in the failure process. Hence, for

inhomogeneous deformations the failure location nearly becomes a deterministic quantity. However, in two out of fifteen calculations failure occurs for $2 \leq x < 4$. A typical realization for failure between $2 \leq x < 4$ is considered in Figs. 6.11 and 6.12. In Fig. 6.11 the dimensionless end point deflection v/v_0, with v_0 the maximum deflection in the first cycle, is shown as a function of the number of cycles. The characters (a), (b), (c), (d) mark subsequent stages in the failure process. In Fig. 6.12 the corresponding states are visualized. The damage is characterized by various degrees in darkness; increasingly dark regions express increasing damage. In each plot the damage is scaled to the largest value that has been reached up till the current instant. Thus, the dark zones in Fig. 6.12 (b)–(d) represent the development of a crack. Fig. 6.12 illustrates that failure processes are controlled by the combined effects of deformations and damage, since failure initiation occurs in the subarea in which the conditions for accelerated damage growth are optimally satisfied through a relatively large initial value in combination with relatively large deformations.

In Fig. 6.13 the failure probability is shown as a function of the number of cycles. Curves 1 and 2 show the distribution according to the weakest link hypothesis for the coupled and uncoupled equations respectively. Curves 3 and 4 correspond to structural instability for the coupled and uncoupled equations respectively. The deviations between the coupled and uncoupled solutions are small. The band between curves 1 and 2, and curves 3 and 4 is small compared to the band that was obtained for uni–axial loadings (see Fig. 6.6). These differences arise because local failures in approximately homogeneous deformation fields induce only minor perturbations in the local deformation state, thus giving a more gradual material deterioration.

The instant of structural failure is controlled by the maximum initial damage in the failure region. For homogeneous deformation fields the failure region comprises the total structure, whereas for inhomogeneous fields its dimensions are controlled by the local deformations. Since fewer elementary cells are involved, the expected value of the maximum initial damage in the local failure region is smaller than the expected value of the maximum initial damage in the complete structure. Accordingly, for identical local deformation states a crack is likely to be initiated earlier in a homogeneously loaded structure because of a more serious initial damage. Additionally, the PDF of the maximum damage associated with the failure region in inhomogeneous deformation fields has a larger variance. Consequently, the scatter in observed lifetimes is larger, which can be verified by comparing the CDF's in Figs. 6.6 and 6.13.

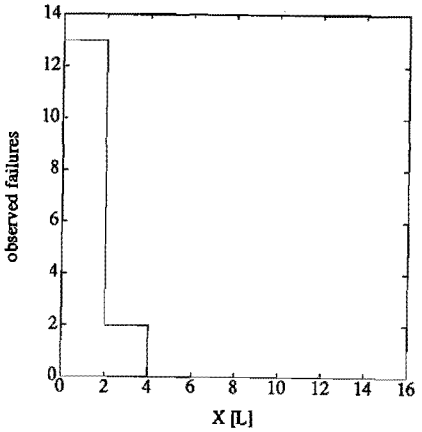

Figure 6.10 Observed failures in bending vs failure location

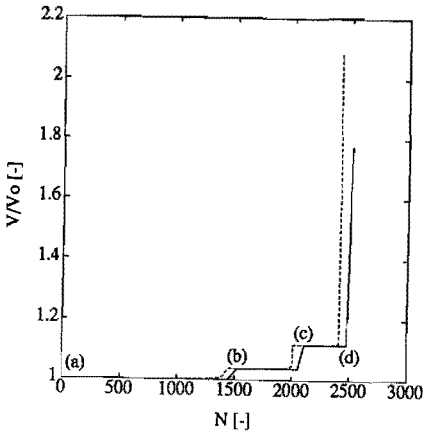

Figure 6.11 v/v_o vs N ;
failure between $2 \leq x < 4$,
----- coupled eq., —— uncoupled eq

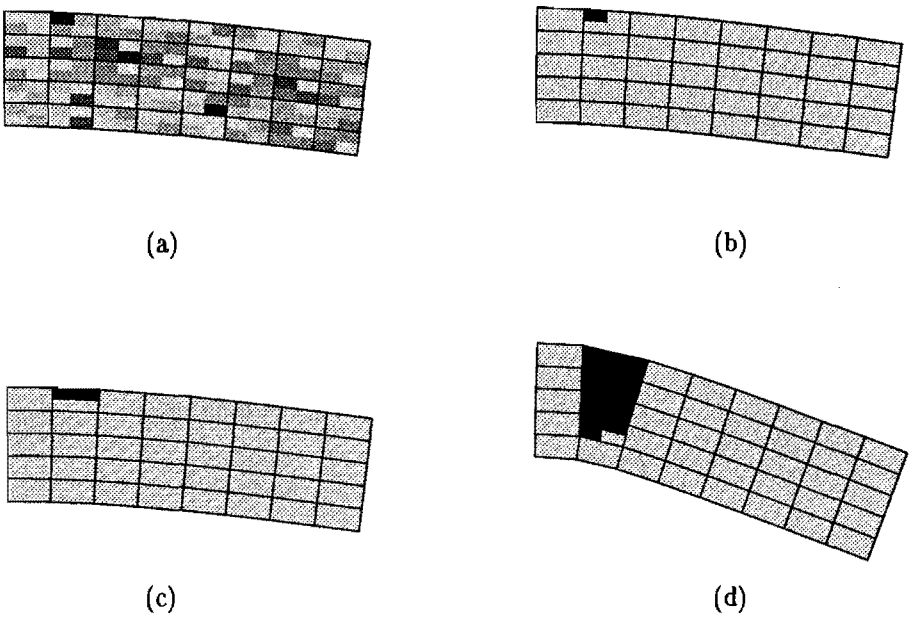

Figure 6.12 Successive stages in the failure process corresponding to Fig. 6.11

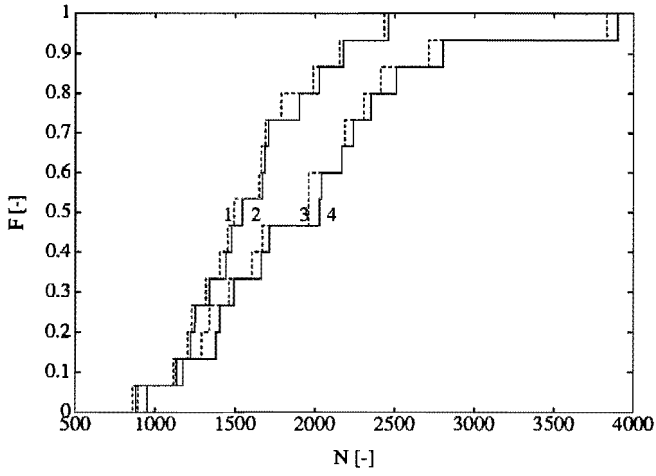

Figure 6.13 Lifetime distributions for bending (case 1) ; ---- coupled eq., —— uncoupled eq. ; curves 1, 2 weakest link ; curves 3, 4 structural instability

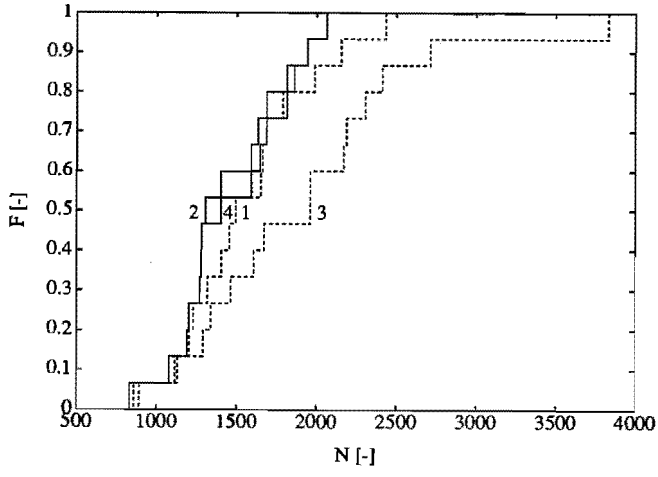

Figure 6.14 Lifetime distributions for bending (case 2) ; ---- h = 0.2, —— h = 1 ; curves 1, 2 weakest link ; curves 3, 4 structural instability

2 *Effects of the equivalent strain definition*

Below, the effects of the equivalent strain definition (3.3.28) on the failure process are investigated by comparing the results for h = 0.2 and h = 1. If h = 0.2 compressive strains are less harmful to the failure process than tensile strains. This means that failure is most likely to be initiated at (0,5). For h = 1 the compressive and tensile strains are weighed equally, implying that failure may be initiated at the

origin (0,0) just as well as at (0,5). Naturally, this will cause a significant decrease in the observed lifetimes as is illustrated in Fig. 6.14. In most cases the structure fails directly after crack initiation, because the equivalent strains in adjacent Gauss points exceed the critical threshold κ_c for static failure (see (6.2.1)).

6.3 Plate with an elliptical hole

In this section crack growth initiation and propagation in a square plate with an elliptical hole is studied. The dimensions of the plate are 100*100*.1 [L^3] and the major and minor axis of the ellipse are 20 [L] and 4 [L]. The plate is loaded at the horizontal edge by a distributed periodical force $q(t)$, which ranges from 0 to 1.28 [$F \cdot L^{-1}$]. As there are two planes of symmetry only a quarter of the structure is analyzed (Fig. 6.15). The structure is modeled using 260 elements. The material data are given in table 6.4.

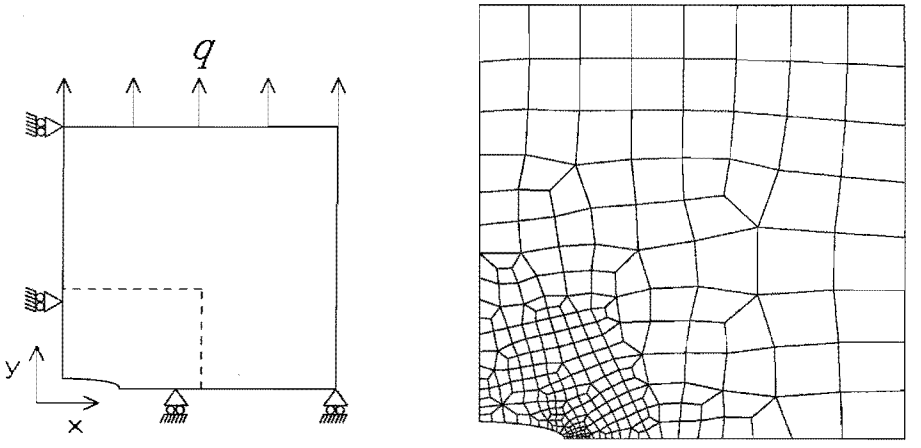

Figure 6.15 Plate with an elliptical hole and finite element discretization

Table 6.4

$E = 3 \cdot 10^3$ [$F \cdot L^{-2}$]	$D_c = 0.995$
$\nu = 0.25$	$\kappa_o = 0$
$\alpha = 1.93 \cdot 10^6$	$\kappa_b = 8 \cdot 10^{-2}$
$\beta = 1.4$	$\lambda = 5000$
$\gamma = 2.6$	$A_{ec} = 0.3$ [L^2]
$h = 0.2$	

Solution strategy and FEM analysis

In section 6.2.3 it was put forward that the local deformation state is the dominant factor in crack growth problems. Then the crack pattern is invariable regardless of the initial state. As the objective of the present example is directed towards the prediction of the crack pattern (completely damaged zone), just one calculation is carried out, in which the values for the initial damage are given by the associated expected values of the PDF (6.2.2): $D_i = E(D; k_i)$. Hence, the application of time consuming simulation techniques is avoided and an averaged structural behaviour is computed. Because of the local mesh refinement some elements become smaller than the EC. A conservative estimate for the initial damage in these elements is given by the expected value for the damage in one EC: $E(D; k_i \leq 1) = E(D; k_i = 1)$. Because the stress gradients in the elements are small, the instants of failure of the element subareas are about equal. This gives rise to adopting a weakest link assumption on element level, i.e. the complete element fails if one subarea fails. A further reduction in computing time can be obtained by employing this assumption. The calculation is performed with the uncoupled constitutive equations.

Due to the high stresses in the vicinity of the hole, a crack starts to develop from this region along the boundary $y = 0$. The deformations in the completely damaged elements are large as a result of crack opening effects. For computational reasons the element stiffness can not be decreased indefinitely. For this reason residual stresses exist in the completely damaged zone. The residual stresses are undesired since they influence the solutions. In the present example the initial stiffness is reduced 200 times in the completely damaged zone (see table 6.4). In Fig. 6.16 the stress component σ_{yy} is shown as a function of the position x at $y = 0$ for different times. The crack growth is characterized by the moving stress peaks. Small residual stresses remain in the damaged zone. For increasing crack lengths the residual stresses become larger due to crack opening effects. The values of the peak stresses strongly depend on the local mesh size. Therefore, the peak stresses tend to decay as a result of the increasingly rougher mesh with growing distance from the hole. This influences the damage evolution and ergo the time to failure. A solution to this problem would be to first carry out an exploratory calculation to study the crack pattern. A second calculation should be carried out with a refined mesh in the regions of the expected crack pattern. A more sophisticated solution is the application of mesh adaptation techniques. Then, crack opening effects can be taken into account correctly and the residual stresses vanish. Additionally, the local mesh refinement can be adapted as the crack proceeds, preventing the peak stresses from falling off.

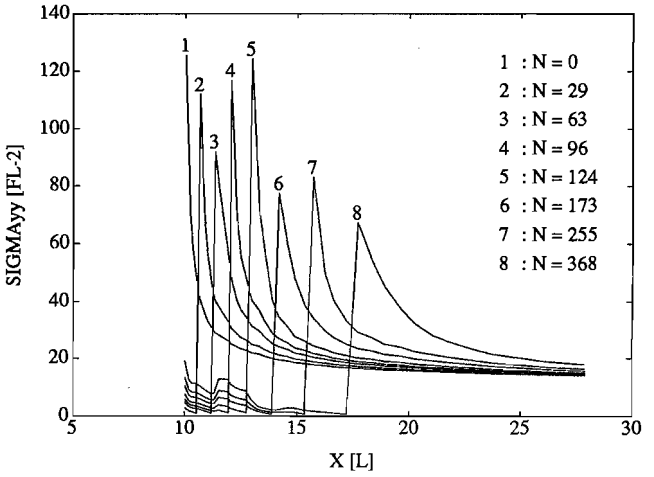

Figure 6.16 σ_{yy} vs x along boundary y = 0 for different N

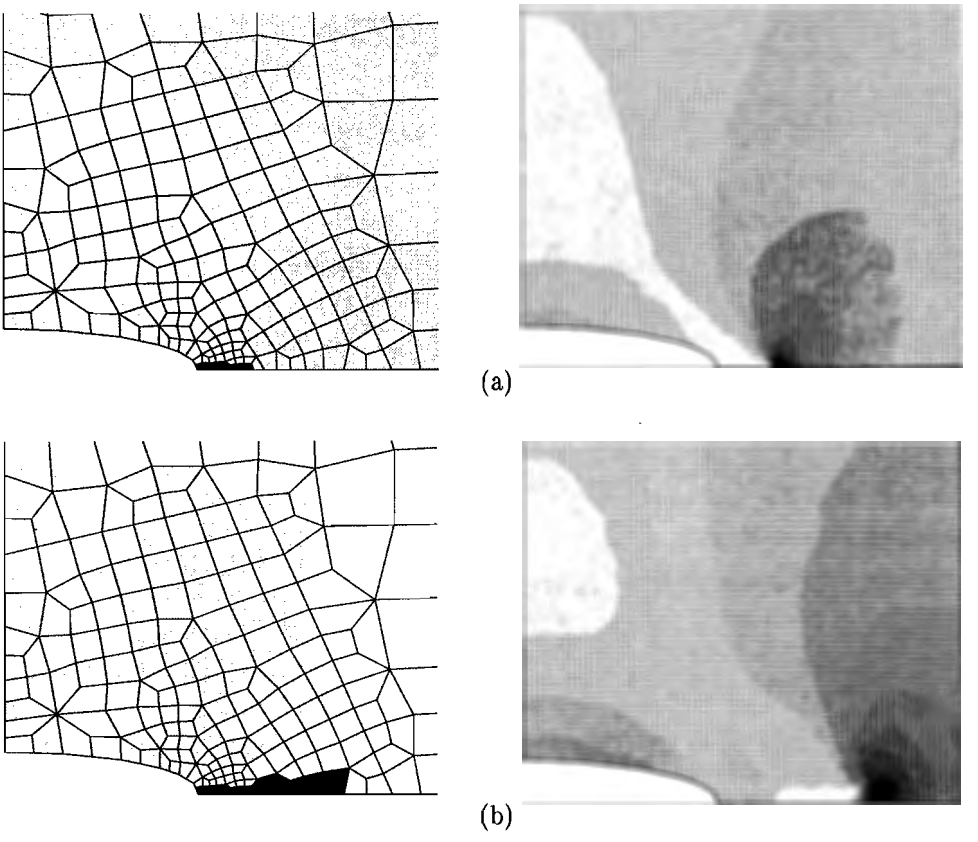

Figure 6.17 Crack pattern and Von Mises stresses after N = 124 cycles (a) and N = 368 cycles (b)

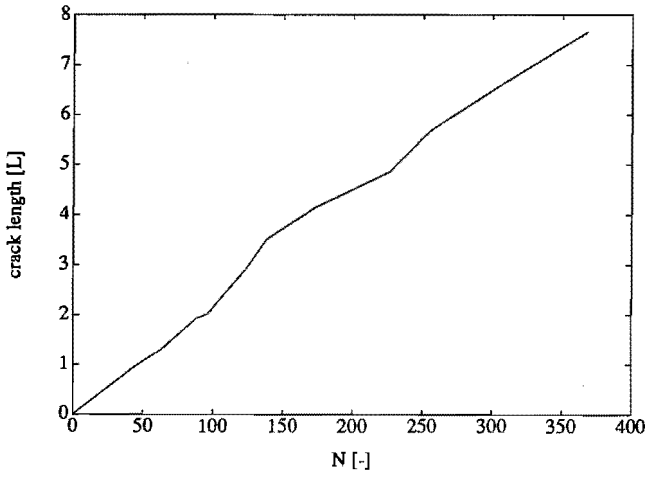

Figure 6.18 Crack length vs N

Two instants in the failure process are shown. Fig. 6.17 (a) shows the crack, which is expressed by the dark zone of failed elements, and the corresponding Von Mises stresses after N = 124 cycles. In Fig. 6.17 (b) the state after N = 368 cycles is depicted. In Fig. 6.18 the crack length is plotted as a function of the number of cycles, showing an almost linear relationship. Thus the crack propagation rate is constant. It is remarked that in the finite element analysis the crack growth rate for about N > 255 cycles is underestimated due to the increasingly rougher mesh as the crack proceeds. Accordingly, in reality the zone of constant crack propagation rate will be smaller.

6.4 Plate with an induced crack

In section 6.3 the direction of crack growth, perpendicular to the direction of the external force, was more or less evident. In this section we discuss a problem in which the direction of crack growth is uncertain in advance. Consider the plate of dimensions 130*130*.1 [L^3] in Fig. 6.19. A crack of length $20\sqrt{2}$ [L] is induced at the origin at an angle of 45°. The plate is loaded in x–direction by a periodical force q_1 and in y–direction by a periodical force q_2. The forces q_1 and q_2 vary between 0 and q_1 and q_2. The plate is modeled with 718 elements (Fig. 6.19). The analysis is performed for the uncoupled constitutive equations. Again only one calculation is carried out using the expected values of the damage distribution (6.2.2). The material data are given in table 6.5.

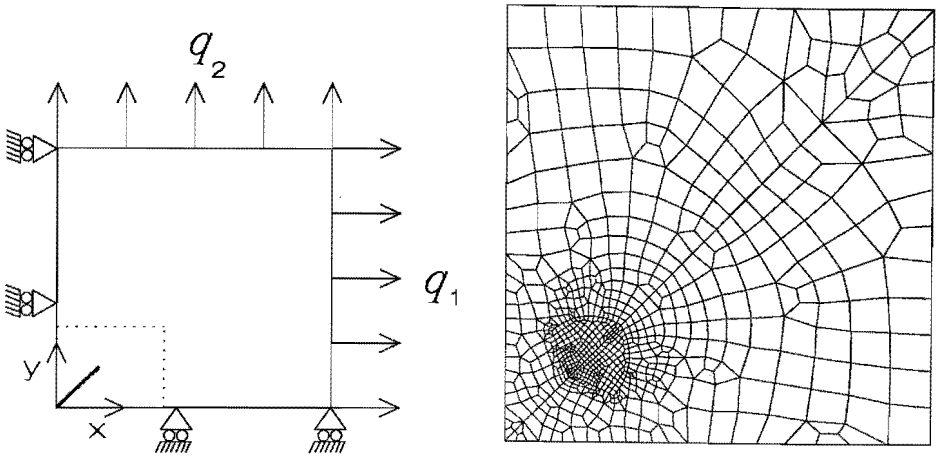

Figure 6.19 Plate with an induced crack and finite element discretization

Table 6.5

$E = 3 \cdot 10^3$ [F·L^{-2}]	$D_c = 0.995$
$\nu = 0.25$	$\kappa_o = 0$
$\alpha = 1.93 \cdot 10^6$	$\kappa_b = 4 \cdot 10^{-2}$
$\beta = 1.4$	$\lambda = 9.6 \cdot 10^4$
$\gamma = 2.6$	$A_{ec} = 0.3$ [L^2]
$h = 0.2$	

Crack initiation and crack growth are predicted for different types of loading. The loading is characterized by the ratio of the force amplitudes $\vartheta = q_2/q_1$. The amplitude q_1 is kept fixed at 96 [F·L^{-1}]. Three cases were studied.

1 $\vartheta = 1$

As the loading is symmetrical and so are the boundary conditions, a crack will develop from the induced crack tip and proceed along the axis of symmetry. In Fig. 6.20 (a) the crack is modeled as a zone of completely damaged elements after $N = 6.65 \cdot 10^3$ cycles. The corresponding Von Mises stresses are shown as well; dark regions mark the position of the current crack tip.

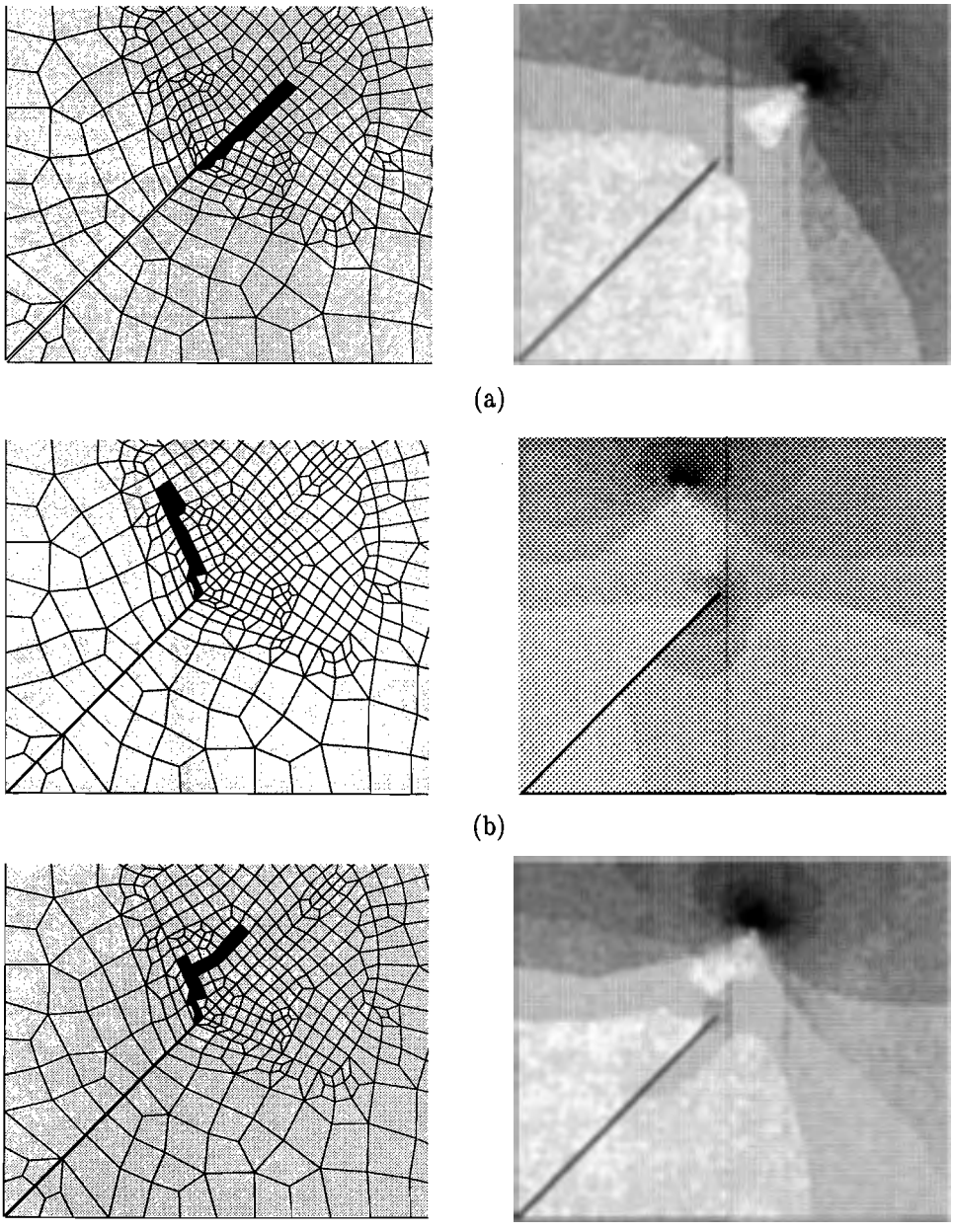

Figure 6.20 Crack patterns and corresponding Von Mises stresses for $\vartheta = 1$ (a), $\vartheta = 0$ (b), and $\vartheta = 0.5$ (c)

2 $\vartheta = 0$

As a result of the non–symmetrical stress–state the crack initiation and propagation will occur to the left of the crack tip. In Fig. 6.20 (b) the crack and the corresponding Von Mises stresses are shown after $N = 1.4 \cdot 10^4$ cycles.

3 $\vartheta = 0.5$

In this case we get a combination of the failure processes under 1 and 2 as is illustrated in Fig. 6.20 (c), where the crack and the corresponding Von Mises stresses are depicted after $N = 1.4 \cdot 10^4$ cycles. In contrast with the cracks that have developed for $\vartheta = 1$ and $\vartheta = 0$, the crack for $\vartheta = 0.5$ is not straight. Until some transition phase is reached the crack proceeds identically to the crack for loading in x–direction ($\vartheta = 0$). Thereafter the crack proceeds in accordance with the crack for equal loading amplitudes ($\vartheta = 1$). Most likely this process will repeat itself, as a result of which the crack will zigzag through the plate.

To conclude this chapter, it is stated that CDM is well suited for the analysis of crack growth problems. Both crack initiation and propagation can be analyzed in a natural manner by representing the crack as a zone of completely damaged elements. Although no reference can be made to other studies, the results of the simulations presented in this chapter can be qualified as promising. The mesh sensitivity is reduced by the notion of the elementary cell. Future investigations into the correct description of the stress state as the crack proceeds are recommended. This can be achieved using mesh adaptation techniques (Schreurs et al. 1986).

7 Discussion

On the theory

In the present study Continuum Damage Mechanics was adopted to describe brittle failure mechanisms. The theory of CDM can be developed using thermodynamics with internal state variables. The introduction of internal state variables to represent dissipative mechanisms requires the establishment of rate equations for these variables, the so–called evolution equations. The ensuing approach has a great generality, since all constitutive equations can be derived from two potentials: the Helmholtz free energy and the dissipation potential. Thus, different mechanisms such as plasticity, damage or creep, can be handled in a similar fashion.

Brittle failure processes are characterized by the fact that damage evolution is the predominant dissipative mechanism. Additionally, time can be considered as a pseudo variable. A complete description of the current state requires the establishment of the stress–strain relation and the damage evolution equation together with a criterion for damage growth. From the thermodynamical framework a natural coupling between the stress–strain relation and the evolution equation is obtained. The stress–strain relation was determined using the concepts of effective stress and strain equivalence. For isotropic damage states the correctness of these concepts can be demonstrated. The damage criterion encloses a surface in strain space. This requires the definition of an equivalent strain. The employed equivalent strain accounts for the fact that tensile and compressive loadings may contribute differently to the failure process. For instance in fatigue tensile loadings are more harmful than compressive loadings. Further research concerning the proper choice of the parameter that weighs the contribution of tensile and compressive strains, is recommended. Most likely this parameter is a true material property, which can be related to the tensile and compressive strength.

A distinction, which is based on the formulation of the damage criterion, was made between brittle and fatigue damage. The model developed for brittle damage is capable of predicting the behaviour of polystyrene (PS) and concrete. The model for fatigue damage was kept as simple as possible to expedite the parameter characterization. Nevertheless, some widely accepted cumulative damage models, such as the Palmgren–Miner rule, could be derived from it. The parameters in the evolution law were considered as constants. This assumption is confirmed by the results in chapter 4 regarding the effects of the mean stress on the lifetime of polystyrene specimens.

Anisotropic damage models were considered. Problems concerning the choice of a proper damage variable were signalled. The directional nature was taken into account using dyadic vector products. For isotropic damage the macro symmetry is left unaltered by this choice. Since this is not the case for the vector representation as applied by Talreja (1985), dyadic products are to be preferred. The constitutive equations were derived by Taylor series expansions of the independent variables. This straightforward elaboration, however, yields unworkable expressions. In case of small deformations it is advisable to derive the constitutive equations using a micromechanical approach (Krajcinovic and Sumarac 1989), which reflects the underlying physics of the failure process.

On the experimental evaluation

The experimental characterization of the evolution equation for fatigue is extremely difficult due to the high degree of damage localization. This implies that conventional methods, which measure variations in global material properties, are useless. In the present study a different method has been adopted. It was assumed, that microdefect growth and macrocrack growth can be represented by identical relations. Several reasons in support of this assumption were given in chapter 4. Further, a relation between an effective defect size and the damage variable is proposed. Then, an evolution equation can be derived, which forms a particularization of the model developed in chapter 3. The parameters in this equation emanate from fracture mechanics. This is very convenient since numerous tests for characterizing fatigue crack growth are reported in literature (see e.g. Sauer and Richardson 1980, Williams 1984).

Due to the presence of microdefects with unknown positions and dimensions, damage evolution is a stochastic process. This phenomenon was accounted for by considering the initial damage as a random variable. This is a new point of view, since in CDM it is assumed that initially a material is in a perfect state, resulting in a deterministic analysis. A procedure was developed to determine the probability distribution function (PDF) of the initial damage. For this purpose the PDF of the initial damage was associated with some characteristic size, the elementary cell (EC). Based on the fact that under homogeneous loading conditions the reliability of a structure is determined by the largest damage, statistics of extremes was employed to render the PDF for the maximum damage in the structure. Two methods were presented for determining the parameters in the initial damage distribution and the associated EC. In both methods these quantities are obtained

by minimizing the deviations between a model distribution function and an experimental distribution function. The choice between the methods is imposed by the question, whether local failure occurs in static loading. If this is the case, the experimental distribution of the maximum initial damage can be determined from two static tests. In case of non–local damaging in static tests, lifetime data are required. This method can be applied if the discrepancies between coupled and uncoupled solutions stay small, which is definitely true for fatigue as was demonstrated in chapters 4 and 5. Of course, the second method can be applied also if static loadings show local damaging. It is stated that the second method finds a broader applicability. Furthermore the data acquisition requires relatively little effort.

Lifetime distributions of Biomer were predicted fairly well. A further point in support of the developed theory is that the dimensions of the EC were within the scale of the representative volume element (RVE) for polymers. Then, there might be a correspondence between the EC and the RVE, which can solve the problem of characterizing the scale of the RVE as discussed by Lemaitre and Dufailly (1987). Instead of using micrographic measurements, the scale follows directly from the present minimization procedure. This, however, needs further investigations.

Failure processes in PS were investigated. The mean maximum initial defect size resulting from the present model agrees well with the size as reported by McMaster et al. (1974). The effect of the mean stress on the lifetime was tested. The results agreed well with data from Sauer et al. (1976).

Chen et al. (1981) applied optical measurements to study failure processes in PS. Optical measurements give direct information about the local damage state. A striking resemblence was observed between the reflected light intensity and the damage in fatigue loading. This similarity provides further evidence for the validity of the developed model. In addition, it makes clear that the evolution equation for fatigue can be characterized with optical methods. However, the major benefit of these measurements is that they can be applied to characterize different damage processes, which no longer satisfy the hypothesis of identical crack growth relations on the micro and macro level. For example, failure processes in composite materials consist of different phases, involving matrix cracking, interface delamination, and fiber rupture. These mechanisms are very complex and require different evolution laws. Therefore, it is strongly recommended to further investigate the feasibility of optical and ultrasonic damage measurements.

On the numerical procedure

The balance equation and the constitutive equations were solved numerically. Due to the continuous coupling between the constitutive equations large computing times may evolve for complex problems. A substantial reduction of computing time is achieved by employing an adaptive stepsize algorithm. The algorithm is based on estimates for the local truncation error in the numerical integration of the evolution equation. It is noted that the time stepping algorithm is applied to the most critical damage evolution in the mesh. As the damage effects are localized, substructuring (Zienkiewicz 1976) may become an important device in the modeling of damage phenomena with less computational effort. A further reduction in computing time is achieved by uncoupling the constitutive equations. In section 5.6 it was demonstrated that for failure mechanisms, which show an explosive increase in the damage state, the uncoupling produces satisfactory results.

Stochastic failure processes were analyzed using simulation techniques. The simulations consist of finite element calculations for different realizations of the initial state. Lifetime distributions were predicted by performing calculations with different realizations of the initial state. Under homogeneous loading conditions failure is initiated in the element with the largest initial damage. Under inhomogeneous loading conditions the local deformation state is the dominating factor in the failure mechanism.

An important issue is the dependence on the finite element modeling (mesh sensitivity). Several solutions to this question were suggested. Chaboche (1988) states that the local mesh size has to be fixed in every application after checking a particular one. Another approach is to introduce a nonlocal definition for damage growth (Bazant and Pijaudier–Cabot 1988). Billardon et al. (1987) introduced an energy criterion which is associated with a characteristic size. In the present study the PDF of the initial damage was associated with the EC. The mesh sensitivity was studied under homogeneous loading conditions, because then the results are not disturbed by the local deformation state and crack initiation is completely dictated by the maximum initial damage in the structure. The PDF of the maximum initial damage and consequently the PDF for the time to crack initiation do not depend upon the finite element modeling. In section 6.2.2 it was demonstrated that the time to complete failure displayed only a minor mesh sensitivity that originated from a less accurate description of the local deformation state in case of a small number of elements. Further investigations concerning the role of the EC as a characteristic

size in the reduction of the mesh sensitivity are highly recommended.

In chapter 6 it was pointed out that CDM can be used to predict both crack initiation and propagation by representing the crack as a zone of completely damaged elements. Crack growth is modeled in a natural way through growth of this zone. Hence, the crack tip is a process zone in which the damage continually changes. This should be compared to fracture mechanics, where given some stress state in the vicinity of a crack tip, it is checked, whether crack growth occurs. In crack growth problems the failure processes are dominated by the local deformation state leading to identical crack patterns for all realizations of the initial state. As our main concern was directed towards the qualitative prediction of the crack pattern, only one calculation was carried out by attributing the expected values of the initial damage distribution to the Gauss points in the mesh. This analysis yields an averaged structural behaviour. It is noted that in situations where the time to failure is of paramount importance, simulation techniques must be used. Crack propagation in a plate with an induced crack was studied for three distinct loadings. Although no reference can be made to other studies, the results are qualified as promising, since the computed crack patterns come up to our expectations.

In the present study the meshes were kept fixed. Due to the fact that the interconnections between the elements are maintained, crack opening effects cause large deformations in the completely damaged zone. The rigidity of this zone can not be decreased indefinitely, since errors with respect to the solution of the linearized set of equations can be expected to be large if structures of widely varying stiffness are analyzed. As a consequence residual stresses may take on considerable values in the completely damaged zone. A solution to this problem is the application of mesh adaptation techniques. By adapting the local mesh refinement as the crack proceeds crack opening effects can be modeled correctly, thus ruling out residual stresses and the downward trend of the peak stresses at the crack tip. In future research attention should be given to mesh adaptation techniques.

To conclude this thesis, it is stated that CDM provides for an attractive theory in the modeling of failure processes. The experimental characterization of damage is feasible through the stochastic nature of damage. Implementation in finite element codes renders a powerful tool for the analysis of (stochastic) processes involving crack initiation and propagation. However, the discussion above indicates a number of issues to be investigated further. For example in the characterization of damage states optical measurements may contribute substantially. Investigations in

the numerical field are required with respect to the mesh sensitivity, the application of mesh adaptation techniques and substructuring. Priority, however, should be given to the implementation of the model into a standard finite element code. The implementation should be set up in a general way, such that damage processes can be analyzed by user supplied routines for the evolution equation and the damage criterion. Advantage can be gained of common features that different dissipative mechanisms display.

Appendices

Appendix A Elaboration for anisotropic damage

The constitutive theory in section 3.4 will be elucidated for isotropic material behaviour. In this case the constitutive equations are completely independent of the orientation of the coordinate reference system. Hence, the free energy potential must obey the following relation for any proper orthogonal tensor **Q**

$$\psi(\mathbf{E},\mathbf{D}) = \psi(\mathbf{Q}\cdot\mathbf{E}\cdot\mathbf{Q}^c,\mathbf{Q}\cdot\mathbf{D}\cdot\mathbf{Q}^c) \qquad \forall\, \mathbf{Q} \tag{A1}$$

Using the representation theorems for isotropic scalar functions (Spencer 1971), it follows that the free energy can only depend on a set of 10 scalar invariants

$$I_1 = E_{kk}\ ;\ I_2 = E_{ij}E_{ji}\ ;\ I_3 = E_{ij}E_{jk}E_{ki}\ ;\ I_4 = D_{kk}\ ;\ I_5 = D_{ij}D_{ji}\ ;$$

$$I_6 = D_{ij}D_{jk}D_{ki}\ ;\ I_7 = D_{ij}E_{ij}\ ;\ I_8 = D_{ij}D_{jk}E_{ki}\ ;\ I_9 = D_{ij}E_{jk}E_{ki}\ ;$$

$$I_{10} = D_{ij}D_{jk}E_{kl}E_{li} \tag{A2}$$

Expanding $\psi(\mathbf{E},\mathbf{D})$ in powers of **E**, terminating at the second power, we obtain

$$\rho_0\psi = A_0 + A_1I_1 + A_2I_7 + A_3I_8 + \tfrac{1}{2}A_4I_1^2 + \tfrac{1}{2}A_5I_2 + A_6I_1I_7 + A_7I_1I_8 +$$

$$+ A_8I_7I_8 + \tfrac{1}{2}A_9I_7^2 + \tfrac{1}{2}A_{10}I_8^2 + A_{11}I_9 + A_{12}I_{10} \tag{A3}$$

where $A_i = A_i(I_4,I_5,I_6)$ for $i = 1,\ldots,12$. In view of eq. $(3.4.9)_1$ it follows that

$$P_{pq} = A_1\delta_{pq} + A_2D_{pq} + A_3D_{qj}D_{jp} + A_4E_{kk}\delta_{pq} + A_5E_{pq} + A_6(D_{ij}E_{ij}\delta_{pq} +$$

$$+ D_{pq}E_{kk}) + A_7(D_{qj}D_{jp}E_{kk} + D_{ij}D_{jk}E_{ki}\delta_{pq}) + A_8(D_{pq}D_{ij}D_{jk}E_{ki} +$$

$$+ D_{ij}E_{ij}D_{qk}D_{kp}) + A_9D_{pq}D_{ij}E_{ij} + A_{10}D_{qj}D_{jp}D_{ik}D_{kl}E_{li} + A_{11}(D_{ip}E_{qi}$$

$$+ D_{qi}E_{ip}) + A_{12}(D_{ij}D_{jp}E_{qi} + D_{qj}D_{ji}E_{ip}) \tag{A4}$$

If it is required that the body is stress free in the reference configuration, the following condition must be satisfied

$$A_1\delta_{pq} + A_2D_{pq} + A_3D_{qj}D_{jp} = 0 \tag{A5}$$

A_1, A_4 and A_5 should reduce to the classical moduli in the absence of damage. Thus, we must have $A_1 = 0$, $A_4 = \lambda_o$ and $A_5 = 2\mu_0$, where λ_o and μ_o are the so–called Lamé–constants. If it is assumed that the A_i do not depend on the damage state the generalized force X_{pq} is given by

$$\begin{aligned} X_{pq} = {} & (A_2 + A_6I_1 + A_8I_8 + A_9I_7)E_{pq} + \\ & + (A_3 + A_7I_1 + A_8I_7 + A_{10}I_8)(D_{qk}E_{kp} + D_{ip}E_{qi}) + \\ & + A_{11}E_{qk}E_{kp} + A_{12}(D_{qk}D_{kl}E_{lp} + D_{ip}E_{li}E_{ql}) \end{aligned} \tag{A6}$$

After specification of the damage criterion (3.3.21) and the consistency condition (3.4.11), the constitutive theory is completely defined together with eqs. (A4), (A6) and (3.4.14).

Appendix B Kolmogorov–Smirnov test of fit

The Kolmogorov–Smirnov test is useful for testing whether two distributions are different. It is based on the deviate $\underline{\Delta}$

$$\underline{\Delta} = \max_{x} [\, F_{\underline{n}}(x) - P_{\underline{x}}(x)] \tag{B1}$$

where $F_{\underline{n}}(x)$ is the cumulative frequency distribution of a sample of size n. $F_{\underline{n}}(x)$ is regarded as a discrete random variable whose possible values are 0, 1/n, 2/n,...,1. Kolmogorov's theorem offers the possibility to estimate the distribution function of $\underline{\Delta}$. In particular if the CDF of $\underline{x}$, $P_{\underline{x}}(x)$, is continuous, the theorem states that

$$\lim_{n\to\infty} P[\underline{\Delta} < y/\sqrt{n}] = Q(y) = \begin{cases} 0 & y \leq 0 \\ \sum_{k=-\infty}^{\infty} (-1)^k \exp(-2k^2y^2) & y > 0 \end{cases} \tag{B2}$$

which is a monotonic function with the limiting values $Q(0) = 0$ and $Q(\infty) = 1$. Assume that a CDF $P_{\underline{x}}(x)$ has been guessed for $\underline{x}$ and that $F_{\underline{n}}(x)$ has been built up from an observed sample. Then compute

$$\Delta = \max_{x} \mid \hat{F}_{\underline{n}}(x) - \hat{P}_{\underline{x}}(x) \mid \tag{B3}$$

i.e. the realization of the random variable corresponding to the observed sample. If the sample size is sufficiently large it is possible to calculate from equation (B2) the significance level of an observed value of Δ.

$$P(\underline{\Delta} \geq \Delta) \cong 1 - Q(\sqrt{n}\,\Delta) \tag{B4}$$

Small values of P show that the CDF of $F_{\underline{n}}(x)$ is significantly different from $P_{\underline{x}}(x)$. It should then be concluded that $\hat{P}_{\underline{x}}(x)$ cannot be used to describe the random variable $\underline{x}$. However, if P is sufficiently large, the calculated deviate Δ is a value that is likely to be found in a single test. In this case the sample test is not in conflict with the hypothetical CDF $P_{\underline{x}}(x)$.

Appendix C Scheme of the solution process

In this Appendix the solution strategy, which is employed for the coupled as well as the uncoupled set of equations is highlighted. For notational simplicity the damage column $\underset{\sim}{D} = \{ {}_1D, {}_2D, \ldots, {}_{4n_i}D \}$ with n_i the number of integration (Gauss) points, is introduced. Then, for times $t_n > 0$ the solution procedure is as follows

1 $t_{n+1} \longleftarrow t_n + \Delta t_n$

$a \longleftarrow 1$

$\underset{\sim}{D}^a_{n+1}$

if ($\exists\, j \in \{1, 2\ldots, 4n_i\} \mid {}_jD^a_{n+1} > D_c$) *go to* 2

if (*equations are uncoupled*) *then*

Δt_n

go to 1

else

2 $\underline{\underline{K}}(\underset{\sim}{x}^a_{n+1}, \underset{\sim}{D}^a_{n+1})\ \delta\underset{\sim}{x} = \underset{\sim}{r}(\underset{\sim}{x}^a_{n+1}, \underset{\sim}{D}^a_{n+1})$

$\underset{\sim}{x}^a_{n+1} \longleftarrow \underset{\sim}{x}^a_{n+1} + \delta\underset{\sim}{x}$

$\underline{F}^a_{n+1}, \underline{E}^a_{n+1}, \underline{\sigma}^a_{n+1}$

if ($|\underset{\sim}{r}| < \alpha$) *then*

Δt_n

go to 1

else

$a \longleftarrow a+1$

$\underset{\sim}{D}^a_{n+1}$

go to 2

endif

endif

References

Allen, D.H., Harris, C.E., and Groves, S.E. 1987, A thermomechanical constitutive theory for elastic composites with distributed damage–I. Theoretical development, *Int. J. Solids Struct.* **23**, 1301–1318.

Allix, O., Ladeveze, P., Le Dantec, E., and Vittecoq, E. 1987, Damage mechanics for composite laminates under complex loading, *Proceedings I.U.T.A.M./I.C.M. Symposium Yielding, damage and failure of anisotropic solids*, August 24–28, Grenoble, France.

Andrews, E.H. 1969, Fatigue in polymers, *Testing of polymers*, John Wiley & Sons, New York.

Augusti, G., Baratta, A., and Casciati, F. 1984, *Probabilistic methods in structural engineering*, Chapman and Hall, London.

Bathe, K.J. 1982, *Finite element procedures in engineering analysis*, Prentice–Hall, Englewood Cliffs.

Bazant, Z.P., and Pijaudier–Cabot, G. 1988, Nonlocal continuum damage, localization instability and convergence, *J. Appl. Mech.* **55**, 287–293.

Billardon, R., and Moret–Bailly, L. 1987, Fully coupled strain and damage finite element analysis of ductile fracture, *Nucl. Eng. Des.* **105**, 43–49.

Broek, D. 1986, *Elementary engineering fracture mechanics*, Sijthof and Noordhof.

Budianski, B., and O' Connel, R.J. 1976, Elastic moduli of a cracked solid, *Int. J. Solids Struct.* **12**, 81–97.

Cassenti, B.N. 1984, Static failure of composite material, *AIAA Journal* **22**, 103–110.

Chaboche, J.L. 1988, Continuum Damage Mechanics, Parts 1 and 2, *J. Appl. Mech.* **55**, 59–72.

Chaboche, J.L., and Lesne, P.M. 1988, A nonlinear continuous fatigue damage model, *Fatigue Fract. Eng. Mater. Struct.* **12**, 81–97.

Chen, C.C., Chheda, N., and Sauer, J.A. 1981, Craze and Fatigue resistance of glassy polymers, *J. Macromol. Sci. – Phys.* **B19**, 565–588.

Chow, C.L., and Wang, J. 1988, Ductile fracture characterization with an aniso–tropic damage theory, *Eng. Fract. Mech.* **30**, 547–563.

Coleman, B.D., and Gurtin, M.E. 1967, Thermodynamics with internal state variables, *J. Chem. Phys.* **47**, 597–613.

Crum Mc, N.G., Buckley, C.P., and Bucknall, C.B. 1988, *Principles of Polymer Engineering*, Oxford Science Publications.

Davison, L., and Stevens, A.L. 1973, Thermomechanical constitution of spalling elastic bodies, *J. Appl. Phys.* **44**, 668–674.

Davison, L., Stevens, A.L., and Kipp, M.E. 1977, Theory of spall damage accumu–lation in ductile metals, *J. Mech. Phys. Solids* **25**, 11–28.

Dumont, J.P., Ladeveze, P., Poss, M., and Remond, Y. 1987, Damage mechanics for 3–D composites, *Composite Structures* **8**, 119–141.

Gadkaree, K.P., and Kardos, J.L. 1984, Prediction and measurement of fatigue life distributions for elastomeric biomaterials, *J. Appl. Polymer. Sci.* **29**, 3041–3055.

Georgiadis, C. 1984, Probability of failure models in finite element analysis of brittle materials, *Comp. & Struct.* **18**, 537–549.

Germain, P., Nguyen, Q.S., and Suquet, P. 1983, Continuum Thermodynamics, *J. Appl. Mech.* **50**, 1010–1020.

Griffith, A.A. 1920, The phenomena of rupture and flow in solids, *Phyl. Trans. Roy. Soc. London* **A221**, 163–198.

Hashin, Z. 1983, Analysis of composite materials, *J. Appl. Mech.* **50**, 481–505.

Hashin, Z. 1983, Statistical cumulative damage theory for fatigue life prediction, *J. Appl. Mech.* **50**, 571–579.

Horii, H., and Nemat–Nasser, S. 1983, Overall moduli of solids with microcracks: load induced anisotropy, *J. Mech. Phys. Solids* **31**, 155–171.

Hunter, S.C. 1983, *Mechanics of continuous media*, Ellis Horwood, Chichester, England.

Hwang, W., and Han, K.S. 1986, Cumulative damage models and multi stress fatigue life prediction, *J. Comp. Mat.* **20**, 125–153.

Jansson, S., and Stigh, U. 1985, Influence of cavity shape on damage parameter, *J. Appl. Mech.* **52**, 609–614.

Kachanov, L.M. 1986, *Introduction to Continuum Damage Mechanics*, Martinus Nijhoff, Dordrecht.

Kam, T.Y., and Chew, H.C. 1987, Reliability analysis of brittle structures under random loadings, *Comp. & Struct.* **26**, 1005–1010.

Kestin, J., and Bataille, J. 1978, Irreversible thermodynamics of continua and internal variables, *Continuum models of discrete systems*, Provan, J.W., ed., Univ. of Waterloo Press.

Krajcinovic, D., and Fonseka, G.U. 1981, The continuous damage theory of brittle materials, Parts 1 and 2, *J. Appl. Mech.* **48**, 809–824.

Krajcinovic, D., and Silva, M.A.G. 1982, Statistical aspects of the continuous damage theory, *Int. J. Solids Struct.* **18**, 551–562.

Krajcinovic, D. 1983, Constitutive equations for damaging materials, *J. Appl. Mech.* **50**, 355–360.

Krajcinovic, D. 1984, Continuum Damage Mechanics, *Appl. Mech. Rev.* 37, 1–6.

Krajcinovic, D. 1986, Micromechanical basis of phenomenological models, *CISM course on Continuum Damage Mechanics*, Udine, Italy.

Krajcinovic, D., and Sumarac, D. 1989, A mesomechanical model for brittle deformation processes parts 1 and 2, *J. Appl. Mech.* **51**, 51–62.

Laws, N., and Brockenbrough, J.R. 1987, The effect of microcrack systems on the loss of stiffness of elastic solids, *Int. J. Solids Struct.* **23**, 1247–1268.

Lemaitre, J. 1986, Formulation and identification of damage kinetic constitutive equations, *CISM course on Continuum Damage Mechanics*, Udine, Italy.

Lemaitre, J. 1986, Local approach of fracture, *Eng. Fract. Mech.* **25**, 523–537.

Lemaitre J., and Dufailly, J. 1987, Damage measurements, *Eng. Fract. Mech.* 28, 643–661.

Lewis, E.E. 1987, *Introduction to reliability engineering*, John Wiley & Sons.

Malvern, L.E. 1969, *Introduction to the mechanics of a continuous medium*, Prentice–Hall, Englewood Cliffs, N.J..

Master Mc, A.D., Morrow, D.R., and Sauer, J.A. 1974, Nature of fatigue behavior and effect of flaw size in Polystyrene, *Polym. Eng. Sci.* **14**, 801–805.

Mazars, J. 1982, Mechanical damage and fracture of concrete structures, *Advances in Fracture Research* (Fracture 81), 1499–1506, Pergamon Press.

Müller, I. 1984, *Thermodynamics*, Pitman, London.

Murakami, S., and Ohno, N. 1981, A continuum theory of creep and creep damage, *Creep in structures*, Ponter and Hayhurst, eds., Springer Verlag, 422–444.

Murakami, S. 1988, Mechanical modeling of material damage, *J. Appl. Mech.* **55**, 280–286.

Paas, M.H.J.W., Oomens, C.W.J., Schreurs, P.J.G., and Janssen, J.D. 1990, The mechanical behaviour of continuous media with stochastic damage, *Eng. Fract. Mech.* **36**, 255–266.

Paas, M.H.J.W., Schreurs, P.J.G., Oomens, C.W.J., and Janssen, J.D. 1990, A stochastic approach to fatigue damage modeling, *Mechanics and mechanisms of damage in composites and multimaterials*, D. Baptiste ed., 22–36.

Paas, M.H.J.W., Schreurs, P.J.G., and Janssen, J.D. 1990, The application of Continuum Damage Mechanics to fatigue failure mechanisms, *Proceedings of the Dutch National Applied Mechanics Congress 1990*, Kluwer, Dordrecht, Holland.

Press, W.H., Flannery, B.P., Teukolsky, S.A., and Vetterling, W.T. 1986, *Numerical recipes*, Cambridge University Press.

Rabinowitz, S., Krause, A.R., and Beardmore, P. 1973, Failure of polystyrene in tensile and cyclic deformation, *J. Mater. Sci.* **8.**, 11–22.

Rabotnov, Y.N. 1969, *Creep problems of structural members*, North Holland.

Rooyackers, H.F.L. 1988, *A numerical implementation of the schapery model for nonlinear visco–elasticity*, Ph.D. thesis, Eindhoven University of Technology, The Netherlands.

Rice, J.R. 1970, On the structure of stress–strain relations for time–dependent plastic deformations in metals, *J. Appl. Mech.* **37**, 728–737.

Rivlin, R.S., and Thomas, A.G. 1953, Rupture of rubber I. Characteristic energy for tearing, *J. Polym. Sci.* **10**, 291.

Sauer, J.A., Mc Master, A.D., and Morrow, D.R. 1976, Fatigue behavior of polystyrene and effect of mean stress, *J. Macromol. Sci. – Phys.* **B12**, 535–562.

Sauer, J.A., Foden, E., and Morrow, D.R. 1977, Influence of molecular weight on the fatigue behavior of polyethelyne and polystyrene, *Polym. Eng. Sci.* 17, 246–250.

Sauer, J.A., and Richardson, G.C. 1980, Fatigue of polymers, *Int. J. Fract.* 16, 499–532.

Sauren, A.A.H.J. 1981, *The mechanical behaviour of the aortic valve*, Ph.D. thesis, Eindhoven University of Technology, The Netherlands.

Schoofs, A.J.G. 1987, *Experimental design and structural optimization*, Ph.D. thesis, Eindhoven University of Technology, The Netherlands.

Schreurs, P.J.G., Veldpaus, F.E., and Brekelmans, W.A.M. 1986, Simulation of forming processes, using the arbitrary Eulerian–Lagrangian formulation, *Comp. Meth. Appl. Mech. Eng.* **58**, 19–36.

Simo, J.C., and Ju, J.W. 1987, Strain– and stress–based continuum damage models–I. Formulation, *Int. J. Solids Struct.* **23**, 821–840.

Singh, U.K., and Digby, P.J. 1989, A continuum damage model for simulation of the progressive failure of brittle rocks, *Int. J. Solids Struct.* **25**, 647–663.

Sheikh, A.K., and Ahmad, M. 1987, A reliability model for a nonlinear damage process, *Reliability Eng.* 18, 73–99.

Skibo, M.D., Hertzberg, R.W., and Manson, J.A. 1976, Fatigue fracture processes in polystyrene, *J. Mater. Sci.* **11**, 479–490.

Spencer, A.J.M. 1971, Theory of invariants, *Continuum physics Vol 1: Mathematics*, A.C. Ehringen, ed., Academic Press, New York, 268–293.

Steenhoven van, A.A. 1979, *The closing behaviour of the aortic valve*, Ph.D. thesis, Eindhoven University of Technology, The Netherlands.

Talreja, R. 1985, A continuum mechanics characterization of damage in composite materials, *Proc. R. Soc. London* A**399**, 195–216.

Ven van der, R.N.H.J. 1988, *A statistical model for the description of failure mechanisms* (in Dutch), Report WFW–88.031, M.Sc. thesis, Eindhoven University of Technology, The Netherlands.

Weibull, W. 1953, A statistical distribution function of wide applicability, *J. Appl. Mech.*, 293–297.

Weitsman, Y. 1988, Damage coupled with heat conduction in uniaxially reinforced composites, *J. Appl. Mech.* **55**, 641–647.

Weitsman, Y. 1988, A continuum damage model for viscoelastic materials, *J. Appl. Mech.* **55**, 773–780.

Wijngaarden van, H. 1988, *Constitutive equations for metals with an application to the extrusion of lead*, Ph.D. thesis, Eindhoven University of Technology, The Netherlands.

Williams, J.G. 1984, *Fracture mechanics of polymers*, Ellis Horwood, Chichester.

Young, R.J. 1983, *Introduction to polymers*, Chapman and Hall, London.

Zienkiewicz, O.C. 1977, *The Finite Element Method*, McGraw–Hill, London.

Zweben, C., and Rosen, B.W. 1970, A statistical theory of material strength with application to composite materials, *J. Mech. Phys. Solids* **18**, 189–206.

Samenvatting

In de modelvorming van faalmechanismen is de toepassing van geavanceerde theoretische en numerieke methoden onmisbaar. In dit onderzoek wordt continuum damage mechanics (CDM) gebruikt om faalmechanismen te beschrijven. CDM is een tak van de continuümsmechanica, waarbij de lokale verdeling van microdefecten wordt gekarakteriseerd met een continue (schade)variabele. Als gevolg van de introductie van de schadevariabele moet een extra relatie bepaald worden, de (schade)evolutievergelijking, die aangeeft hoe de schade verandert. In CDM wordt een continue koppeling tussen de schade en deformaties verkregen. Algemene uitdrukkingen voor de constitutieve vergelijkingen, te weten de spannings–rek relatie en de evolutie vergelijking, kunnen worden afgeleid uit twee potentialen: de Helmholtz vrije energie functie en de dissipatie potentiaal.

In deze studie wordt vooral aandacht besteed aan brosse faalmechanismen, hetgeen betekent, dat schade–evolutie het overheersende dissipatieve mechanisme is. Verder hangt de huidige toestand niet af van de snelheid waarmee deze toestand bereikt is. Gebaseerd op de formulering van het criterium voor schadegroei, wordt een verder onderscheid gemaakt tussen brosse schade en schade door vermoeiing. Voor beide mechanismen zijn modellen ontwikkeld. Het model voor brosse schade is in staat om het gedrag van beton en polystyreen in eenvoudige belasting situaties te beschrijven. Het model voor vermoeiing kan desgewenst tot enkele algemeen aanvaarde cumulatieve schademodellen vereenvoudigd worden. Anisotrope schade wordt behandeld, waarbij de richtings–afhankelijkheid wordt verdisconteerd met behulp van dyadische vector produkten.

Voor een volledige beschrijving van faalmechanismen moeten de evolutie–vergelijking en de initiële schade bekend zijn. Om de parameters in de evolutie–vergelijking te karakteriseren wordt verondersteld, dat microscheur– en macro–scheurgroei door identieke relaties beschreven worden. Vervolgens kan de evolutie–vergelijking afgeleid worden met behulp van concepten uit de breukmechanica. Op grond van het feit dat faalprocessen in werkelijkheid stochastische processen zijn, kan beredeneerd worden dat de initiële schade een random variabele is. Door de initiële schade te associëren met een karakteristieke afmeting, de zogenaamde elementaire cel, kunnen de bijbehorende statistische eigenschappen bepaald worden. De geldigheid van het ontwikkelde statistische model wordt aangetoond voor vermoeiing bij rubbers en polystyreen.

Voor praktische toepassingen zijn de evenwichtsvergelijking en de constitu–

tieve vergelijkingen numeriek opgelost. Gebaseerd op het principe van de gewogen residuën is een iteratieve procedure ontwikkeld om de niet–lineaire vergelijkingen op te lossen. Aanzienlijke rekentijdwinst wordt verkregen door de toepassing van een adaptief stapgrootte algoritme bij de numerieke integratie van de evolutievergelijking en door ontkoppeling van de constitutieve vergelijkingen.

Simulatie–technieken worden toegepast om stochastische faalprocessen te analyseren. De simulaties bestaan uit eindige elementen berekeningen voor verschillende begintoestanden. De statistische eigenschappen van de faalprocessen volgen uit het geheel van de responsies. De simulaties tonen aan dat de oplossingen, die verkregen zijn met de gekoppelde en ontkoppelde constitutieve vergelijkingen, slechts in geringe mate verschillen. Bovendien wordt de afhankelijkheid van de mesh op de resultaten verminderd door het concept van de elementaire cel.

In CDM is scheurgroei equivalent aan de groei van een zone van volledig beschadigde elementen. Zowel de initiatie alsook de groei van scheuren worden voorspeld.

Levensbericht

25–2–1963	Geboren te Heerlen
1975–1981	Gymnasium B aan het Bernardinus College te Heerlen
1981–1986	Studie Werktuigbouwkunde aan de Technische Universiteit Eindhoven
1986–1990	Wetenschappelijk assistent aan de Technische Universiteit Eindhoven, afdeling Werktuigbouwkunde

Stellingen

behorende bij het proefschrift

CONTINUUM DAMAGE MECHANICS
WITH AN APPLICATION TO FATIGUE

1) Met behulp van "continuum damage mechanics" kunnen de processen, die optreden bij vermoeiing en brosse breuk, op vrijwel identieke wijze gemodelleerd worden.
   - Marigo, J.J. 1985, Modelling of brittle and fatigue damage for elastic material by growth of microvoids, *Eng. Fract. Mech.* **21**, 861–874.
   - Dit proefschrift, hoofdstuk 3.

2) Wanneer de microstructuur niet nauwkeurig bekend is, dient de initiële schade, een essentiële grootheid in de beschrijving van faalmechanismen, opgevat te worden als een stochast.
   - Dit proefschrift, hoofdstuk 4.

3) De toepassing van een adaptief stapgrootte algoritme en (indien toelaatbaar) de ontkoppeling van de spannings–rek relatie en de schade–evolutie vergelijking leveren een enorme winst in rekentijd op bij de numerieke uitwerking van schademodellen.
   - Dit proefschrift, hoofdstuk 5.

4) Continuum damage mechanics is niet alleen een methode om scheurinitiatie te voorspellen, maar is ook uitermate geschikt om scheurvoortplanting te beschrijven.
   - Lemaitre, J. 1986, Local approach of fracture, *Eng. Fract. Mech.* 25, 523–537.
   - Dit proefschrift, hoofdstuk 6.

5) Het concept van de elementaire cel en de hiermee geassocieerde kansdichtheidsfunctie van de initiële schade reduceren de mesh–afhankelijkheid bij bezwijkanalyses gebaseerd op de eindige elementen methode.
   - Dit proefschrift, hoofdstuk 6.

6) Structurele modellen dienen slechts dan geprefereerd te worden boven fenomenologische modellen, als men beschikt over een gedetailleerd inzicht in de microstructuur en de zich op micro–niveau manifesterende processen.

7) Optimaliseringsmethoden zijn van groot belang bij de ontwikkeling van constructies. Een zwak punt echter is de keuze van de ontwerpvariabelen en de te minimaliseren objectfunctie(s).
   – Vanderplaats, G.N. 1984, *Numerical optimization techniques for engineering design*, McGraw–Hill, New York.

8) Het merendeel van de studenten in de technische wetenschappen beschikt over een gebrekkige kennis van gestructureerd programmeren. Als gevolg hiervan wordt programmeren door hen veelal gezien als een intuïtief te bedrijven ambacht.

9) Onderzoek gehoorzaamt aan darwinistische principes. Alleen de beste theorieën worden voortdurend verder ontwikkeld. Overbodige theorieën verdwijnen of leven voort binnen een geïsoleerde gemeenschap.

10) De rustpols verstrekt belangrijke informatie omtrent de fysieke en mentale conditie. Fysieke en/of mentale overbelasting kunnen door een regelmatige registratie van de rustpols in een vroeg stadium worden opgespoord.

11) De belangrijkste taak van een coach is de training zodanig in te richten, dat ieder individu het maximale rendement haalt uit de geleverde inspanning.

12) Oost west, thuis werkt best.

Eindhoven, september 1990 Michel Paas